Coupling of Thermal Field-Flow Fractionation and FTIR Spectroscopy for the Fractionation and Analysis of Complex Polymers

by
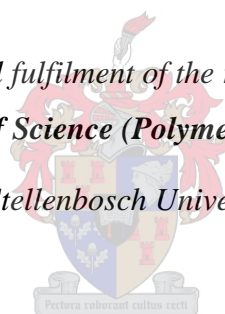
Nonkululeko Winnie Radebe

Thesis presented in partial fulfilment of the requirements for the degree
Master of Science (Polymer Science)

at Stellenbosch University

Supervisor: Prof Harald Pasch

Faculty of Science

Department of Chemistry and Polymer Science

December 2017

Declaration

By submitting this thesis electronically, I declare that the entirety of the work contained therein is my own, original work, that I am the sole author thereof (save to the extent explicitly otherwise stated), that reproduction and publication thereof by Stellenbosch University will not infringe any third party rights and that I have not previously in its entirety or in part submitted it for obtaining any qualification.

December 2017

ii

Abstract

The fast-paced growth and production of complex polymers has accelerated the need for advancement in characterization techniques. The structural complexity of polymers is described using the concept of molecular heterogeneity in molar mass, chemical composition, molecular architecture. The task of characterizing complex polymeric materials is a challenge, and has accelerated the need for hyphenated techniques that provide adequate information regarding the different microstructure distributions. The increased use of hyphenated techniques has prompted the development of online coupling of thermal field flow fractionation (ThFFF) and Fourier transform infrared spectroscopy (FTIR). ThFFF is a powerful channel-based fractionation tool for microstructure analysis of complex polymers as it has the ability to separate according to both molar mass and composition in a single experiment. FTIR, coupled to a separation technique, provides concentration profiles as well as detailed chemical structure information of macromolecules as a function of ThFFF elution volume.

The presented coupled method will significantly decrease the time needed for ThFFF-FTIR as compared to collecting fractions from ThFFF separation and subsequent offline analysis by FTIR. The inherent problem with the online coupling of ThFFF to FTIR is the combination of strong solvent signals and relatively low sample concentration necessary for ThFFF separation. To overcome this, a specialized flow cell was constructed and a mathematical solvent suppression routine was used to subtract the solvent signals. In the present study, the setup of the method as well as data treatment and example measurements are presented. Blends of polystyrene (PS) and poly (methyl methacrylate) (PMMA) as well as copolymers of styrene and methyl methacrylate (SMA) are analyzed and quantified using the method. By selecting spectral bands that are unique to each analyte, the distribution of the individual analyte components across the elution profile are measured and presented. Even when quantification is not possible, the technique can be used as a means of qualitative analysis, as seen for styrene-acrylonitrile (SAN) copolymers. In one integrated procedure, ThFFF -FTIR is shown to provide detailed microstructural characterization of complex multicomponent samples.

iii

Opsomming

Die vinnige groei en produksie van komplekse polimere het die behoefte aan vooruitgang in karakteriseringstegnieke versnel. Die strukturele kompleksiteit van polimere word beskryf deur gebruik te maak van die molekulêre heterogeniteit konsept in molêre massa, chemiese samestelling, molekulêre argitektuur. Die taak om hierdie polimeerstowwe te karakteriseer, is 'n uitdaging en het die behoefte aan koppeltekstegnieke versnel wat voldoende inligting verskaf oor die verskillende mikrostruktuurverdelings. Die toenemende gebruik van koppeltekens het daartoe gelei dat die ontwikkeling van aanlynkoppeling van termiese veldstroomfraktasie (ThFFF) en Fourier-transform infrarooi spektroskopie (FTIR) ontwikkel is. ThFFF is 'n kragtige kanaalgebaseerde breukinstrument vir mikrostrukture-analise van komplekse polimere, aangesien dit die vermoë het om volgens 'n enkele eksperiment volgens beide molêre massa en samestelling te skei. FTIR, gekoppel aan 'n skeidingstegniek, verskaf konsentrasieprofiele sowel as gedetailleerde makromolekule chemiese struktuurinligting as 'n funksie van elueringsvolume.

Die aangebied gekoppelde metode sal aansienlik verminder die tyd wat nodig is om breuke te versamel vanaf FFF skeiding en daaropvolgende offline analise deur FTIR. Die inherente probleem met die aanlyn koppeling van ThFFF tot FTIR, is 'n kombinasie van hoë oplosmiddel seine en relatief lae monster konsentrasie wat nodig is vir ThFFF skeiding. Om dit te oorkom, is 'n gespesialiseerde vloeisel gebou en 'n wiskundige oplosmiddelonderdrukkingsroetine gebruik om die oplosmiddel seine af te trek. In die huidige studie word die opstel van die metode sowel as data behandeling en voorbeeldmetings aangebied. Blends van poli (styreen) (PS) en poli (metiel-metakrylaat) (PMMA) sowel as kopolimere van styreen-metiel-metakrylaat (SMA) -kopolimere word geanaliseer en gekwantifiseer volgens die metode. Deur spektrale bande wat uniek is aan elke analiet te selekteer, word die verspreiding van die individuele analtekomponente oor die elutieprofiel gemeet en aangebied. Selfs wanneer kwantifisering nie moontlik is nie, kan die tegniek as kwalitatiewe analise gebruik word, soos gesien vir styreen-akrietonitril (SAN) kopolimere. In een geïntegreerde prosedure word THFFF -FTIR getoon om gedetailleerde mikrostrukturele karakterisering van komplekse multikomponentmonsters te verskaf.

Acknowledgements

Firstly, I would like to thank my supervisor, Prof Harald Pasch, for affording me the opportunity to work in his group and for providing me with funding. I truly appreciate his guidance, support and mentorship throughout the past two years.

I would like to thank my fellow researchers in the group, particularly A. Ndiripo, U.L Muza and Dr G. Greyling as well as the Department of Chemistry and Polymer Science for their unwavering support. A special thanks goes to Dr T. Beskers and Prof M. Wilhelm of Karlsruhe Institute of Technology (KIT), Germany, for collaborating with us on this project and always being available to help.

Thank you to my family and friends for motivating me daily. Most importantly, thank you to my mother, Brenda Radebe, for her love, support and many sacrifices throughout my studies.

Lastly, I would like to thank my ancestors for paving the way for me to get to this point.

Table of Contents

List of Figures

xi

List of Tables

List of symbols and abbreviations

2D	Two-dimensional
AF4	Asymmetric flow field-flow fractionation
AN	Acrylonitrile
ATR	Attenuated total reflection
CCD	Chemical composition distribution
Đ	Dispersity index
D	Normal diffusion coefficient
D_h	Hydrodynamic diameter
DLS	Dynamic light scattering
DMF	Dimethylformamide
dn/dc	Specific refractive index increment
DP	Depth of penetration
DRI	Differential refractive index detector
D_T	Thermal diffusion coefficient
FFF	Field-flow fractionation
FTIR	Fourier transform infrared spectroscopy
HPLC	High pressure liquid chromatography
IR.	Infrared spectroscopy
LC	Liquid chromatography
LOD	Limit of detection
LOQ	Limit of quantification
LS	Light scattering
MALLS	Multiangle laser light scattering
MIR	Mid-infrared
MMD	Molar mass distribution
M_p	Peak molar mass
M_w	Molar mass
NMR	Nuclear magnetic resonance spectroscopy

xiii

PAN	Polyacrylonitrile
PMMA	Poly(methyl methacrylate)
PS	Polystyrene
R_g	Radius of gyration
S/N	Signal-to-noise ratio
SAN	Styrene-acrylonitrile (copolymer)
SEC	Size exclusion chromatography
SMA	Styrene-methyl methacrylate (copolymer)
S_T	Soret coefficient
THF	Tetrahydrofuran
ThFFF	Thermal field-flow fractionation
$\frac{S/N}{\sqrt{t}}$	Time independent signal-to-noise ratio
TIMO	Time Resolved Infrared Spectroscopy for Molecular Online SEC Detection
t_r	Retention time
UV-Vis	Ultraviolet-Visible
wt. %	Weight percentage
ZnSe	Zinc selenide
ΔT	Applied temperature gradient

Chapter 1 : Introduction

1.1   Background

Synthetic polymeric materials are highly complex multicomponent materials. These complex materials are characterized by their chemical composition, molar mass, architecture, functionality as well as their respective distributions[1]. This structural complexity of macromolecules is described as molecular heterogeneity. Molecular heterogeneity can dramatically influence a polymer's properties, therefore, it is critical to determine the various distributions within each type of heterogeneity in order to fully characterize these macromolecules.

It is possible to determine functional groups and concentrations of monomer units present in a sample using traditional polymer analysis techniques such as nuclear magnetic resonance spectroscopy (NMR) or infrared spectroscopy (IR). However, using these methods in isolation do not yield information on the distribution of the monomer units or the functional groups in the polymer material (inter- and intramolecular distribution). Furthermore, IR does not provide information of molar mass. Techniques such as light scattering (LS), viscosimetry or osmometry provide molar mass averages for macromolecules but, similar to IR and NMR, when used in isolation they only measure average bulk properties[2]. Therefore, these techniques lack information regarding molecular distributions. For the characterization of polymeric materials according to molecular heterogeneity, it is necessary to use a wide range of analytical techniques which are selective towards a specific type of distribution[1,3–5]. By combining two different analytical techniques, it is possible to provide two-dimensional (2D) information on the molecular heterogeneity.

Chromatographic and other fractionation methods are able to separate complex materials according to the distributions present in that sample, therefore, if more than one type of distribution exits, more than one type of separation will be required. Multidimensional separations are required when the distributions are interdependent e.g. CCD and MMD[3]. Two common multidimensional approaches include the coupling of different chromatographic modes in 2-D liquid chromatography (2D-LC) or coupling chromatographic or fractionation techniques with either molar mass sensitive detectors and/or spectroscopic techniques[1]. In this work, we are interested in the latter approach, especially the hyphenation of field-flow

fractionation (FFF) and Fourier transform infrared spectroscopy (FTIR). Previous work has explored and reported on the coupling of IR and size exclusion chromatography (SEC) using a liquid flow cell [6–10]. Obtaining an acceptable signal-to-noise (S/N) ratio has proven to be the most significant challenge. However, Beskers and Wilhelm recently developed a fully online coupled technique using SEC and FTIR [11]. Here, the FTIR spectra are obtained online at the highest sensitivity using a custom designed flow cell. Thereafter, a mathematical approach called the "Time Resolved Infrared Spectroscopy for Molecular Online SEC Detection (TIMO)" software is used to subtract the solvent signal, decrease noise and reduce baseline drift.

Coupling of FFF with FTIR is valuable when there are compositional changes as a function of the separation period (elution time). The purpose of detector coupling or multidetector techniques is to identify and quantify the amount of heterogeneous components in a polymer material. FTIR has broad applications in many fields of science and engineering. Over the years, FTIR spectroscopy has become one of the most important tools for both qualitative and quantitative characterization of organic materials, in particular, polymers. However, FTIR as a technique on its own, cannot tell whether a sample is a mixture, a copolymer or a blend, regardless of the functional groups. For a precise determination of the composition of a complex polymer, which includes the chemical composition and the molar mass distribution of the components, a separation step is required.

Chromatography is a powerful tool for resolving/separating analytes, but does not provide molecular identification without a suitable detector[12]. Moreover, measuring chemical composition and molar mass in an online manner is preferred to manually collecting fractions and characterizing them one at a time. The online FFF-FTIR method will significantly decrease the labour and time as compared to fraction collection from FFF and subsequent offline analysis by FTIR. In addition to the above-mentioned advantages for coupling FTIR, all wavenumbers of IR can be measured simultaneously[13]. Furthermore, accurate wavenumber calibration will enable precise post run spectral manipulation such as subtraction or ratio techniques.

Combining multiple detectors online to a fractionation platform has proven to be useful. A hyphenated system that combines the high-resolution capabilities of FFF with the absolute and independent molar mass determination of light scattering (i.e. multiangle laser light scattering, MALLS) eliminates the need to calibrate the FFF system. Furthermore, light scattering detectors, when used together with a differential refractive index detector (DRI), give a signal

2

that is a function of both molar mass and concentration and can be used to obtain the average molar mass, and molar mass distribution. The advantage of using FFF instead of SEC is in avoiding the underestimation of the molar mass of ultrahigh molar mass polymers. This is because the long chains of such polymers undergo pronounced shear degradation in the porous stationary phase of a column-based fractionation device [14].

1.2   Research gap

Some disadvantages of complex LC techniques are:

1. The use of many solvents (e.g. in a solvent gradient and in 2D- LC).
2. Not all concentration detectors can be used in a solvent gradient. An LC-Transform system has to be used in order to couple chromatographic techniques to FTIR which is time consuming and labour intensive.
3. 2D-LC experiments are very long compared to FFF experiments, which give information on molar mass and chemical composition in one single experiment.
4. HPLC instrumentation is complex and expensive as compared to the simple FFF channel.

Since a single or isocratic solvent is used in ThFFF, a multidetector approach is possible. This makes a single short experiment more informative as compared to complex instrumentation such as in 2D-LC.

Furthermore, the use of FTIR in a multidetector set-up has an advantage when the solvent and the analyte combination have the same refractive index. This is because the DRI detector will not be able to distinguish between the solvent and analyte. The same challenge is faced when using a multiangle light scattering detector. In cases where the polymer does not absorb radiation in the UV-VIS range the UV detector becomes obsolete. In addition, viscosity and light scattering detectors cannot be used quantitatively without a concentration detector. Examples of isorefractive systems are poly(lactic acid) (PLA) in chloroform or polydimethylsiloxane (PDMS) in THF[11]. FTIR is able to detect signals regardless of the refractive index of the samples, therefore, FTIR can be used as a universal concentration detector. At the same time it provides information on the chemical composition of the analyte.

3

1.3   Limitations

The most important limitation of using FTIR as a means of chemical composition analysis for polymer solutions is the absorbance behaviour of the solvent. Most solvents have functional groups and exhibit strong absorptions in the mid-infrared (MIR) radiation region (4000 to 400 cm^{-1})[13]. Thus far, chloroform has been identified as the solvent that is most transparent to IR radiation. However, for non-transparent solvents, software has been developed to compensate for solvent absorbance. This fixes the problem of signal overlap. However, sensitivity of the technique is decreased as a consequence. An example of polymer/solvent signal overlap can be found when polystyrene (PS) is dissolved and analysed in toluene[15]. Even in this case, the TIMO software is able to subtract the toluene signals and allow the PS to be analysed.

1.4   Aims and objectives

The aim of this study is to develop an online FTIR detection method for ThFFF in order to directly identify and quantify the chemical composition of the eluting species. As such, the following objectives are defined:

1. To couple the FTIR flow cell to the ThFFF and subsequently optimize the flow cell, in order to satisfy the fractionation needs

2. To prepare complex samples consisting of:

    a) blends of PS and PMMA homopolymers

    b) copolymer samples such as poly(styrene-methyl methacrylate) (SMA) and poly(styrene-acrylonitrile) (SAN)

3. To characterize these samples by a multidetector ThFFF approach consisting of online UV, MALLS, DRI, dynamic light scattering (DLS) and FTIR detection

4. To extract quantitative information on chemical composition, molar mass, molecular size and diffusion coefficients from this complex multi-detector setup.

1.5   Layout of Thesis

Chapter 1

Here, the advantages and possible limitations of the coupling method are introduced. A broad overview on coupling FFF and FTIR is given and concepts about previous attempts of coupling spectroscopy and chromatography are highlighted.

Chapter 2

The theoretical background of FFF, ThFFF and FTIR is discussed in detail. Hyphenated techniques involving FFF and FTIR are introduced.

Chapter 3

The experimental procedures, instrumental set-up and instrumental procedures are outlined. Data processing methods and techniques are introduced.

Chapter 4

Chapter 4 summarizes the results and discussions on the characterization of the polymer blends and copolymers. Results from each detector are presented and explained.

Chapter 5

In this chapter, conclusions are given and relevant recommendations are made.

1.6   References

1.   Pasch, H. & Malik, M. I. *Advanced Separation Techniques for Polyolefins*. (Springer: New York, U.S.A, 2014).

2.   Held, D. & Kilz, P. Characterization of Polymers by Liquid Chromatography. *Macromol. Symp.* **231,** 145–165 (2006).

3.   Pasch, H. Analysis of complex polymers by multidimensional techniques. *Phys. Chem. Chem. Phys.* **1,** 3879–3890 (1999).

4.   Ahmad, I. A. H. & Striegel, A. M. Determining the absolute , chemical-heterogeneity-corrected molar mass averages , distribution , and solution conformation of random copolymers. *Anal. Bioanal. Chem.* **396,** 1589–1598 (2010).

5.   Ahmad, I. H. Studying Chemical and Sequence Length Heterogeneities in Copolymers. (Doctoral Thesis: Florida State University, 2011).

6.   Somsen, G. W. & Gooijer, C. Liquid chromatography – Fourier-transform infrared spectrometry. *J. Chromatogr. A* **856,** 213–242 (1999).

7.   Kok, S. J., Wold, C. A., Hankemeier, T. & Schoenmakers, P. J. Comparison of on-line flow-cell and off-line solvent-elimination interfaces for size-exclusion chromatography and Fourier-transform infrared spectroscopy in polymer analysis. *J. Chromatogr. A* **1017,** 83–96 (2003).

8.   Aust, N. & Lederer, K. A New IR Detector Cell with Optimized Optical Path Length for High-Temperature SEC of Polyolefins. *Int. J. Polym. Anal. Charact.* **3,** 219–229 (1999).

9.   Brown, R. S., Hausler, D. . & Taylor, L. Fourier Transform Infrared Spectrometric Detection in Size-Exclusion Chromatographic Separation of Polar Synfuel Material. *Anal. Chem.* **9,** 197–201 (1981).

10. Kok, S. J., Hankemeier, T. & Schoenmakers, P. J. Comprehensive two-dimensional liquid chromatography with on-line Fourier-transform-infrared-spectroscopy detection for the characterization of copolymers. *J. Chromatogr.* **1098,** 104–110 (2005).

11. Beskers, T. F., Hofe, T. & Wilhelm, M. Development of a chemically sensitive online SEC detector based on FTIR spectroscopy. *Polym. Chem.* **6,** 128–142 (2015).

12. Dwyer, J. L. & Zhou, M. Polymer Characterization by Combined Chromatography-Infrared Spectroscopy. *Int. J. Spectrosc.* **2011,** (2011).

13. Griffiths, P. R. & de Haseth, J. A. *Fourier transform Infrared Spectroscopy*. (John Wiley & Sons: New Jersey, U.S.A, 2007).

14. Pasch, H. Advanced fractionation methods for the microstructure analysis of complex polymers. *Polym. Adv. Technol.* **26,** 771–784 (2015).

15. Beskers, T. F., Hofe, T. & Wilhelm, M. Online Coupling of Size-Exclusion Chromatography and IR Spectroscopy to Correlate Molecular Weight with Chemical Composition. *Macromol. Rapid Commun.* **33,** 1747−1752 (2012).

6

Chapter 2 : Literature review

2.1.   Polymer characterization

Advanced characterization of materials is important in the product development cycle. The way in which a material/polymer is designed affects its properties and ultimately its performance. The increasing need for polymers with superior performance in polymer-related industries (i.e. car tires), has resulted in the production of more complex polymers and has therefore created a need for more sophisticated characterization methods[1]. Polymer characterization can include six important methods (among others): (1) fractionation and particle size distribution, (2) morphological studies, (3) spectroscopic studies (4) dynamic mechanical analysis, (5) rheology and (6) thermal properties[2].

In order to fully characterize a complex polymer by chemical composition and molar mass distributions, a separation technique is required. The most widely used separation technique for polymers is size exclusion chromatography (SEC) [3]. SEC separation is based on separation of macromolecules according to their size in solution using a multi-porous packed column. The larger molecules are excluded from the porous packing material because, unlike smaller particles, they cannot traverse through the pores. Therefore, large particles elute sooner than smaller particles because they travel a shorter path.

Field-flow fractionation (FFF) is a complementary separation technique where the sample is injected into and flows through an empty channel. FFF relies on an externally generated field that is applied perpendicular to the flow, for separation[4–6]. FFF is sensitive to both the molar mass and chemical composition, depending on the applied external field. The channel-based approach enables the analysis of sensitive and fragile analytes such as complex macromolecules, aggregates, particles and colloids[7].

2.2.   Fractionation by field–flow fractionation (FFF)

FFF separation takes place in a thin ribbon–like channel, comprising of a spacer clamped between two plates. The extent of the separation is due to the strength of the externally applied field, as schematically shown in Figure 2.1. The laminar flow conditions (i.e. the highest flow velocity at the centre of the channel and the slowest velocity at the walls [5]) within the channel

shown in Figure 2.1, results in a parabolic flow velocity profile across the channel. The component of a sample that is influenced more strongly by the applied field and/or has a lower diffusion coefficient, will establish a steady state closer to the accumulation wall of the FFF channel[6]. This component will have a longer retention than the component which is weakly influenced by the applied field. The ability of the analyte to diffuse is dependent on the molecular size, where the small components diffuse faster than the larger components. This results in a distribution of macromolecules with respect to their hydrodynamic size in the channel.
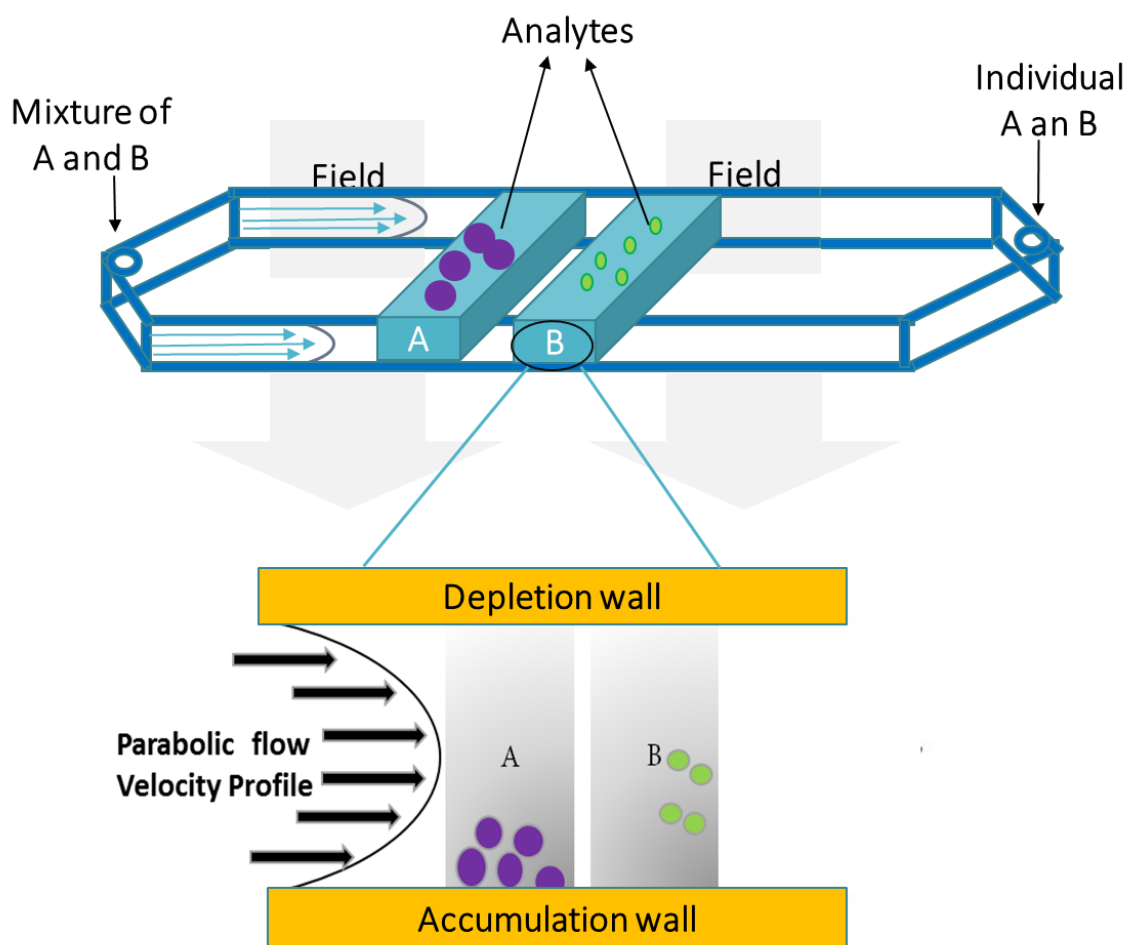
Figure 2.1: Representation of the FFF separation mechanism.

Advantages of FFF over column–based separation techniques

SEC and high- pressure liquid chromatography (HPLC) are the standard methods used for the analysis of complex polymers. However, due to the absence of a stationary phase in FFF, this technique has several advantages over SEC/HPLC, which include:

- Minimized shear degradation[8]

- Separation of molecules over a wide molecular size range ($10^3 – 10^9$ Da) [3]

- Open–channel setup eliminates the need for filtration [6, 9]

- Sensitive and fragile analytes such as supramolecular assemblies and protein aggregates can be accurately analysed [5]

- Adsorption is avoided [10]

- Complex mixtures containing gels, suspended particles and soluble polymers are analysed in one run [5,11,12]

FFF sub–techniques

FFF consists of a family of sub-techniques which operate under different fields. Each type of field used in each sub-technique has a different range and area of applicability. For example, flow FFF (FlFFF) separates according to diffusion coeffcient differences with an application range of 0.001–50 µm, mostly in aqueous solvents[7]. Centrifugal or sedimentation FFF (CFFF or SdFFF) separate according to the diffusion coefficient as well as density differences[5]. Another sub-technique that has been extensively used is thermal FFF, which separates according to thermal diffusivity and normal diffusion coefficients. Other FFF techniques include electrical FFF (FlFFF)[9], hollow fiber FFF (HFFFF)[9] as well as magnetic FFF (MgFFF)[13].

2.3. Thermal field–flow fractionation (ThFFF)

ThFFF is a sub–technique of FFF that uses a temperature gradient across the channel in order to fractionate analyte molecules according to size or chemical composition and most recently according to tacticity distributions[12]. The analytes are subjected to a temperature gradient (ΔT) where they migrate from the hot wall to the cold (accumulation) wall of the channel. Such a lateral migration of the analytes that is due to a temperature gradient (Figure 2.2) can be used

for fractionation. The migration is characterised by the thermal diffusion coefficient, D_T. D_T is calculated using Equation 2.1, where t_0 and t_r are the retention times related to the peak maxima and of the retained and unretained peaks, respectively[7].

$$D_T = \frac{6Dt_r}{\Delta t_0} \qquad\qquad 2.1$$

Normal diffusion (Brownian motion), D, is the migration of the analyte molecules away from the cold wall towards the centre of the channel and it counteracts thermal diffusion. D can be calculated using the Einstein–Stokes law as presented in Equation 2.2, where η is the solvent viscosity, and D_h is the polymer hydrodynamic diameter.

$$D = \frac{kT}{3\pi\eta D_h} \qquad\qquad 2.2$$

The Soret coefficient, S_T, as defined by Equation 2.3, is the average distance from the accumulation wall. A variation in this value allows for separation according to both chemical composition (D_T) and molar mass (D)[14].

$$S_T = \frac{D_T}{D} \qquad\qquad 2.3$$

The distribution of polymer formed at the cold wall under steady–state conditions can be described by the effective thickness which is the distance from the cold wall to the center of gravity of the polymer zone [4, 6]. For homopolymers, species with higher D (or lower polymer M_W) elute first and those with the lowest D elute last.

10
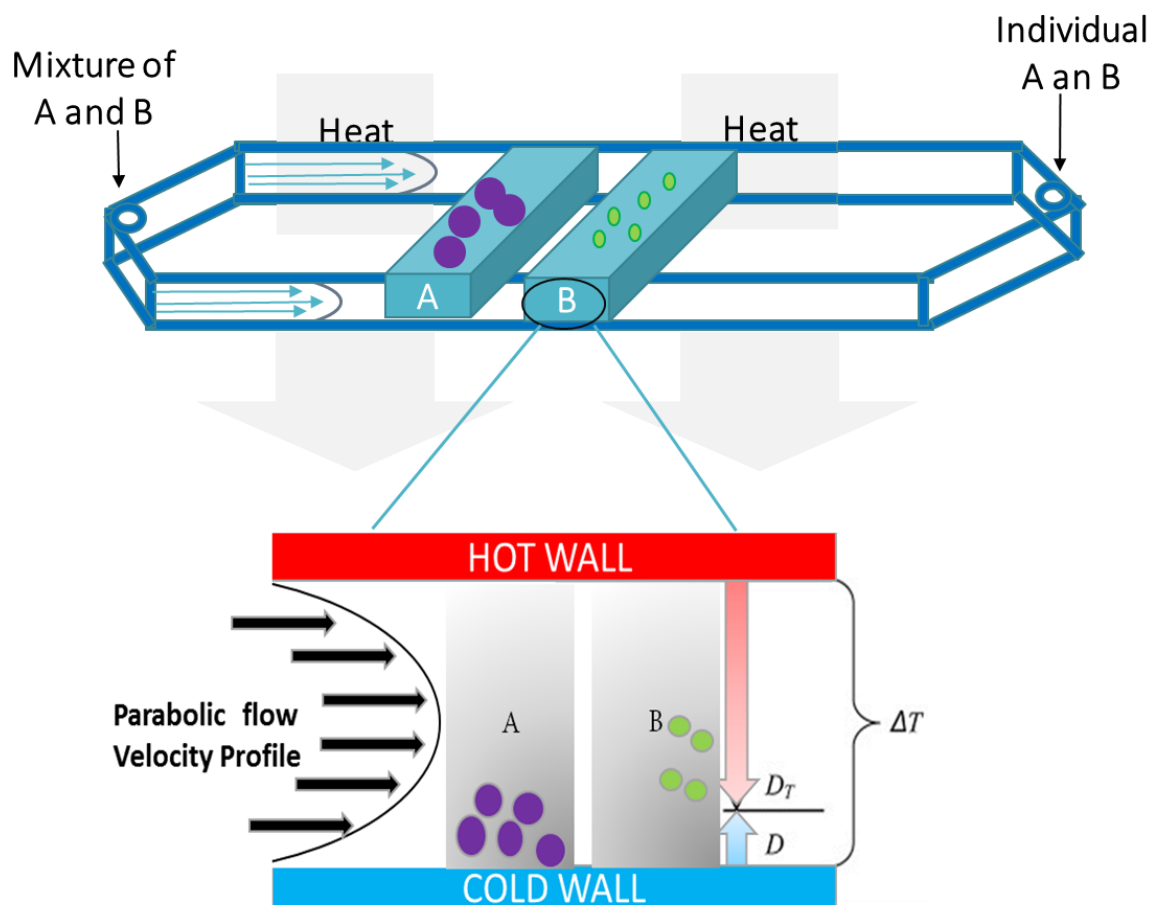
Figure 2.2: Representation of the thermal FFF separation mechanism.

Detectors

Concentration detectors such as the differential refractometer (RI) or the ultraviolet-visible (UV-Vis) detector and molar mass-sensitive detectors like the multiangle laser light scattering (MALLS) detector are the most common detectors used with FFF fractionations[10-12,15-17].

Hyphenated techniques, unlike detector coupling, specifically refer to the combination of chromatographic and spectroscopic methods to exploit the advantages of both. Coupling and hyphenation have, however, been used interchangeably. Hyphenated techniques include gas chromatography-mass spectrometry (GC-MS), LC-NMR, capillary electrophoresis–mass spectrometry (CE-MS) and LC-IR[18]. Examples of these techniques using field-flow fractionation are FFF-NMR and FFF-MALDI-TOFMS. Work on FFF-FTIR, to the best of our knowledge, has not yet been reported on.

11

FFF–NMR

The coupling of ThFFF online with ^{1}H NMR was done, for the first time, by van Aswegen et al.[19] in 2013. NMR is a powerful technique which, when used as a detector, can replace the need for a multiple detector setup. By successfully coupling ThFFF and NMR the authors were able to comprehensively analyse homopolymers and block copolymers of different molar masses and chemical compositions. Through the NMR chromatograms, they were able to obtain qualitative and quantitative information about the polymers with regard to microstructure[19]. Furthermore, comparative studies were done with SEC-NMR and the molar mass analysis of the homopolymer and copolymer samples (PS-b-PMMA, PI-b-PMMA and PS-b-PI block copolymers) were in good agreement, proving that coupling of ThFFF-NMR provided a robust and reproducible method for complex polymer analysis. In addition, they were able to comprehensively investigate the molecular heterogeneity of PB-b-PVP-b-PtBMA triblock copolymers by ThFFF-NMR[17]. One of the few disadvantages of FFF-NMR is that it is expensive and requires sophisticated setups.

FFF–MALDI–TOFMS

ThFFF and matrix-assisted laser desorption/ionization time-of-flight mass spectrometry (MALDI-TOFMS) were coupled by Kassalainen and Williams to yield a powerful combination of techniques for polymer analysis[20]. MALDI-TOFMS is able to analyse low-volatility polymers up to 10^3 kDa, depending on the instrumentation used, while ThFFF is able to separate polymers with molar mass well above 10^4 kDa[21,22]. Therefore, the focus was to optimize the experimental conditions that will allow for analysis over a wide range of molar masses. Thereafter, the ThFFF-MALDI-TOFMS technique was successfully applied to polydisperse polymers[20]. The main objective of this coupling was to simultaneously use ThFFF as a means to collect fractions for MALDI-TOFMS and as technique to validate the accuracy of MALDI-TOF molar mass distribution results[20]. Unfortunately, MALDI-TOF relies on desorption and ionization of molecules from a solid surface layer and therefore, it is intrinsically not compatible with ThFFF for online analysis. Furthermore, this method is expensive which makes it inaccessible to many laboratories.

12

2.4. Fundamentals of Fourier transform infrared spectroscopy (FTIR)

The interaction of light with molecules is the basis of FTIR spectroscopy. The energy absorbed by chemical bonds generates their FTIR spectrum. The energy absorbed is directly proportional to the wavenumber as follows:

$$E = hcW \hspace{4cm} 2.4$$

Where E and W represent energy (J) and wavenumber (cm^{-1}), respectively, and h is Planck's constant (6.63 x 10^{-34} Js) and C is the velocity of light (~3 x 10^{10} cm/s). All materials with temperatures above absolute zero emit infrared (IR) radiation. When materials are radiated with and absorb IR light, the absorbed energy causes vibrations of the atomic bonds. Different atomic groups absorb at different wavenumbers and this can be used to identify the structure of those groups. In the case of infrared spectroscopy, the quantized states are vibrational states, with the fundamental tones of bonds occurring in the MIR region[23,24].

Peak positions are a result of the frequency (Hz) of light that a molecule will absorb when excited by light as follows:

$$v = \frac{1}{2\pi} \left(\frac{k}{\mu}\right)^{1/2} \hspace{4cm} 2.5$$

Where, v is the frequency in cm^{-1}, k is the force constant in N/cm, μ is the reduced mass in kg. The reduced mass and the force constant determine the wavenumber at which a molecule will absorb infrared light. No two chemical substances have the same force constants and atomic masses, which is why the infrared spectrum of each chemical substance is unique.

An IR spectrum is a plot of the wavenumber against the measured IR absorbance[23]. The rate of change of the dipole moment in a molecule is proportional to the intensity of the IR absorption[25]. The absorbance of these bands is proportional to the concentration based on the Bouguer–Lambert–Beer law as follows:

$$A = \varepsilon lc \hspace{4cm} 2.6$$

Where A is the absorbance, ε is the absorptivity, l is the pathlength and c is the concentration.

Molecules with inherent dipole moments exhibit stronger responses than molecules with induced dipole moments. Hence, groups such as –NH and –OH with strong dipole moments typically give strong absorption bands[23].

13

2.4.1. FTIR instrumentation

At the core of every FTIR instrument is an optical device called an interferometer [23]. It is used to measure interference between two beams of light. The oldest and most common interferometer is the Michelson Interferometer. It consists of a beam splitter, a mirror that moves back and forth, a fixed mirror and an infrared source. The beam splitter is designed such that it transmits incident light and reflects some of the light incident upon it. Once, the radiation source strikes the beam splitter and separates into two beams. One light beam is transmitted through the beam splitter to the fixed mirror and the second is reflected off the beam splitter to the moving mirror[23,24]. Thereafter, the light beams recombine and again, half of the reflected radiation is transmitted and half is reflected at the beam splitter. This results in one beam passing to the detector and the second back to the source. Due to the effect of interference, the intensity of each beam, one passing to the detector and the other returning to the source, depends on the difference of path lengths in the two arms of the interferometer. This principle is illustrated in Figure 2.3.

The Michelson interferometer regulates the incoming optical radiation by changing the optical path difference (OPD) between the two possible paths in the interferometer in a continuous fashion. A change in path difference, termed retardation, is done by moving one of the two mirrors at a constant velocity over a fixed distance[26]. When the moving mirror has travelled the required distance, which is governed by the required spectral resolution, it is quickly returned to the start position to begin the next scan[23,24]. During the motion of the moving mirror, each wavelength of the collected radiation is modulated at a unique frequency that is a function of the wavelength of the radiation and the velocity of the moving mirror. Our experiments were carried out using a Bruker spectrometer where the best signal-to-noise ratio (S/N) was achieved at mirror velocity of 30 kHz and 60 kHz.

A plot of light intensity as function of OPD is called an interferogram. An interferogram is the fundamental measurement acquired by FTIR. After mathematical manipulation (i.e. Fourier Transformation), the interferogram yields a spectrum, hence the term Fourier transform infrared (FTIR) spectroscopy. An infrared spectrum contains two pieces of vital information namely, light intensity and wavenumber.
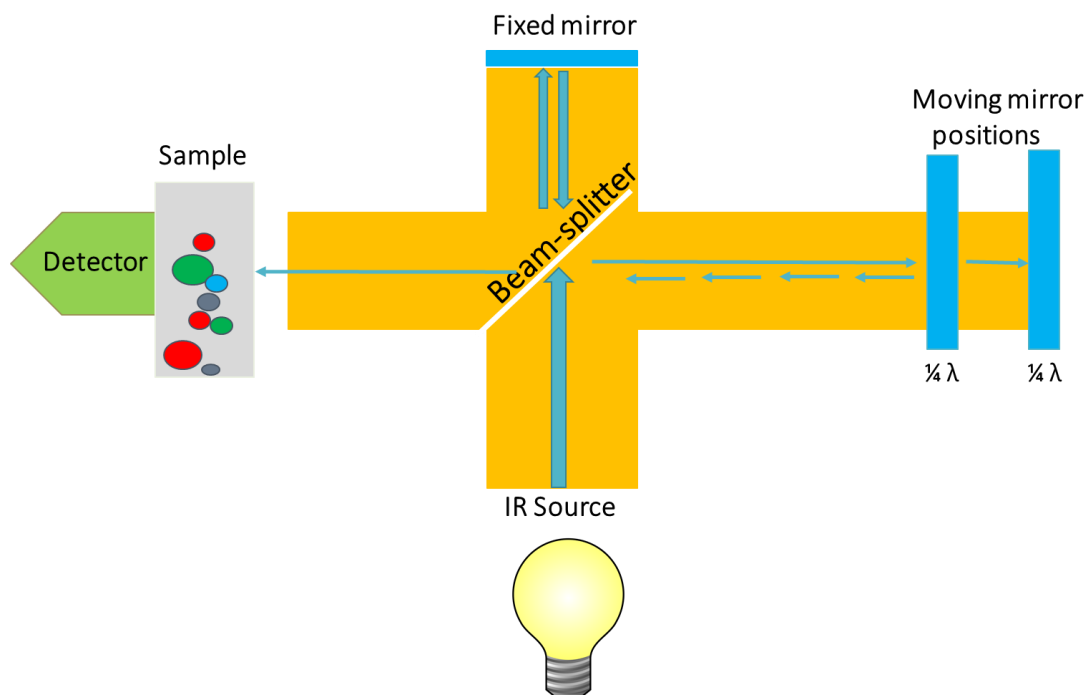
Figure 2.3: Representation of the FTIR – Michelson Interferometer.

The FT technique has several advantages for infrared spectroscopy including an improved S/ N ratio[27], because unlike in the conventional spectrometer where the noise of the detector affects the individual wavenumber, FT simultaneously applies all wavelengths allowing the noise to be distributed through the entire spectrum[24].

Another major advantage of FTIR spectroscopy is its rapid scanning capabilities. FTIR is able to continuously monitor molecular absorbances in short time intervals which requires small differences between the spectra. FTIR can be used to do kinetic studies of polymerization reactions. Using the rapid scanning capabilities of FTIR, one can monitor the chemical changes in a sample held in a heated cell [28]. Conversion curves as a function of time and temperature for each species involved in a cure process can be generated. A practical example of the rapid-scan FTIR technique is to study the cure kinetics of isocyanate coatings, where the absorbance peak of 2256 cm^{-1} was monitored as a function of time during the reaction[28].

2.4.2. FTIR trading rules

In FTIR, the relationship between scanning parameters, spectral quality and analysis time is important for efficiency. The signal-to-noise ratio (S/N) is a number used to assess performance of an IR spectrometer. The S/N ratio is directly proportional to the resolution. The resolution of a spectrum is the ability of the spectrometer to separate two characteristic bands in a spectrum. An IR spectrum appears as a continuous function but it is made up of a number of discrete data points. The line segments that connect the data points specify the "smoothness" of the spectrum, which is in essence the resolution. The resolution of an instrument dictates the number of data points. For example, a spectrum with 16 cm^{-1} resolution contains a data point every 16 cm^{-1}. A limiting factor for FTIR measurements with a high resolution is that more time is required for a larger number of data points. High-resolution spectra contain more information than low-resolution spectra but are inherently more noisy. Noise (N) limits detectability but it cannot be completely removed[24]. Each measurement is accompanied by noise and is defined by random fluctuations in the baseline.

Noise contributions can be minimized in several different ways. These all involve either enhancing the signal by smoothing or using a digital filter, or by modifying the instrumental method. Noise (N) by definition is the standard deviation (σ) of several measurements. A noise value is only meaningful in relation to the signal (S) intensity from which the S/N results. The S/N virtually reflects the uncertainty or the measurement error in the signal intensity. Therefore, a limit value of S/N $\geq$ 3 for the detection of a substance is generally established in spectroscopy and also in chromatography. This is called the limit of detection (LOD). Signals are usually quantified only from a limit value of S/N $\geq$ 10, which corresponds to an uncertainty of 10%. This is referred to as limit of quantification (LOQ)[29]. The S/N can be improved by adding up or averaging several measurements, also known as signal averaging[30].

2.5.   Coupling with FTIR

To date there have been two main approaches used in interfacing chromatography and FTIR. These are namely, the solvent elimination interface and a flow cell. The former approach involves the removal of the eluent prior to offline detection[31], it is the preferred approach for chromatography-IR operation because it sensitively acquires analyte spectra that are free of spectral interferences from the solvent[32]. In both approaches, solvent–analyte combinations

16

have to be such that their signals do not overlap. If so, it will be difficult to detect a frequency line with sufficient S/N ratio for detection.

2.5.1. Solvent elimination approach

The most successful solvent elimination technique for HPLC/FTIR is the LC-Transform interface, developed by Lab Connections[24]. Figure 2.4 shows the design concept of the interface. There are two main devices/modules, namely the collection and the optics components. In this technique, the solvent from the separation technique (i.e SEC/LC, FFF) is evaporated by using either a thermospray or a flow nebulizer. The solvent is removed at a high temperature and almost simultaneously, the separated analytes are deposited on a rotating sample collection disc. The sample collection disc is made from germanium and it is optically transparent in the range 6,000–450 cm^{-1}. After the analyte components have been deposited, IR spectra from the immobilized chromatogram are acquired. When a chromatogram has been collected on the sample collector disc, it is transferred to the optics module in the FTIR instrument for analysis. A control module defines the sample collection disc position and rotation rate in order to be compatible with the run time and peak resolution of the chromatographic separation. The lower surface of the disc is covered with a reflecting aluminium layer[1,33]. One fundamental drawback of this technique is the inability to identify components of a mixture in real time[24]. This is because the process takes place in two steps namely deposition and spectral measurement.

The solvent elimination approach has several advantages over the flow cell approach. Firstly, as previously mentioned, the absence of interfering solvent absorption bands allows spectral interpretation over the entire wavenumber range, therefore, allowing full exploitation of the identification possibilities of IR spectroscopy. Secondly, solvent elimination measurements are compatible with gradient elution LC by varying the nebulizer temperature[31]. Thirdly, the immobilized chromatogram/fractogram is still available after the separation has been completed which means that with an increase in the scanning time the S/N ratio can be greatly enhanced. Lastly, analyte deposits can be concentrated thus increasing sensitivity[32,34].
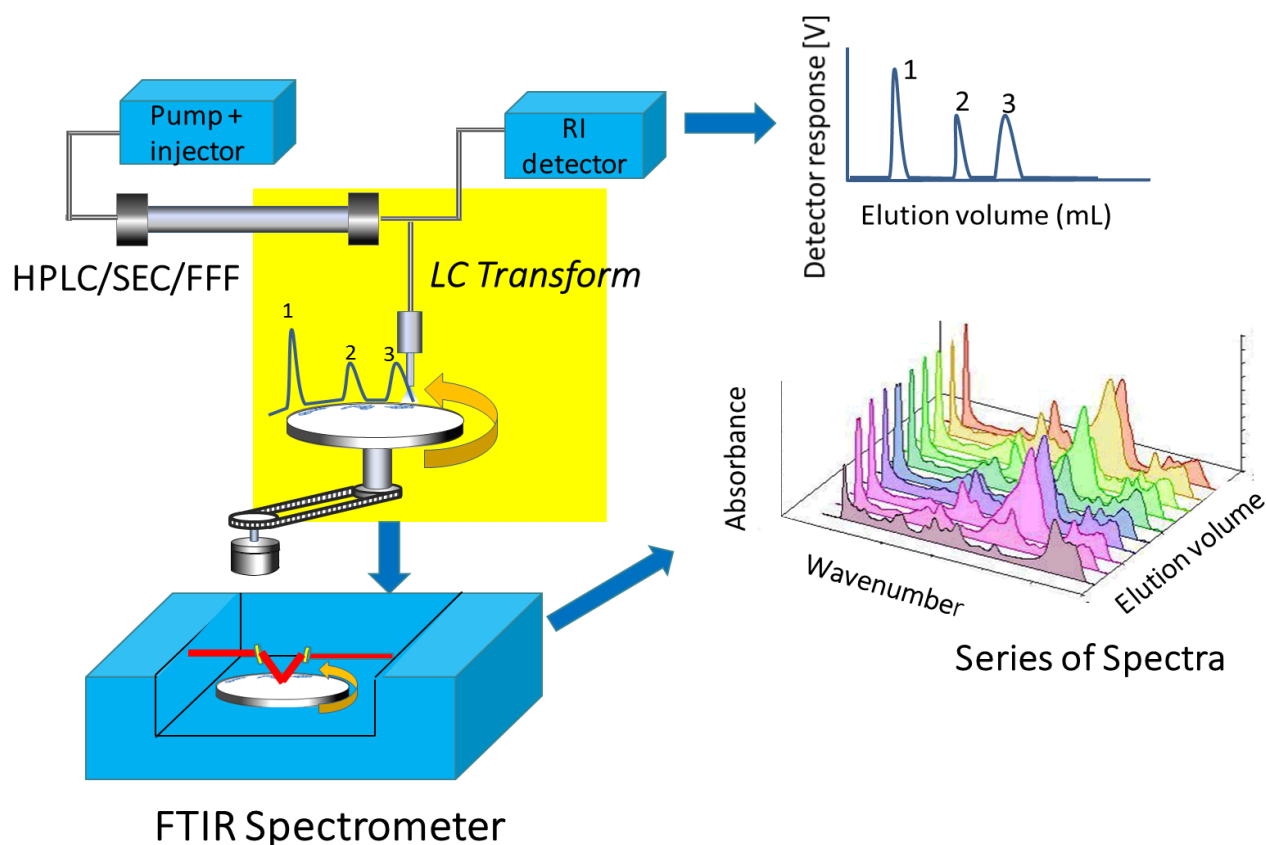
Figure 2.4: Schematic representation of SEC/LC/FFF-FTIR coupling using the LC-Transform interface

Applications

There have been several uses for SEC-FTIR and LC-FTIR using the solvent elimination method. These include the characterization of styrene-butadiene rubbers (SBR) which are used

18

in automotive tyre manufacturing, using a SEC column and an interface based a pneumatic nebulizer design[35]. Quantitative SEC-FTIR analysis of the composition of polystyrene (PS) and poly(methyl methacrylate) (PMMA) was done using a linear regression calibration and external calibration[36]. Here, a custom-built solvent evaporation interface was used. The solvent elimination approach has become more popular than the use of flow cells for HPLC or SEC coupled to FTIR. A polycarbonate/aliphatic polyester (PC/APE) blend and a polycarbonate-co-polydimethylsiloxane (PC-co-PDMS) copolymer in dichloromethane (DCM) were analyzed using SEC-FTIR by both the flow cell (potassium bromide windows) and the solvent elimination methods. Sensitivity was found to be higher for the solvent elimination interface. For both the blend and the copolymer samples, the homopolymer and comonomer ratios were found to be comparable for both methods[31]. 2D-LC coupled online with FTIR was used to study styrene-co-methylacrylate copolymers with varying styrene contents in dichloromethane. The IR absorption band ratios for SMA copolymers using the functional group contour plots were used to determine the styrene content as a function of molar mass[34].

2.5.2. Online flow cell approach

The online approach is where the effluent of the chromatograph passes through a flow cell and the IR spectra are acquired in real-time. Online coupling via a flow cell is based on one of three methods namely, transmission, attenuated total reflection (ATR) and specular-reflection measurements[31]. There are several drawbacks of the flow cell method, one of which is the limit in the number of mobile phases that show a sufficiently large spectral window[37]. There are, however, some transparent regions of the mid-IR range that produce a possibility of detection e.g. the use of deuterated solvents/mobile phases such as deuterium oxide or perdeuterated methanol. IR is able to monitor many organic compounds that have C–H structures in the molecules[38]. Important problems include obtaining a sufficient S/N ratio and using flow-through cells with minimum path lengths[18,29].

Furthermore, attempts to subtract the mobile phase absorption from the IR bands have resulted in inaccurate conclusions when there are no absorptions of the analyte in the corresponding spectral regions. This renders it nearly impossible to apply this solvent subtraction approach to gradient elution because the eluent composition changes over time[39].

There have been efforts to use FTIR detection with liquid flow-through cells and high performance columns, however, they have not been successful. This is due to the fact that

significantly less sample is need for efficient separation[18]. There has however been considerable progress made with flow cells and SEC[29,40].

Transmission flow cells

Transmission flow cells can consist of either an IR transparent cavity or two IR transparent windows, which are separated by a metal or Teflon spacer. Capillary tubing is used to allow eluent to enter and exit the cell[23]. As the eluent passes, it is sampled by an IR beam passing perpendicularly. It is possible to adjust the internal volume vs. path length of the cell, depending on the application. A high temperature option for these flow cells is available. In addition, flow cells with a so-called "zero-dead volume" (ZDV) have been developed for use in microbore LC [41,42]. An example of this type of flow cell is presented in Figure 2.5. Here, the eluent passes a sample cavity that has a 0.75 mm hole drilled in a block of either calcium fluoride (CaF_2) or potassium bromide (KBr). The IR beam crosses perpendicularly through the eluent stream[42].
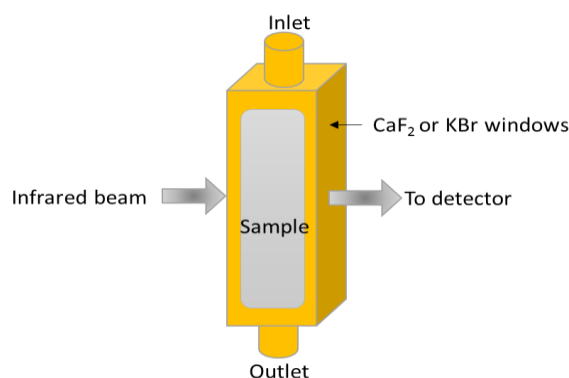
Figure 2.5: Principle of transmission flow cell

ATR flow cells

An attenuated total reflectance (ATR) accessory operates by measuring the changes that occur in a totally internally reflected infrared beam when the beam comes into contact with a sample. An infrared beam is directed onto an optically dense crystal with a high refractive index at a certain angle. This internal reflectance creates an evanescent wave that extends beyond the surface of the crystal into the sample held in contact with the crystal[43]. This evanescent wave

20

protrudes only a few microns (0.5-5 µm) beyond the crystal surface and into the sample. This is referred to as depth of penetration (DP). The total path length of an ATR experiment is equal to the DP of the beam into the sample for each point of reflection multiplied by the number of reflections that cover the surface of the crystal. Single reflection ATR is not always adequate because of the low sensitivity observed (see Figure 2.6). Improvement in sensitivity can be obtained by the use of multiple internal reflection systems which increases the path length[29]. For our work, we used an ATR flow cell with six reflections as shown in Figure 2.7.

Furthermore, in ATR experiments, the spectrum obtained is independent of the sample thickness[44]. Subsequently, there must be good contact between the sample and the crystal surface. In regions of the infrared spectrum where the sample absorbs energy, the evanescent wave will be attenuated or altered. The refractive index of the crystal must be considerably greater than that of the sample or else internal reflectance will not occur – the light will be transmitted rather than internally reflected in the crystal[23,44].
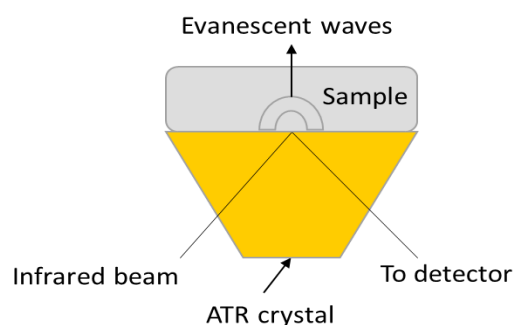
Figure 2.6: ATR flow cell with one reflection
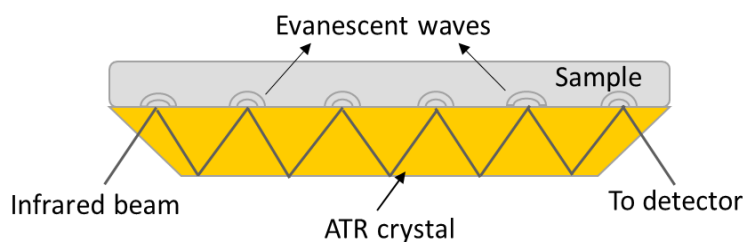
Figure 2.7: ATR flow cell with six reflections

Specular–reflection flow cells

Specular-reflection is also known as infrared reflection absorption spectroscopy (IRRAS). The flow cells consist of a trough-shaped stainless steel cell body, covered with an IR transparent window (i.e. ZnSe, Ge, CaF). The IR beam, under near-normal incident angles, is directed using an external mirror and this reduces the reflection losses at the air-window interface[42]. One of the IR beams passes the cell window, it is reflected inside the cell cavity, by a mirror surface. The beam passes the effluent flow path twice and is directed towards the detector via a second external mirror. This is illustrated in Figure 2.8. The optical path length is twice the thickness of the sample cavity[42].
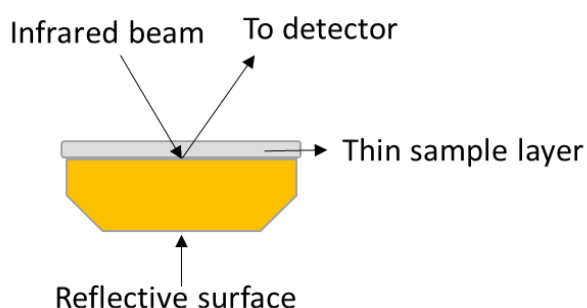
Figure 2.8: Principle of specular–reflection flow cell

Flow cell window materials

Each of the above mentioned flow cell techniques utilizes a flow cell window material, which is most often a crystal. Zinc selenide (ZnSe) and germanium (Ge) are the most commonly used but diamond is the best crystal material due to its robustness and durability. However, it is the least used as it is the most expensive. Although, ZnSe and Ge are prone to scratching if improperly used[44], they have several advantages. ZnSe is a relatively low cost ATR crystal material and is ideal for analyzing liquids and non-pastes and gels but it is not particularly robust with a working pH range of 5–9. Ge, on the other hand, has a much better working pH range and, therefore, can be used to analyse weak acids and alkalis[44]. Ge has the highest refractive index of all the cell window materials available, which means that the effective depth of penetration is approximately 1 μm[23]. This is an advantage when analyzing highly absorbing materials[42].

22

Cheaper crystal alternatives include sodium chloride (NaCl) and KBr which are completely transparent in the mid IR region. They have refractive indices of 1.49 and 1.39, respectively, which is low compared to 4.0 and 2.4 for Ge and ZnSe, respectively[24,42]. This is an advantage only for minimizing the risk of spectral fringes, however, these materials are not suitable for ATR flow cells, as they cannot maintain total reflection at the crystal boundaries[42].

Applications

As previously mentioned, the major limitation of all flow–through cells is the limited selection of solvents/mobile phases that exhibit sufficiently large spectral windows for measurements with high sensitivity. SEC-FTIR has, however, been used several times to analyze polyolefins. Using SEC-FTIR is of particular interest when it comes to compositional analysis of polyolefins. The methyl group ($-CH_3$) has at least two associated absorption bands. Using either one of these bands as well as the methylene group ($-CH_2-$) bands, their ratios can be calibrated against polymer standards. This "ratio method" can be applied to short-chain branching[45]. DesLauriers and co-workers showed that the compositional heterogeneity (short chain branching) in polyolefins can be analyzed sensitively by on-flow SEC-FTIR. Here, the SEC and FTIR were connected through a heated transfer line and a flow cell made from KBr windows[46]. Furthermore, compositional heterogeneity in Ziegler–Natta produced ethylene-1-olefin copolymers were characterized according to their comonomer content as function of molar mass in 1,2,4-trichlorobenzene (TCB)[47]. TCB is relatively transparent in the range of 2700–3000 cm^{-1} and it is often used for polyolefin analysis[48].

SEC-FTIR was further used to investigate the preferential solvation effects of water on alternating copolymers of maleic anhydride and styrene and styrene-maleimide copolymers in THF. A flow cell with ZnSe windows and elliptical Teflon spacers was used and spectra were collected online in 2 s intervals. One spectrum was a result of eight co-added scans. The SEC-FTIR experiments confirmed the preferential solvation of these polymers by water as compared to THF[49].

2.5.3. Coupling of SEC-FTIR through a modified ATR flow cell

In 2012, Beskers and Wilhelm presented a new SEC-FTIR coupling set-up were FTIR was shown to serve as a true online detector[40]. The idea was to measure FTIR spectra in an online fashion. Thereafter, a mathematical approach was used to subtract the solvent signals in order

23

to minimize the noise and reduce spectral drifts[29,40]. Initially, for pre-test purposes a transmission flow cell and another ATR-style cell were built. Later, they built three flow cells of different inner cell volumes all based on a ZnSe crystal with a trapezoidal shape, which allowed for six reflections of the IR beam. The inner cell volumes were made using perfluorinated elastomers called FFKM or Kalrez®[29]. The flow cell used had to meet several requirements including sufficient sensitivity. This means that the ATR should have an appropriate amount of reflections (or for transmission: a certain path length). It also has to be suitable for through–use applications. They investigated the influence of cell volume to band broadening and came to a conclusion that the flow cell with the lowest volume (170 µL) exhibited the least amount of band broadening. They attributed this to less mixing as compared to the larger cells. More importantly through sharper peaks, the signal height was increased by ca. 20%, which lead to a better S/N ratio. Lastly, they had to ensure that the flow cell is stable against as many solvents as possible. For this reason, they opted to use ZnSe. The development of a sensitive online detector that was based on FTIR spectroscopy was successful in providing chemical composition information as a function of elution volume for several polymers in an isocratic solvent.

Solvent suppression

Although the individual spectra differed from those found in literature due to residual characteristic peaks from the solvent, the spectra were still characteristic of the analyzed polymer. Beskers et al. developed a solvent suppression software that is able to eliminate the solvent signals as completely as possible. The aim was to assign characteristic absorption peaks to different components. The solvent suppression works in three steps, which are (1) solvent subtraction, (2) drift correction and (3) noise reduction. This improves the time $\frac{S/N}{\sqrt{t}}$ by a factor of 1.4. A MATLAB (matrix laboratory) coding program was used to develop the solvent suppression which is known as the TIMO software.

(1) Solvent subtraction

Spectral subtraction is a straightforward processing technique that is used to remove unwanted contributions to a spectrum such as solvents, water vapor, CO_2 and other impurities[23]. First, a background spectrum which is in essence the solvent spectrum is measured. Thereafter, it is subtracted from the data set.

24

(2) Drift correction

The drift correction in the MATLAB program removes all the parts that are constant in the spectra, which ensures the same result for background spectrum. Drifts occur on a much larger timescale than that of the chromatographic experiment; therefore, drift is fitted to a blank solvent before and after the chromatogram. A second order polynomial was used for each wavenumber. The software calculates a parabola for each wavenumber and then subtracts it from the data set. For this, it is still required to keep the conditions as constant as possible.

(3) Noise reduction

For the noise reduction, a signal-free area is required in the spectrum (i.e. no IR peaks) whose width and position can be selected. For most polymers, the region at 1800 to 2000 cm^{-1} is suitable. The average value from this region is then subtracted from the complete spectrum. The noise is then reduced in the time axis because each spectrum's baseline is "artificially" set to zero. Therefore, changes or fluctuations between the different spectra are levelled out as the spectra are measured one after the other. This levels out noise in the time axis and it does not reduce noise within the spectrum. The software warns against non–sensible inputs, (i.e. a chromatogram boundary outside the data set). Since the parameters only change when the separation set-up changes and not for different samples, the parameters can be stored and saved. This means that a user only needs to click "Calculate" for a routine measurement, which causes the calculation and saving of the file. The TIMO software processes files exported to OPUS after the measurement.

Applications

With this method, a number of coupled SEC separations could be chemically detected using the FTIR spectrometer. Coupled measurements, using different polymers in different solvents were carried out. The method has also been applied successfully to scientific and industrial questions, mainly in analytics for novel syntheses or synthetic pathways. For example, multiblock copolymers of poly(styrene)-b-poly(tetrahydrofuran) synthesized via RAFT end group switching were characterized using the online SEC-FTIR with TIMO detection. Here, the average block fractions as well as the chemical composition distribution of each block was determined   successfully[50]. Furthermore, SEC-FTIR was used to determine the chemical composition of poly(styrene)–poly(L-lactide) block copolymers in cloroform[51].

25

The limits of the method concerning selectivity and sensitivity were evaluated. Examples for low sensitivity are polymers with only small dipole moments, such as conformational and constitutional isomers of polybutadienes (PB). Three isomers were evaluated, cis-1,4-PB, trans-1,4-PB and 1,2-PB. These are chemically quite similar and, therefore, have very similar infrared spectra. A challenge of practical relevance was the detection of cis-1,4-PB on the basis of a specific peak. This isomer is distinguished from the others by its absorption at 735 cm^{-1}. After the investigation it was concluded that quantification of the cis-PB moiety is not possible without a strong overloading of the column and should preferably take place in the solid state, without molar mass dependence[29]. Additionally, samples with similar spectra to the solvent were regarded as potentially challenging for the method. Therefore, PS in toluene as well as poly(ethylene glycol), and poly(tetrafuran) in THF were measured. All three samples could be detected successfully[29].

2.6. References

1. Pasch, H., Malik, M. I. & Macko, T. Recent Advances in High – Temperature Fractionation of Polyolefins. *Adv. Polym. Sci*. **251**, 77–140 (2013).

2. Craver, C. D. & Provder, T. *Polymer Characterization: Physical property, Spectroscopic, and Chromatographic Methods*. (American Chemical Society, Washington DC, 1990).

3. Runyon, J. R. & Williams, S. K. R. A theory – based approach to thermal field -flow fractionation of polyacrylates. *J. Chromatogr. A* **1218**, 7016–7022 (2011).

4. Schimpf, M. E. & Giddings, J. C. Characterization of thermal diffusion in polymer solutions by thermal field – flow fractionation: effects of molar mass and branching. *Macromolecules* **20**, 1561–1563 (1987).

5. Ratanathanawongs Williams, S. K. & Lee, D. Field – flow fractionation of proteins polysaccharides, synthetic polymers, and supramolecular assemblies. *J. Sep. Sci*. **29**, 1720–1732 (2006).

6. Dolan, J. W., Hinshaw, J. V. & Majors, R. E. Field Flow Fractionation for analyzing biological, natural, and synthetic polymers. *Chromatogr. Online* **16**, 8 – 16 (2013). Available Online: www.chromatographyonline.com

7. Schimpf, M., Caldwell, K. & Giddings, J. C. *Field flow Fractionation Handbook*. (John Wiely & Sons, New York, 2000; Vol. 4.).

8. Pasch, H. Advanced fractionation methods for the microstructure analysis of complex polymers. *Polym. Adv. Technol*. **26**, 771–784 (2015).

9. Messaud, F. A., Sanderson, R. D., Runyon, J.R., Otte, T., Pasch, H. & Ratanathanawongs Williams, S.K. An overview on field – flow fractionation techniques and their applications in the separation and characterization of polymers. *Prog. Polym. Sci*. **34**, 351–368 (2009).

10. Malik, M. I. & Pasch, H. Field – flow fractionation : New and exciting perspectives in polymer analysis. *Prog. Polym. Sci*. **63**, 42–85 (2016).

11. Muza, U. L., Greyling, G. & Pasch, H. Characterization of Complex Polymer Self – Assemblies and Large Aggregates by Multidetector Thermal Field – Flow Fractionation. Anal. Chem. **89**, 7216−7224 (2017).

12. Greyling, G. & Pasch, H. Multidetector thermal field – flow fractionation as a unique tool for the tacticity – based separation of poly(methyl methacrylate) – polystyrene block copolymer micelles. *J. Chromatogr*. A **1414**, 163–72 (2015).

13. Kowalkowski, T., Buszewski, B., Cantado, C. & Dondi, F. Field-Flow Fractionation: Theory, Techniques, Applications and the Challenges. *Anal. Chem.* **8347,** 129–135 (2016).

14. Schimpf, M. E. Polymer analysis by thermal field – flow fractionation. *J. Liq. Chromatogr. Relat. Technol*. **25**, 2101–2134 (2002).

15. Greyling, G. & Pasch, H. Multidetector Thermal Field – Flow Fractionation: A Unique Tool for Monitoring the Structure and Dynamics of Block Copolymer Micelles. *Macromolecules* **49**, 1882–1889 (2016).

16. Greyling, G. & Pasch, H. Multidetector Thermal Field – Flow Fractionation as a Novel Tool for the Microstructure Separation of Polyisoprene and Polybutadiene. *Macromol. Rapid Commun*. **35**, 1846–1851 (2014).

17. van Aswegen, W., Hiller, W., Hehn, M. & Pasch, H. Comprehensive Triblock Copolymer Analysis by Coupled ThFFF-NMR. *Macromol. Rapid Commun*. **34**, 1098–1103 (2013).

18. Pasch, H., Colfen, H., Antonietti, M., Engelhardt, H. & Groshe, O. *Advances in Polymer Science* (Springer: Verlag Berlin Heidelberg, 1999)

19. Hiller, W., van Aswegen, W., Hehn, M. & Pasch, H. Online ThFFF − NMR: A Novel Tool for Molar Mass and Chemical Composition Analysis of Complex Macromolecules. *Macromolecules* **46**, 2544–2552 (2013).

20. Kassalainen, G. E. & Williams, S. K. R. Coupling Thermal Field – Flow Fractionation with Matrix – Assisted Laser Desorption / Ionization Time – of – Flight Mass Spectrometry for the Analysis of Synthetic Polymers. *Anal. Chem.* **75**, 1887–1894 (2003).

21. Byrd, H. C. M. & McEwen, C. N. The Limitations of MALDI – TOF Mass Spectrometry in the Analysis of Wide Polydisperse Polymers. *Anal. Chem.* **72**, 4568–4576 (2000).

22. El – Aneed, A., Cohen, A. & Banoub, J. Mass Spectrometry, Review of the Basics : Electrospray, MALDI, and Commonly Used Mass Analyzers. *Appl. Spectrosc. Rev.* **44**, 210 – 230, (2017).

23. Smith, B. C. *Fundamentals of Fourier Transform Infrared Spectroscopy*. (CRC Press : Florida, United States, 2011).

24. Griffiths, P. R. & de Haseth, J. A. *Fourier Transform Infrared Spectroscopy*. (John Wiley & Sons, New Jersey, 2007).

25. Escobar – Barrios, V. a, Rangel – Méndez, J. R., Pérez – Aguilar, N. V, Andrade – Espinosa, G. & Dávila – Rodríguez, J. L. *Infrared Spectroscopy – Materials Science, Engineering and Technology* (ed. Theophile, T.) 195–212 (InTech, 2012).

26. Bhargava, R., Wang, S. & Koenig, J. L. FTIR Microspectroscopy of Polymeric Systems. *Adv. Polym. Sci.* **163**, 137–191 (2003).

27. Fellgett, P. B. On the Ultimate Sensitivity and Practical Performance of Radiation Detectors. *J. Opt. Soc. Am.* **39**, 970–946 (1949).

28. Koenig, J. *Spectroscopy of Polymers*. (Elsevier Science Inc: New York, 1992).

29. Beskers, T. F., Hofe, T. & Wilhelm, M. Development of a chemically sensitive online SEC detector based on FTIR spectroscopy. *Polym. Chem*. **6**, 128–142 (2015).

30. Skoog, D. A., Holler, J. F. & Crouch, S. R. *Principles of Instrumental Analysis.* (Cengage Learning: Boston, 2007).

31. Kok, S. J., Wold, C. A., Hankemeier, T. & Schoenmakers, P. J. Comparison of on – line flow – cell and off – line solvent – elimination interfaces for size – exclusion chromatography and Fourier – transform infrared spectroscopy in polymer analysis. *J. Chromatogr. A* **1017**, 83–96 (2003).

32. Kok, S. J. Fourier transform infrared spectroscopy with a sample deposition interface as a quantitative detector in size – exclusion chromatography. *J. Chromatogr. A* **948**, 257–265 (2002).

33. Pasch, H. Recent Developments in Polyolefin Characterization. *Macromol. Symp.* **165,** 91–98 (2001).

34. Kok, S. J., Hankemeier, T. & Schoenmakers, P. J. Comprehensive two – dimensional liquid chromatography with on – line Fourier – transform – infrared – spectroscopy detection for the characterization of copolymers. *J. Chromatogr.* **1098**, 104–110 (2005).

35. Dwyer, J. L. & Zhou, M. Polymer Characterization by Combined Chromatography – Infrared Spectroscopy. *Int. J. Spectrosc*. **2011**, 1 – 13 (2011).

36. Karami, A., Balke, S. T. & Schunk, T. C. Quantitative interpretation of Fourier – transform infrared spectroscopic data from a size – exclusion chromatography solvent–evaporation interface. *J. Chromatogr. A* 911, 27–37 (2001).

37. Pasch, H. & Malik, M. I. *Advanced Separation Techniques for Polyolefins*. (Springer: New York, 2014).

38. Patel, K., Patel, J., Patel, M. P., Rajput, G. C. & Patel, H. A. Introduction to hyphenated techniques and their applications in pharmacy. *Pharm. Methods* **1**, 2–13 (2010).

39. Somsen, G. W., Gooijer, C., Velthorst, N. H. & Brinkman, U. A. T. Coupling of column liquid chromatography and Fourier transform infrared spectrometry. *J. Chromatogr. A* **811**, 1–34 (1998).

40. Beskers, T. F., Hofe, T. & Wilhelm, M. Online Coupling of Size – Exclusion
     Chromatography and IR Spectroscopy to Correlate Molar mass with Chemical
     Composition. *Macromol. Rapid Commun*. **33**, 1747−1752 (2012).

41. Somsen, G. W. & Gooijer, C. Liquid chromatography – Fourier – transform infrared
     spectrometry. *J. Chromatogr. A* **856**, 213–242 (1999).

42. Kok, S. *Coupling of liquid chromatography and Fourier – transform infrared
     spectroscopy*. (Doctoral Thesis: University of Amsterdam, 2004).

43. Herminghaus, S., Klopfleisch, M. & Schmidt, H. J. Attenuated Total Reflectance as a
     Quantum Interference Phenomenon. *Opt. Lett*. **19**, 293 (1994).

44. Hind, A. R. & Bhargava, S. K. At the solid/liquid interface : FTIR/ATR − the tool of
     choice. *Adv. Colloid Interface Sci.* **93**, 91–114 (2001).

45. Piel, C., Albrecht, A., Neubauer, C., Klampfl, C. W. & Reussner, J. Improved SEC-
     FTIR method for the characterization of multimodal high – density polyethylenes.
     Anal. Bioanal. Chem. **400**, 2607–2613 (2011).

46. Tso, C. C. & Deslauriers, P. J. Comparison of methods for characterizing comonomer
     composition in ethylene 1 – olefin copolymers : 3D – TREF vs. SEC – FTIR. *Polymer*.
     45, 2657–2663 (2004).

47. Deslauriers, P. J., Rohl, D. C. & Hsieh, E. T. Quantifying short chain branching
     microstructures in ethylene - 1 - olefin copolymers using size exclusion
     chromatography and Fourier transform infrared spectroscopy (SEC – FTIR). *Polymer*
     43, 159–170 (2002).

48. Pasch, H. Multidimensional HPLC of Polymers. (Springer: Verlag Berlin Heidelberg,
     2013).

49. Voigt, D., Eichhorn, K., Arndt, K. & Prettin, S. Online Size Exclusion
     Chromatography – Fourier Transform Infrared Spectroscopy (FTIR): Investigation of
     Preferential Solvation Effects. *Int. J. Polym. Anal. Charact.* **5341**, 333–349 (2006).

50. Schmid, C., Falkenhagen, J., Beskers, T.,Nguyen, L., Wilhelm, M., Du Prez, F. &
     Barner – Kowollik, C. Multi – Block Polyurethanes via RAFT End – Group Switching
     and Their Characterization by Advanced Hyphenated Techniques. *Macromolecules*
     45, 6353−6362 (2012).

51.   Malek, A., Dingenouts, N., Beskers, T F., Fehrenbacher, U., Barner, L. & Wilhelm, M. Linear and nonlinear rheological behavior and crystallization of semicrystalline poly (styrene) – poly (L – lactide) block copolymers. *Eur. Polym. J.* **49**, 2704–2720 (**2013**).

Chapter 3 : Experimental procedures

3.1   Chemicals and materials

Polystyrene and poly(methyl methacrylate) homopolymer standards were purchased from Postnova Analytics and Polymer Laboratories (United Kingdom). Polymer Standards Service GmbH (Germany) supplied poly(styrene-co-methyl methacrylate) copolymer samples. The polyacrylonitrile and the poly(styrene-co-acrylonitrile) copolymers were purchased from Sigma-Aldrich (Missouri, United States) and Polymer Source Inc. (Dorval, Canada). Tetrahydrofuran (THF) (99.9%) and dimethylformamide (DMF) (99.9%) were purchased from Sigma-Aldrich.

3.2   Instrumentation set set-up

The ThFFF system (TF2000 Postnova Analytics, Landsberg, Germany) was coupled online to UV (PN 3212 at 254 nm, Postnova Analytics), MALLS (PN 3070, Postnova Analytics), DRI (PN 3150, Postnova Analytics), FTIR Tensor II Spectrometer (Bruker, Ettlingen, Germany) and DLS detectors (Zen 1600, Malvern Instruments, Worcestershire, United Kingdom). The set-up is shown in Figure 3.1. The TF2000 channel has the following dimensions: tip-to-tip length of 45.6 cm, a breadth of 2 cm, a thickness of 127 μm, and a void volume of 1.14 mL.
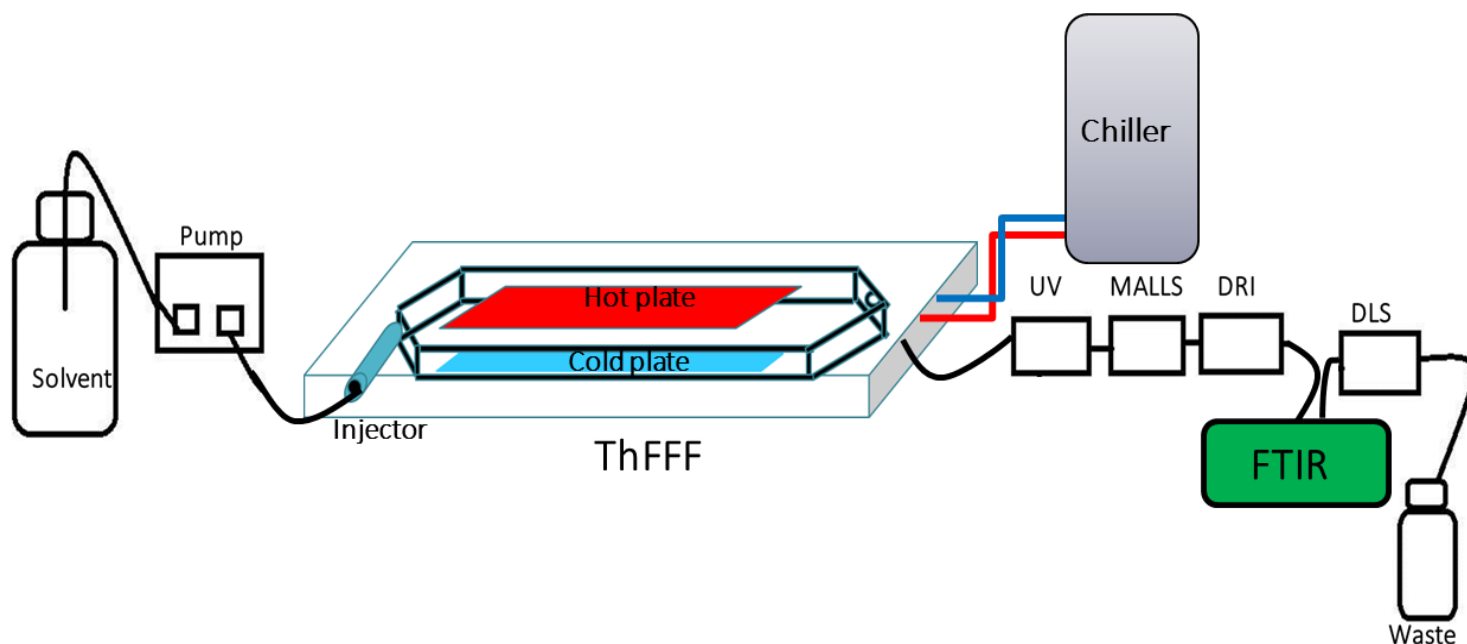
Figure 3.1: Schematic illustration of the ThFFF instrumentation setup.

3.3   ThFFF analysis conditions

All fractionations were conducted under a constant ΔT of 60 K. The temperature of the cold wall was maintained between 20 – 25 °C by an external chiller (Unichiller, Monitoring and Control Laboratories, South Africa). The samples were introduced into the channel via a Rheodyne manual injection valve with the aid of a carrier flow generated by an isocratic pump (PN 1130, Postnova Analytics). THF and DMF were used as carrier liquids at a flow rate of 0.3 mLmin^{-1} and 0.2 mLmin^{-1}, respectively. The samples were injected through a 100 µL capillary sample loop, and fractionations of each sample were performed in triplicate. Overloading concentrations, as was indicated by plateaued and/or irregular detector signals, were investigated as part of the method development and are reported in Chapter 4. Thereafter, variable sample concentrations that had little or no effect on the retention time were used.

3.4   Detectors

The method of coupling an array of detectors like UV, DRI, MALLS and DLS to ThFFF has been used successfully for the analysis of complex polymers[3–7]. The multi-detector approach allows for one integrated measurement to determine hydrodynamic size using DLS, molar mass by MALLS as well as the respective distributions. The chemical composition was monitored using a combination of the UV detector as the selective detector (i.e. chromophore containing materials) and the DRI detector as the universal detector. Furthermore, values for S_T were calculated as shown in Chapter 2, equation 2.3, while values for D_T were calculated from equation 2.1. D_h values were determined by DLS analysis.

3.5   FTIR analysis conditions

The FTIR spectrometer was equipped with a zinc selenite (ZnSe) flow cell. Spectra were recorded at a resolution of 4 cm^{-1} with 64 scans being recorded for the spectrum as well as for background spectrum sampling. The scanner velocity was set to 30 kHz for the SAN copolymers and 60 kHz for all other measurements. The S/N ratio was improved through several experiments and is reported at the beginning of Chapter 4.

3.5.1 FTIR detector

A quantum detector made from a mercury-cadmium-telluride semiconductor material (MCT) was used as the FTIR detector. It had mirror speeds of up to 160 kHz. The spectral range is limited to 600 cm^{-1} - 4000 cm^{-1}. In addition; the detector element must be cooled to -196 °C with liquid nitrogen. The consumption is approx. 0.5 L fresh nitrogen for a maximum of 8 h measurement time. Bruker Optik Opus (version 7.5), Origin (version 8) and time resolved infrared spectroscopy for molecular online SEC detection (TIMO) software were used for data collection and processing. The typical measuring time for one spectrum was 8 to 19 seconds. For one spectrum, 32 to 64 scans were added with each scan consisting of 4 interferograms.

3.5.2 ATR flow cell built in-house

A flow cell constructed in-house with a volume that was reduced to 170 µL through the reconstruction of individual components was utilised. The flow cell resembles the one reported by Beskers et al[1]. The technical drawing for the cell used is shown in Figure. 3.2.
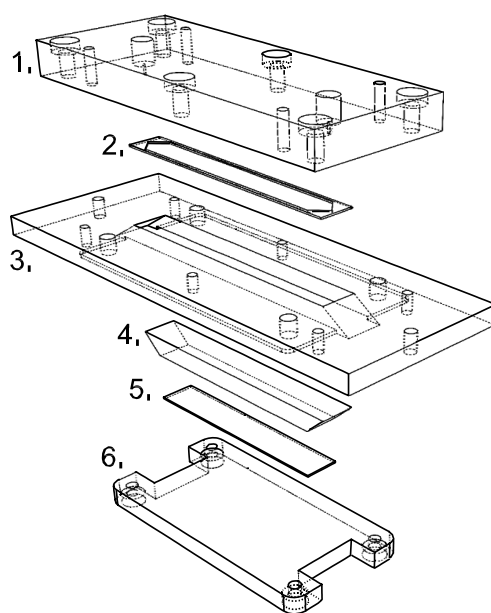
Figure 3.2: The components from the top down can be seen as follows: 1. Cover, made of stainless steel with adaptors for high-pressure connectors; 2. Rubber sealing with a volume of 170 µL; 3. Aluminium backing board; 4. ATR crystal of ZnSe with six reflections; 5. Rubber seal; 6. Aluminum backing.

34

3.5.3 FTIR data processing

Using the TIMO software, the constant solvent signals were suppressed using a second order polynomial that is fitted for every wavenumber in order to reference data taken before and after the fractogram. This polynomial was subtracted from the time evolution at this wavenumber. Thereafter, smoothing and baseline correction was done and a fractogram was obtained[1,2]. Figure 3.3 shows which parameters can be changed. All parameters can be stored so that only the measurement file is loaded for routine measurements and the button "Calculate" is pressed.
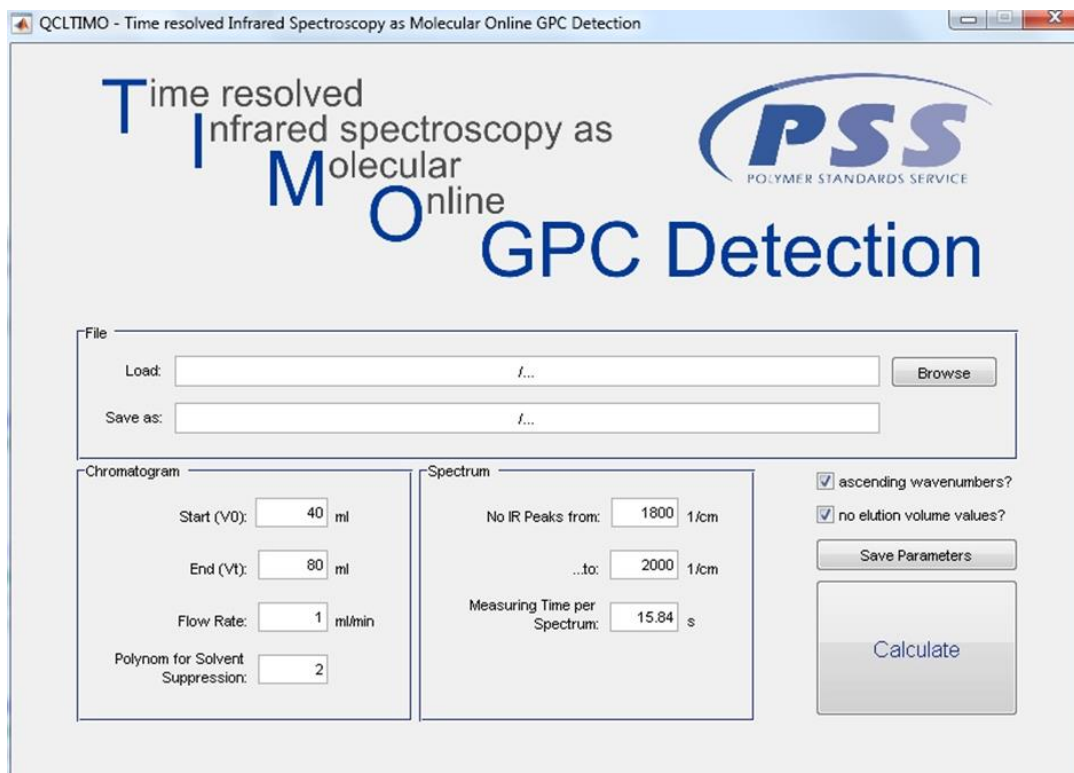
Figure 3.3: Screenshot of the TIMO software

3.6 Refractive index increment (dn/dc)

The samples were dissolved in THF and left overnight to dissolve. The offline determination of dn/dc was performed by three dilutions of each sample of 2 mgmL^{-1} being injected directly into the ThFFF-DRI setup using a glass syringe. The flow rate was 0.3 mLmin^{-1}. Data acquisition and processing were done using the Postnova Analytics TF2000 control software (version 1.0.0.8).

3.7 References

1.   Beskers, T. F., Hofe, T. & Wilhelm, M. Development of a chemically sensitive online

SEC detector based on FTIR spectroscopy. *Polym. Chem.* **6,** 128–142 (2015).

2. Beskers, T. F., Hofe, T. & Wilhelm, M. Online Coupling of Size-Exclusion Chromatography and IR Spectroscopy to Correlate Molecular Weight with Chemical Composition. *Macromol. Rapid Commun.* **33,** 1747−1752 (2012).

3. Greyling, G. & Pasch, H. Multidetector Thermal Field-Flow Fractionation as a Novel Tool for the Microstructure Separation of Polyisoprene and Polybutadiene. *Macromol. Rapid Commun.* **35,** 1846–1851 (2014).

4. Muza, U. L., Greyling, G. & Pasch, H. Characterization of Complex Polymer Self-Assemblies and Large Aggregates by Multidetector Thermal Field-Flow Fractionation. *Anal. Chem.* **89,** 7216−7224 (2017).

5. Greyling, G. & Pasch, H. Multidetector Thermal Field-Flow Fractionation: A Unique Tool for Monitoring the Structure and Dynamics of Block Copolymer Micelles. *Macromolecules* **49,** 1882–1889 (2016).

6. Greyling, G. & Pasch, H. Multidetector thermal field-flow fractionation as a unique tool for the tacticity-based separation of poly(methyl methacrylate)-polystyrene block copolymer micelles. *J. Chromatogr. A* **1414,** 163–72 (2015).

7. Greyling, G. & Pasch, H. Multidetector Thermal Field-Flow Fractionation for the Characterization of Vinyl Polymers in Binary Solvent Systems. *Macromolecules* **50,** 569–579 (2017).

8. Ahmad, I. H. S*tudying Chemical and Sequence Length Heterogeneities in Copolymers*. (Doctoral Thesis: Florida State University, 2011).

Chapter 4 : Results and Discussion

4.1   Introduction

This section outlines the stepwise optimization of the online coupling of ThFFF and FTIR spectroscopy. The coupling was achieved using a flow cell approach. For polymer blends and copolymers, infrared absorbances in solution were measured, and the chemical composition distributions as well as the bulk copolymer compositions were deduced. These results were compared to results obtained by ThFFF coupled to UV and DRI detectors. A penta-detector set-up including additional MALLS and DLS detectors allowed for further comprehensive analysis of molar mass, size and their respective distributions. Furthermore, the thermal and normal diffusion coefficients were calculated from data provided by the DLS and MALLS detectors.

Section 4.1 below outlines the novel approach to determine the optimum experimental conditions and spectrometer specifications for the multidetector ThFFF-FTIR hyphenation.

4.1.1   Optimization of FTIR spectrometer parameters

Using the spectrometer software, the relationship between number of scans, mirror velocity and signal-to-noise ratio (S/N) was studied. Thereafter, the effect of concentration was studied in order to see its influence on detector sensitivity and to determine the minimum amount of material that gives a usable spectrum[1]. Usability is measured by the S/N ratio. A S/N ratio of $\geq$ 3 is regarded as the limit of detection and the limit of quantification is $\geq$ 10. Table 4.1 shows the time dependent S/N ratio. Doubling the number of scans increases the S/N ratio by a factor of approximately $\sqrt{2}$. For this reason it is recommended to calculate the time independent S/N ratio ($\frac{S/N}{\sqrt{t}}$). Doubling the mirror velocity divides the measurement time by two also doubles the S/N ratio for 16 scans, and doubles the S/N ratio for 32 and 64 scans when going from 15 kHz to 30 kHz, respectively. There is also a significant increase in S/N when going from 30 kHz to 60 kHz.

The intensity of an absorption in an IR spectrum relates to the change in dipole moment that occurs during molecular vibrations. Subsequently, vibrations that produce a large change in dipole moment (e.g. C=O stretch) result in a more intense absorption than those that result in a relatively modest change in dipole moment (e.g. C=C). This holds true in transmission IR and does appear to apply to FTIR-ATR. ATR intensities, which are related to depth of penetration,

37

are dependent on the wavenumber. The depth of penetration (DP) of an ATR experiment is given by Equation 4.1:

$$DP = {}^{1}\!/_{[2\pi W n_c (sin^2\theta - n_{sc}^2)^{1/2}]} \qquad 4.1$$

Where W is the wavenumber, n_c and n_{sc} is the refractive index of the ATR crystal and the ratio of the refractive index of the sample and crystal, respectively. A higher depth of penetration means a longer path "through" the sample and therefore a higher signal[1]. According to Equation 4.1 DP is inversely proportional to wavenumber. Therefore, we expect that lower wavenumbers show higher intensity. In general, the S/N ratio for PMMA at 1735 cm^{-1} is higher than for PS at 700 cm^{-1}, shown in Table 4.1. The peak intensity for PMMA is not higher, it appears so because the noise in the central part of the spectrum is lower. This is due to the intensity profile of a single channel spectrum. A higher intensity there will lead to less noise. With less noise, the S/N ratio is better.

Table 4.1: Total injected mass of 0.7 mg consisted of 0.4 mg PS (33 kg/mol) and 0.3 mg PMMA (88 kg/mol). The resolution was kept constant at 8 cm^{-1}.

| Number of scans	Scanner velocity (kHz)	Time per spectrum (sec)	S/N 700 cm^{-1} (PS)	S/N 1735 cm^{-1} (PMMA)
16	15	8	5.63	14.4
16	30	4	8.59	17.3
16	60	2	15.5	30.2
32	15	15	5.72	15.5
32	30	8	14.7	20.0
32	60	4	23.5	35.4
64	15	30	6.83	18.2
64	30	15	15.3	23.5
64	60	8	34.9	49.1

4.1.2 Overloading

The concentration of the injected sample has an observable effect on the quality of the separation. ThFFF has a 'critical concentration' above which interference between the analyte particles occur. The interference occurs either by steric effects, where the particles have insufficient space to reach equilibrium, or aggregation of particles[2]. Polymers, in particular, may experience chain entanglement and, thereby, affect the diffusion rates and increase the viscosity near the cold wall, which subsequently has an effect on the retention times[2].

Injecting a concentration series can reveal the overloading limit for ThFFF-DRI. To determine overloading, PS (33 kg/mol) and PMMA (132 kg/mol) standards were used. Different concentrations were injected under the same ThFFF conditions. Figure 4.1a illustrates a constant peak maximum with higher concentrations, but the signal is cut-off at 0.6 mg injected mass. For the PMMA sample (Figure 4.1 B), the effects of overloading are noticeable above a critical concentration. These effects are seen in the form of peak shoulders as well as a shift to higher elution times. This is due to poor sample solubility and high eluate viscosities at high concentrations[2]. Additional peaks at higher retention volumes are also seen, due to excessive overloading in the PMMA sample at 0.38 and 0.5 mg injected mass.

The sample amount that can be injected without overloading the channel decreases as the molar mass increases. This is clearly illustrated in Figure 4.1a and b. In routine experimental practice, it is necessary to balance the injected amount with the response from the light scattering and concentration detectors. The light scattering detector may show weak responses for polymers with high molar masses that require analysis under low sample load. Unknown samples should, therefore, be analysed at different injected amounts. The absence of overloading is proven by the consistency of distribution curves obtained from different sample loads[3].
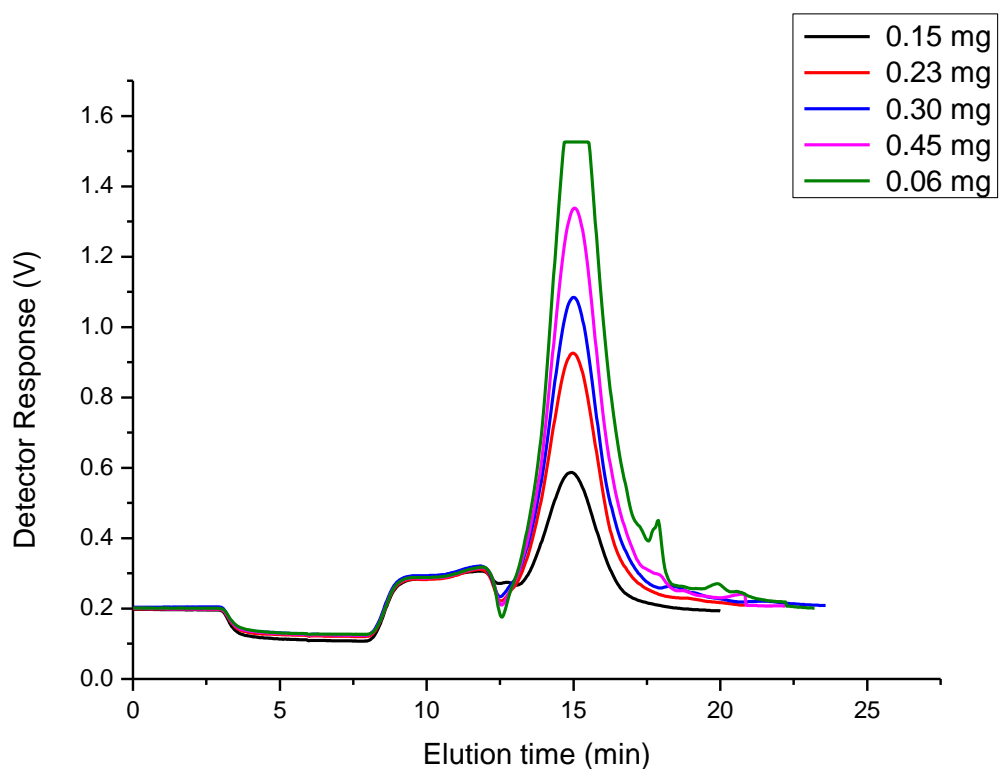
Figure 4.1. A: Elugrams of PS 33 kg/mol at 0.15, 0.23, 0.3, 0.45 and 0.6 mg mass injection, in THF with DRI as the detector
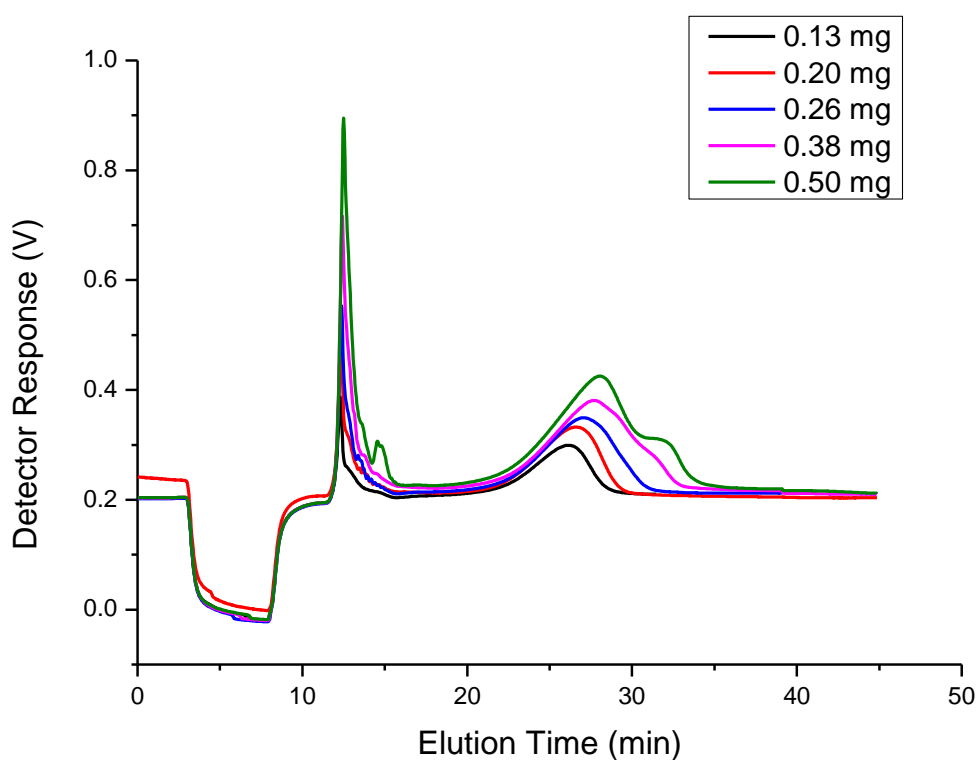
Figure 4.1 B: Elugrams of PMMA 132 kg/mol at 0.13, 0.2, 0.25, 0.38 and 0.5 mg injection mass in THF with DRI as the detector

40

In general, a concentration of 2 mgmL^{-1} of sample at a volume of 100 µL can be injected into the ThFFF channel to obtain good separation results. The concentration necessary for proper detection in FTIR must be high which confirms that FTIR has low sensitivity. Consequently, one needs to inject higher concentrations for FTIR detection which might be above the limit for ThFFF. Therefore, to determine this limit a coupled measurement was done for each sample via a concentration series in order to obtain the best possible S/N ratio with optimum separation. These results are shown in Figure 4.2 and indicate that the measurement method used has a LOQ for PS at 0.3 mg and a LOQ for PMMA at 0.1 mg injected mass. An injected mass less than that leads to difficulties in interpreting the spectra and should be avoided.
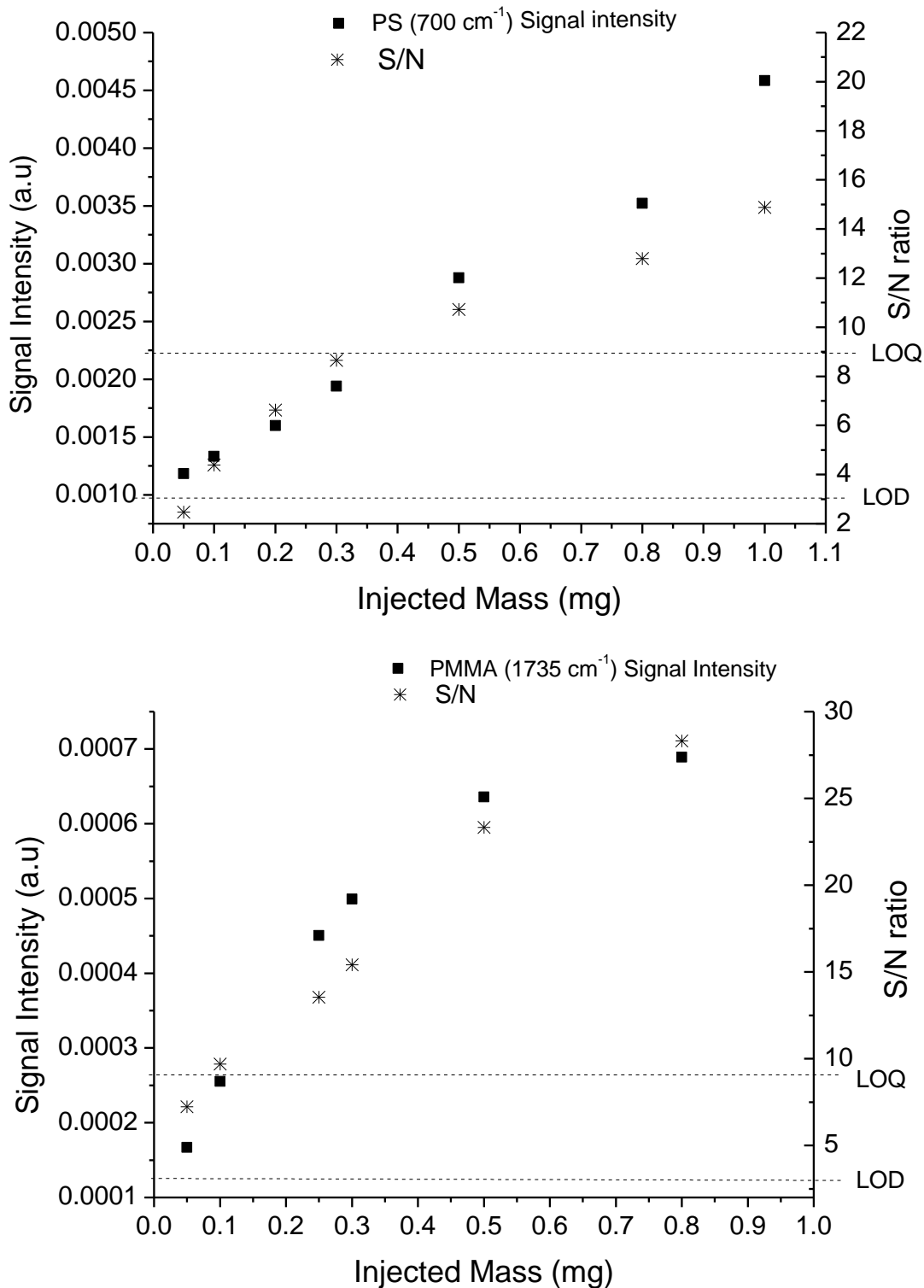
Figure 4.2: The S/N values and signal intensities for polystyrene (PS) at 700 cm^{-1} (M_n 72 kg/mol) and for poly(methyl methacrylate) (PMMA) at 1735 cm-1 (M_n 132 kg/mol) were plotted against injected mass. Quantification is possible without overloading the channel

42

4.2   Blends of polystyrene and poly(methyl methacrylate)

In this section, binary blends of PS and PMMA of different molar masses were prepared and separated using ThFFF. In order to comprehensively quantify the chemical composition of binary blends it was necessary to employ dual concentration detection using the UV and DRI detectors[4]. For the binary blends, UV and DRI were used to calculate the overall bulk chemical composition. The combination of UV and DRI detectors is commonly used for chemical composition determination when a binary blend or copolymer has one comonomer/homopolymer, A or B, absorbing UV (the chromophore) while the other comonomer/homopolymer does not absorb UV at the same wavelength. Quantification is achieved through the calibration of the two detectors in order to determine the response factors of the two different components (monomers or homopolymers).

PS and PMMA were selected as the UV active and non-UV active components, respectively. Known concentrations of each homopolymer in the blend were prepared. The fractionation results were quantified as weight fractions using the UV and DRI detectors and were correlated to the amounts that were injected. Furthermore, for the purpose of FTIR detection, blend samples were selected on the basis of having at least one pair of mutually exclusive absorption bands, namely the carbonyl stretch of PMMA and the phenyl stretch of PS. Using the same method of calibration as for the UV and the DRI detectors, ThFFF-FTIR was used to determine the bulk compositions and chemical composition distributions of the homopolymers as a function of elution time.

Thereafter, the FTIR results were compared to those obtained from the UV and DRI detectors. Five binary blend samples were prepared, two of which were separated and resolved into two peaks and three which did not resolve well. All blend samples were characterized by their chemical composition using the combination of UV/DRI and using FTIR.

4.2.1.   Analysis of average chemical compositions of PS-PMMA blends by ThFFF-UV-RI

Polymer blends were prepared with known amounts in THF using PS and PMMA standards as seen in Table 4.2.

In a first set of experiments, the response factors of both polymers in both detectors were determined. Calibrations of the UV and DRI detectors weres done. We defined F_{PS} and F_{PMMA}

as the response factors of the DRI detector for components A and B. $F_{PS}{'}$ is then the UV detector response factor for component A.

Table 4.2: Concentrations and compositions of the components in blend experiments

Sample name	PS (kg/mol)	PMMA (kg/mol)	PS injected mass (mg)	PMMA injected mass (mg)	PS_{Theo} (wt. %)	$PMMA_{Theo}$ (wt. %)
SM 1	33	138	0.50	0.30	62.5	37.5
SM 2	72	138	0.52	0.18	74.3	25.7
SM 3	72	88	0.52	0.37	58.4	41.6
SM 4	132	88	0.54	0.28	65.9	34.1
SM 5	196	88	0.56	0.28	66.7	33.3

The response factors were determined by injecting known concentrations of PS and PMMA homopolymers into the ThFFF dual detector set-up, calculating the areas of the corresponding fractograms and the dividing the areas by the known concentrations of the homopolymers injected as follows[5]:

$$R_{PS} = F_{PS}G_{PS} \qquad 4.2$$

$$R_{PMMA} = F_{PMMA}G_{PMMA} \qquad 4.3$$

$$R_{PS}{'} = F_{PS}{'}G_{PS} \qquad 4.4$$

Where R_{PS}, R_{PMMA} and $R_{PS}{'}$ are the areas of homopolymers in the DRI detector and of homopolymer PS in the UV detector, respectively. G_{PS} and G_{PMMA} are the concentrations of the homopolymers injected into the dual detector system. The weight fraction W_{PS} of PS, is given by:

$$\frac{1}{W_{PS}} = 1 - \{[(R_{PS}/R_{PMMA})F_{PMMA} - F_{PS}]/[(R_{PS}/R_{PMMA}) - F_{PS}{'}]\} \qquad 4.5$$

and the weight fraction $W_{PMMA} = 1 - W_{PS}$. It is important to note that the retention times for the UV and DRI detector were not equal owing to the fact that detectors are connected in series causing a time delay between the detectors that had to be corrected for[5,6]. Below are the calibration curves obtained using known homopolymer samples of PS and PMMA.
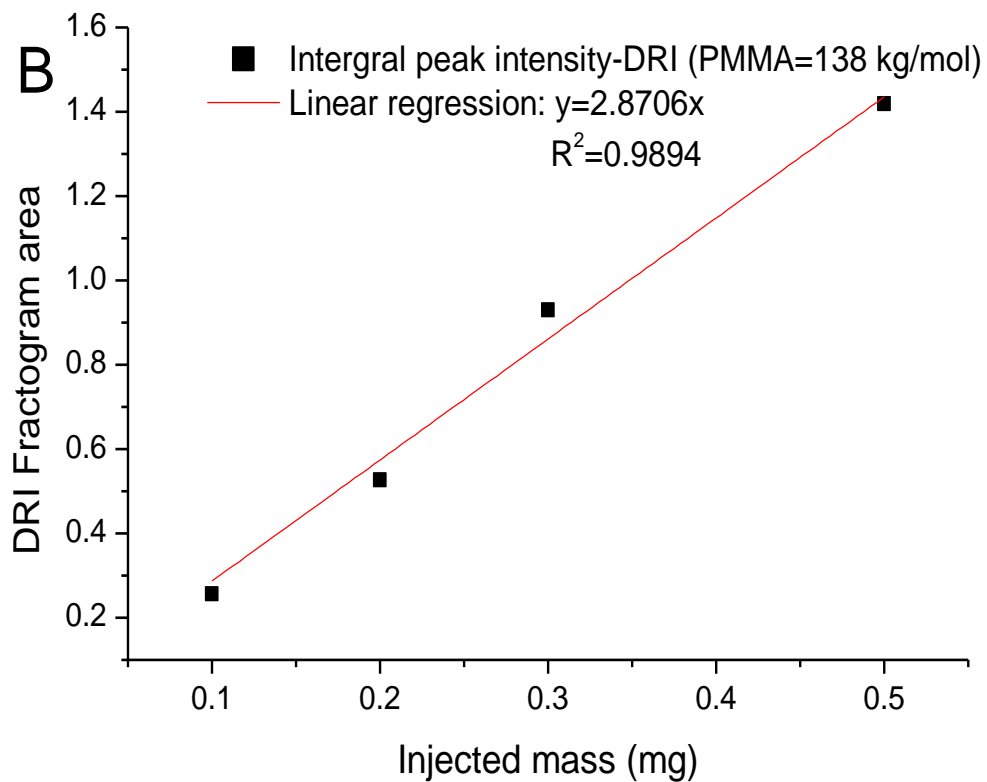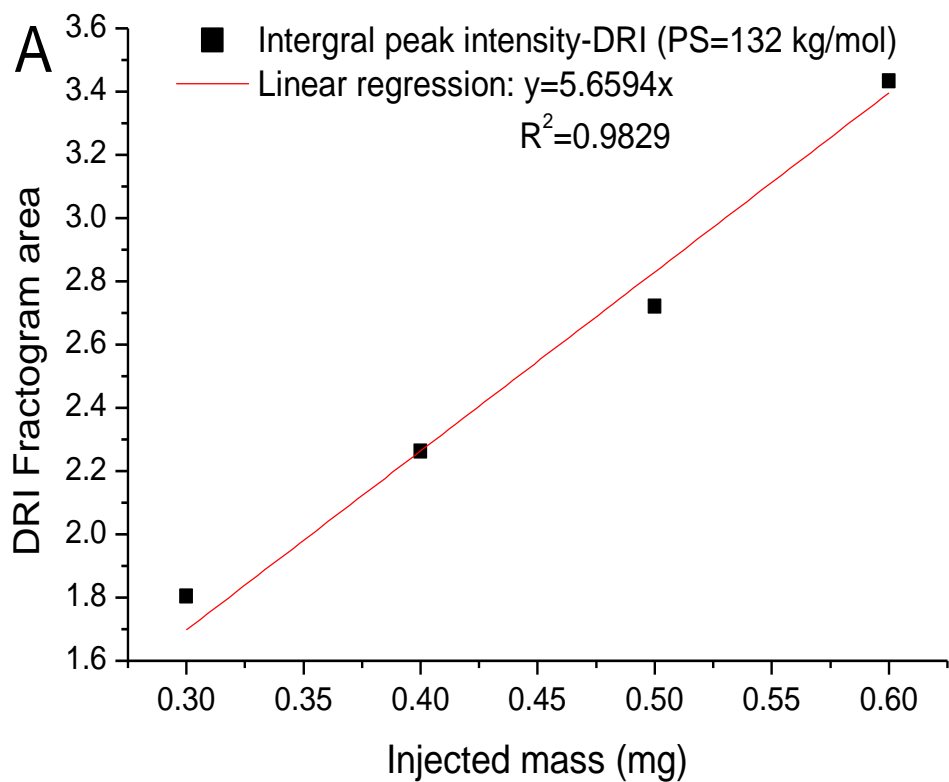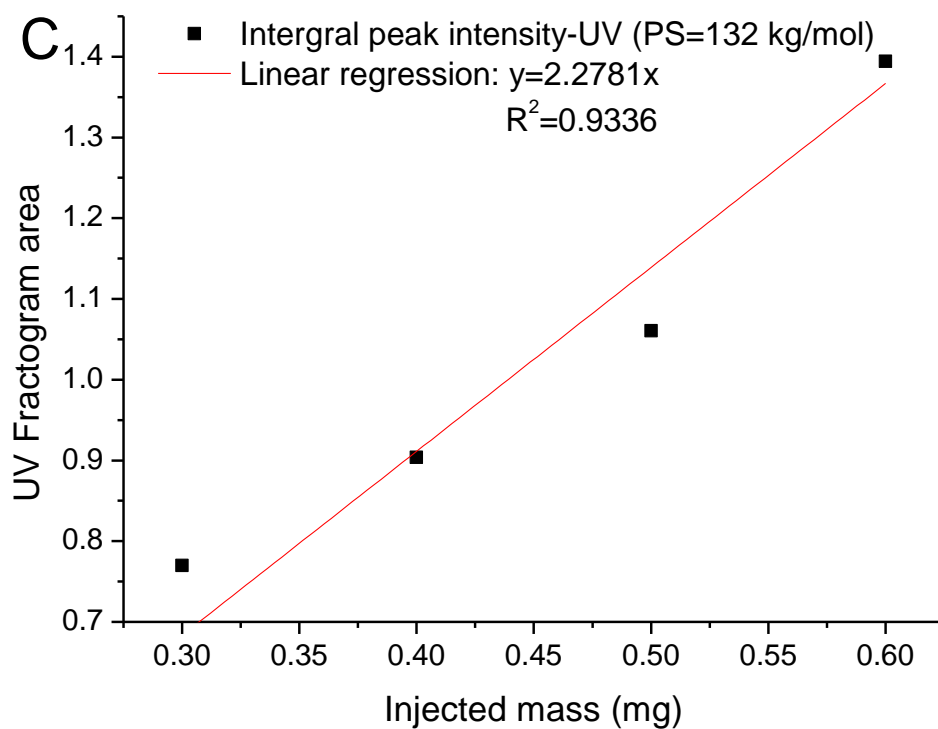
Figure 4.3: (A) DRI calibration using PS 132 kg/mol; (B) DRI calibration using PMMA 138 kg/mol; (C) UV calibration using PS 132 kg/mol

The DRI response factors for PS and PMMA were determined from the slopes of the calibration curves. F_{PS} was 5.659 and F_{PMMA} was 2.871. The UV response factor for PS was 2.278 (F'_{PS}). The response factors and the areas from the UV and DRI fractograms (Figure 4.3) were applied to Equation 4.4 and the bulk compositions were calculated. The results are shown in Table 4.3.

**Table 4.3:** Bulk composition determination by UV/DRI (wt. %) and theoretical wt.% of PS and PMMA in blends

Sample name	PS$_{Exp}$ (wt. %)	PMMA$_{Exp}$ (wt. %)	PS$_{Theo}$ (wt. %)	PMMA$_{Theo}$ (wt. %)
SM 1	59.9	40.1	62.5	37.5
SM 2	70.7	29.3	74.3	25.7
SM 3	51.8	48.2	58.4	41.6
SM 4	62.1	37.9	65.9	34.1
SM 5	63.7	36.3	66.7	33.3

The experimental composition results in Table 4.3 compare well with theoretical compositions. The slight underestimation for PS in SM 1 is attributed to some of the material eluting in the void peak and, therefore, not being accounted for in the DRI peak area (Figure 4.3A). The sensitivity of concentration detectors is known to be dependent on the type of homopolymer, which in the case of a UV detector is due to the different extinction coefficients and for a DRI detector is due to the refractive index increments. Therefore, the measured UV and DRI traces of blend or copolymer samples are not a direct measure of the concentration of eluting chains and need to be corrected according to comonomer/homopolymer-specific detector responses.

UV detection was done at two wavelengths (245 nm and 260 nm). PS can absorb UV light readily and shows strong signals, whereas PMMA absorbs almost no UV light in THF and, therefore, its UV signal intensity is zero. In addition, the molar absorptivity of PS is higher in the region of shorter wavelengths and this is seen with a more pronounced UV detection at 245 nm compared to 260 nm.

In the next step, polymer blend fractionations with blend components having different or similar molar masses were conducted. Blend sample SM 1 consisted of PS (33 kg/mol) and PMMA (138 kg/mol) homopolymers. PMMA was significantly higher in molar mass and the separation was attributed mainly to the different sizes (normal diffusion coefficients) of the polymers in solution. Similarly, SM 2 showed separation according to size in solution. The two blends showed baseline separation as presented in the DRI fractograms in Figure 4.4A. The first eluting components of SM 1 and SM 2 are UV active, as seen in Figure 4.4B, confirming that PS is

only present in the first peak and the second peak of each blend can be attributed to PMMA which is not seen in the UV detector traces.
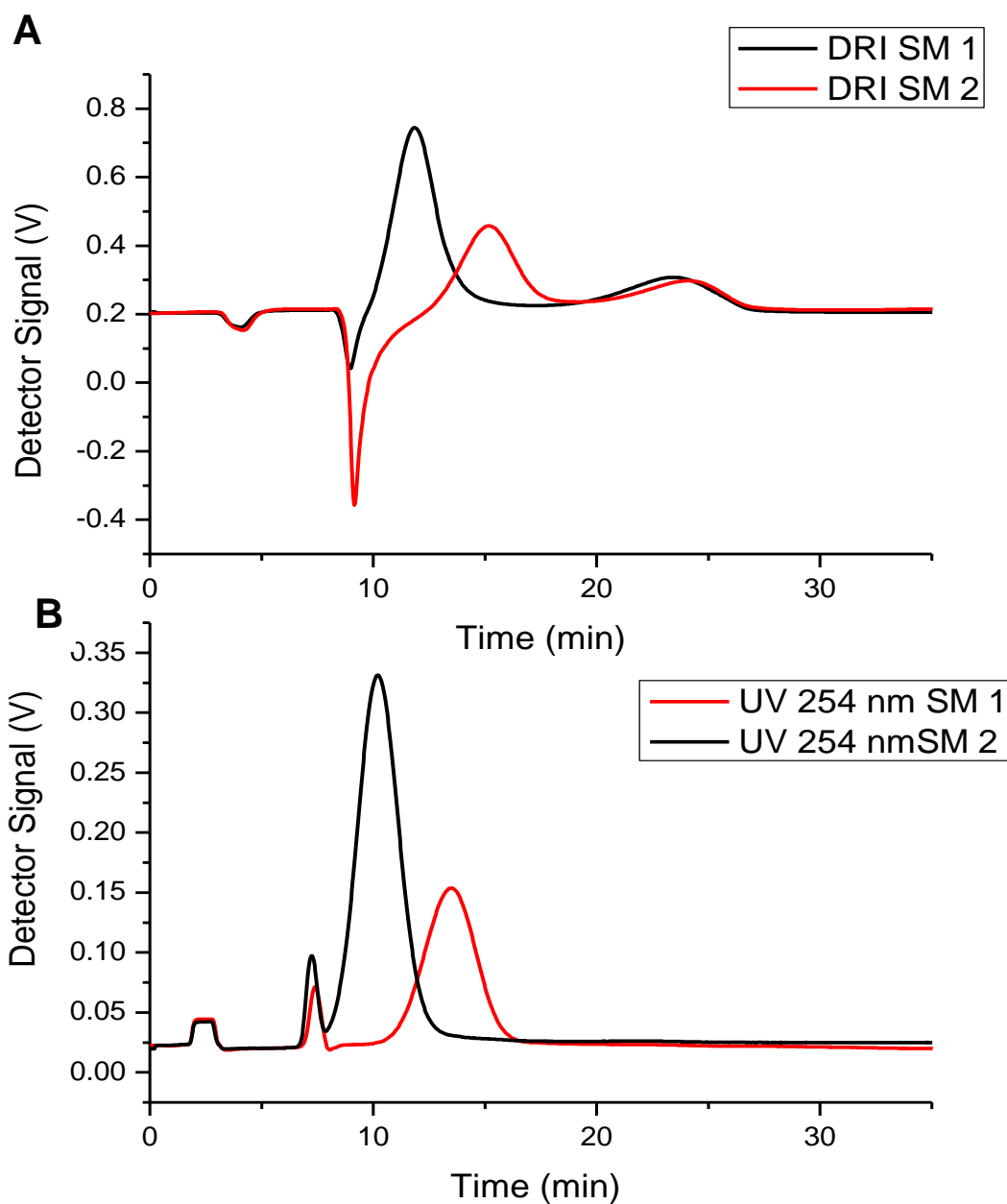
Figure 4.4: Superimposed fractograms of SM 1 and SM 2. Detectors: (A) DRI (B) UV
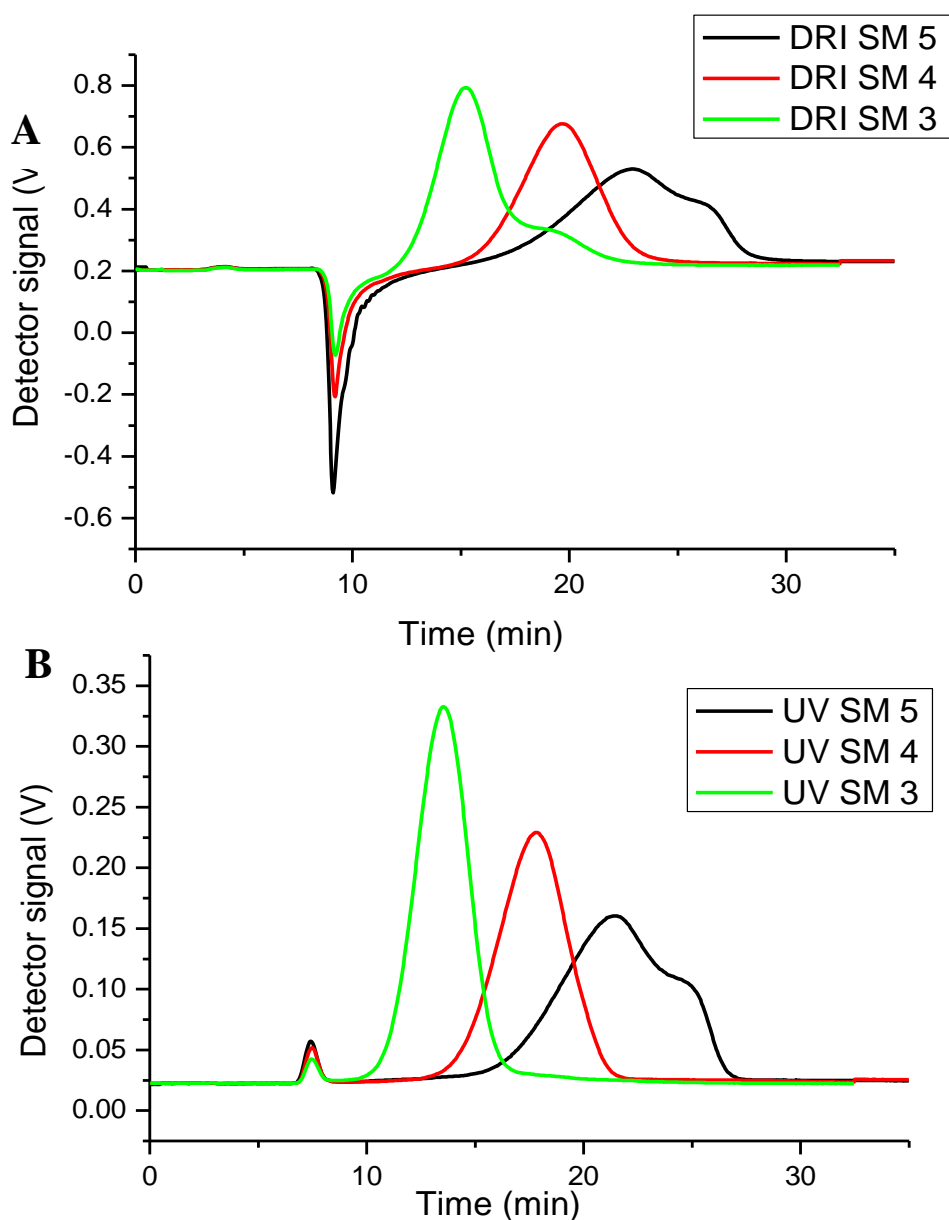
Figure 4.5: Superimposed fractograms of SM 3, SM 4 and SM 5. Detectors: (A) DRI (B) UV

A different scenario is observed for the blends SM 3-5 where the blend components had rather similar molar masses. SM 3 contained PS (72 kg/mol) and PMMA 88 (kg/mol). These homopolymers had rather similar sizes in solution which are 22.5 and 22.8 nm, respectively (see Table 4.4), but had different elution times. The DRI fractogram for SM 3 is an example of a separation that was due to chemical composition and not hydrodynamic size. The main eluting peak is due to PS as can be confirmed by the corresponding UV trace while the later eluting shoulder is due to PMMA. The thermal diffusion coefficient for the PS homopolymer

50

is $2.57\pm0.21\text{x}10^{-7}$ cm^{2}s^{-1}K^{-1}and $3.33\pm0.44\text{x}10^{-7}$ cm^{2}s^{-1}K^{-1} for PMMA, therefore, confirming that the difference in chemical nature was the driving force for the present separation.

Figure 4.6A shows the DRI fractograms for the individual homopolymers of PS (2 mgmL^{-1}) and PMMA (1.5 mgmL^{-1}) superimposed with that of the blend. The two homopolymers that made up SM 4 have the same elution time which explains the appearance of one broad peak for the blend with a very slight shift in retention time. SM 5 has a shoulder peak belonging to the PS (196 kg/mol) in both the UV as the DRI seen in Figure 4.5. Figure 4.6B illustrates an overlay of the homopolymers that make up SM 5 and the DRI for the PS shows a small shoulder peak. A more pronounced shoulder peak is illustrated in the DRI and the UV fractograms for the SM 5 blend (Figure 4.5). This confirms that this peak is due to PS.
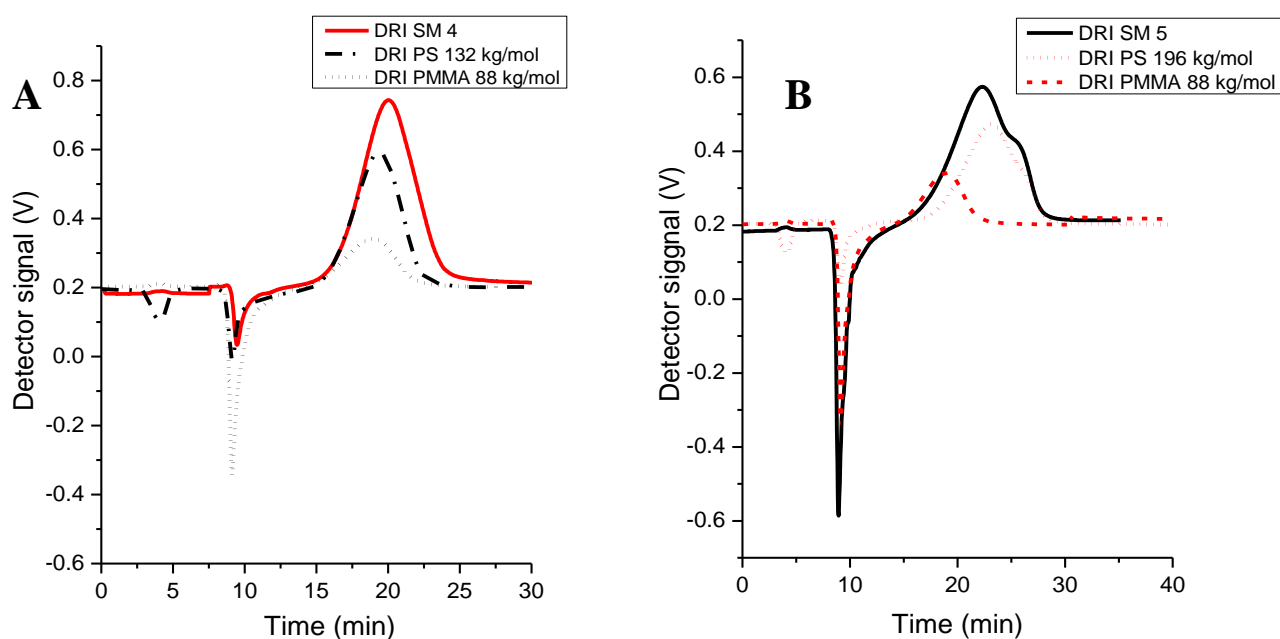
Figure 4.6: Superimposed fractograms of (A) SM 4, PS 132 kg/mol and PMMA 88 kg/mol and (B) SM 5, PS 196 kg/mol and PMMA 88 kg/mol. Detector: DRI

Table 4.4: Retention time (t_r), radius of gyration (R_g), normal diffusion coefficient (D), thermal diffusion coefficient (D_T) and Soret coefficient (S_T) for PS and PMMA homopolymer samples determined by ThFFF at a temperature gradient (ΔT) of 60 K.

Sample name	Molar Mass (g/mol)	t_r (min)	R_g (nm)	D (10^{-10} cm^2 s^{-1})	D_T (10^{-7} cm^2 s^{-1} K^{-1})	S_T (K^{-1})
PS	33 000	10.7	16.7	5.68 ±0.23	2.67 ±0.54	0.0021
PS	72 000	13.9	22.5	4.22 ±0.51	2.57 ±0.21	0.0016
PS	132 000	18.4	31.7	2.99 ±0.44	2.42 ±0.20	0.0012
PS	196 000	22.2	33.2	2.86 ±0.81	2.79 ±0.18	0.0010
PMMA	88 000	18.2	22.8	4.16 ±0.60	3.33 ±0.44	0.0013
PMMA	138 000	31.9	34.2	2.77 ±0.31	3.89 ±0.73	0.0007

The normal diffusion coefficient is dependent on size. The smaller molecules move faster than larger ones, which means they move further away from the accumulation wall towards the centre of the channel (faster flow streams) whereas the larger ones stay closer to the accumulation wall (slower flow streams). Samples with lower molar masses will have larger normal diffusion coefficients regardless of chemical composition and this is shown by the diffusion coefficient values in Table 4.4. Thermal diffusion, is less sensitive to molar mass and mainly dependent on chemical composition. All the PS homopolymers have rather similar thermal diffusion coefficients which is also seen for the PMMA homopolymer samples. The thermal diffusion coefficients of PS and PMMA are distinctively different. This is the reason while PS-PMMA blends can be fractionated by ThFFF over a broad range of blend compositions.

4.2.2. Analysis of PS-PMMA blends regarding chemical composition distribution by ThFFF-FTIR

To determine the content of one comonomer in a blend or copolymer structure, a calibration of the IR signal intensities is required. For this, PS and PMMA homopolymers with known concentrations were injected into the ThFFF-FTIR setup and the signals at 700 cm^{-1} (PS phenyl stretch) and 1735 cm^{-1} (PMMA carbonyl stretch) were detected. At each concentration, three measurements were done and averaged. The signal area as a function of the injected mass was plotted and the slope was determined as the linear regression. The slope values were applied to the absorption peak intensities in the ThFFF-FTIR elugrams and the component concentrations were calculated.

In the online calibration of ThFFF-FTIR, homopolymers of PS (M_n 72 kg/mol) and PMMA (M_n 138 kg/mol) were used. The measured integral intensities are reported in Figure 4.7. Linear regressions were applied to quantify the polymer blend compositions across the FTIR elugrams for a series of PS/PMMA blend ratios. For each sample, the slope values for the PS and the PMMA calibration (0.0038 and 0.0023, respectively) were applied to the respective peak areas to get the injected mass content in wt. % (bulk). The concentrations for both PS and PMMA were then calculated at each elution time by applying the same calibration to each peak intensity at each elution time.

53
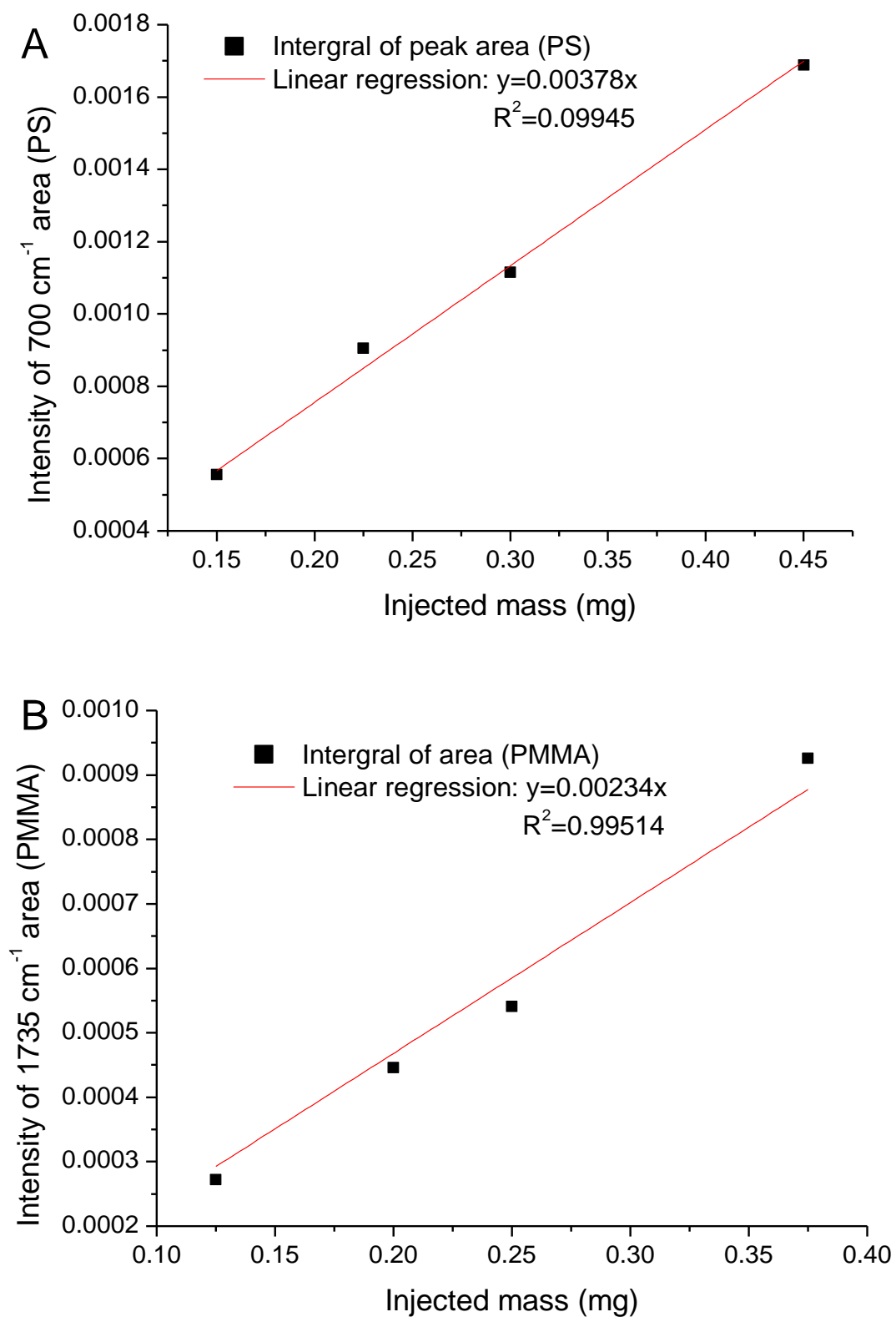
Figure 4.7: Calibration of ThFFF-FTIR. Four concentrations of each homopolymer were used to obtain four signal intensities. Linear regression is applied to obtain a slope; (A) PS 700 cm^{-1} (B) PMMA 1735 cm^{-1}

Table 4.5: Bulk composition by IR (wt. %) from elution profiles at 700 cm^{-1} and 1735 cm^{-1} for PS and PMMA, respectively

| Sample name	PS (wt. %)	PMMA (wt. %)	PS (UV-DRI) (wt. %)	PMMA (UV-DRI) (wt. %)	PS$_{Theo}$ (wt. %)	PMMA$_{Theo}$ (wt. %)
SM 1	63.4	36.6	59.9	40.1	62.5	37.5
SM 2	72.2	27.8	70.7	29.3	74.3	25.7
SM 3	59.8	40.2	51.8	48.2	58.4	41.6
SM 4	67.4	32.6	62.1	37.9	65.9	34.1
SM 5	68.5	31.5	63.7	36.3	66.7	33.3

The blend compositions obtained by ThFFF-FTIR in Table 4.5 compare well with the theoretical values and those obtained using ThFFF-UV-DRI. However, the compositions determined using ThFFF-FTIR are closer to the theoretical values than those determined by ThFFF-UV-DRI. Although FTIR used in coupled measurements has lower sensitivity than when used in isolation, it is more specific and selective than UV spectroscopy. FTIR makes use of a set of absorption bands for identification and is expected to show more specific and accurate results as compared to the UV-DRI approach.

Using ThFFF-FTIR, chemical composition distributions of the blends as a function of elution time were determined. The FTIR elugram of SM 1 shown in Figure 4.8. A confirms what is presented in Figure 4.4. The PS fraction elutes first followed by PMMA exhibiting baseline separation and no co-elution of the two components.
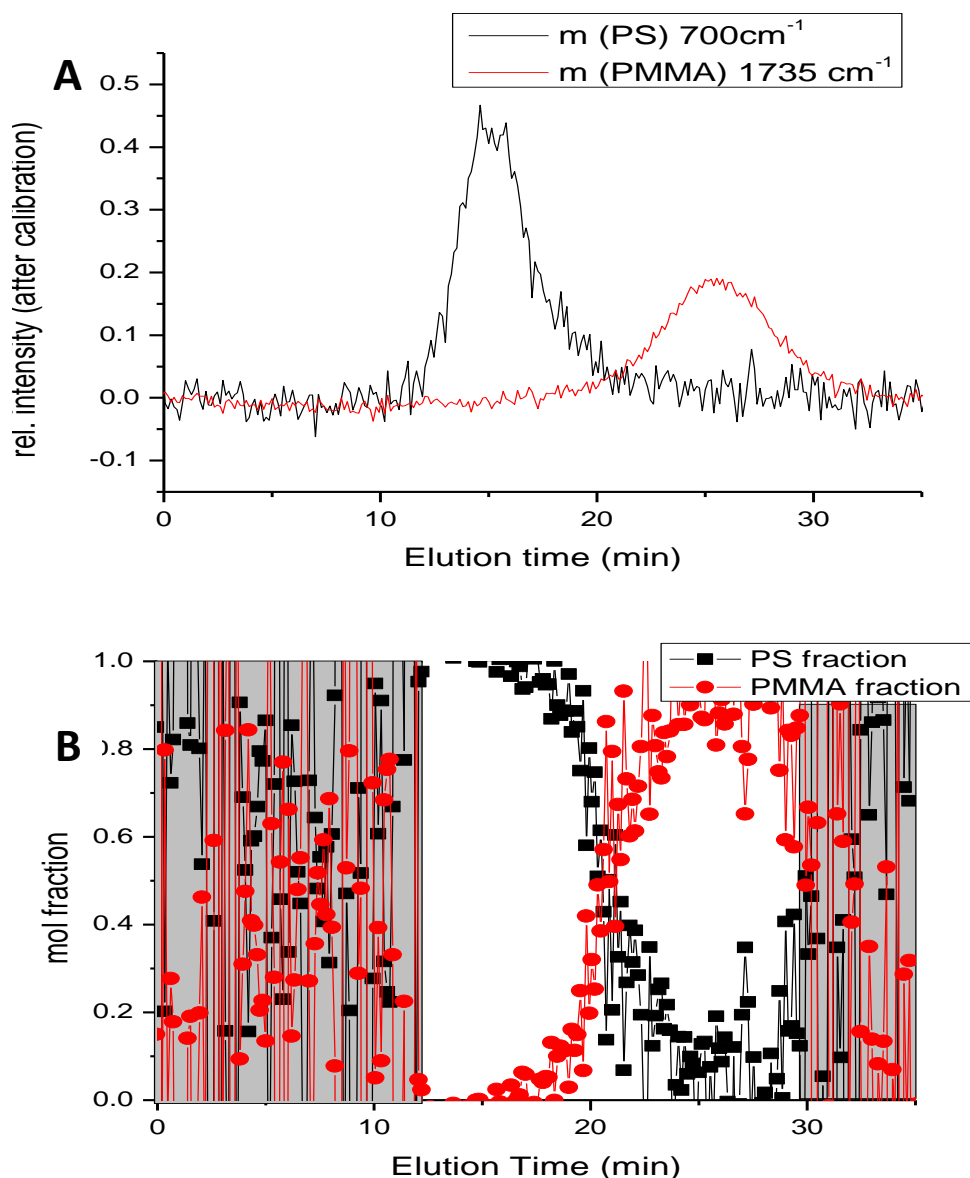
Figure 4.8: (A) FTIR elution profile of SM1, (B) chemical composition distribution for SM 1

The calibrated elugrams (A) and the curves for the elution volume-dependent composition (B) are shown in Figure 4.8 for SM1 and in Figures 4.11-4.13 for SM3, SM4 and SM5. From the calibrated elugrams, the molar fraction of the components can be plotted as chemical composition against the elution volume/time. In areas with low signal intensity (<5% of the peak maximum), calculation and interpretation cannot be achieved and these areas are represented in gray. SM 1 is expected to show no PMMA moieties in the first peak and no PS in the second peak, however the second peak shows 0.2 mole fraction of PS present in the second peak. This can be explained by band broadening effects, explained later in Section 4.2.3.

56
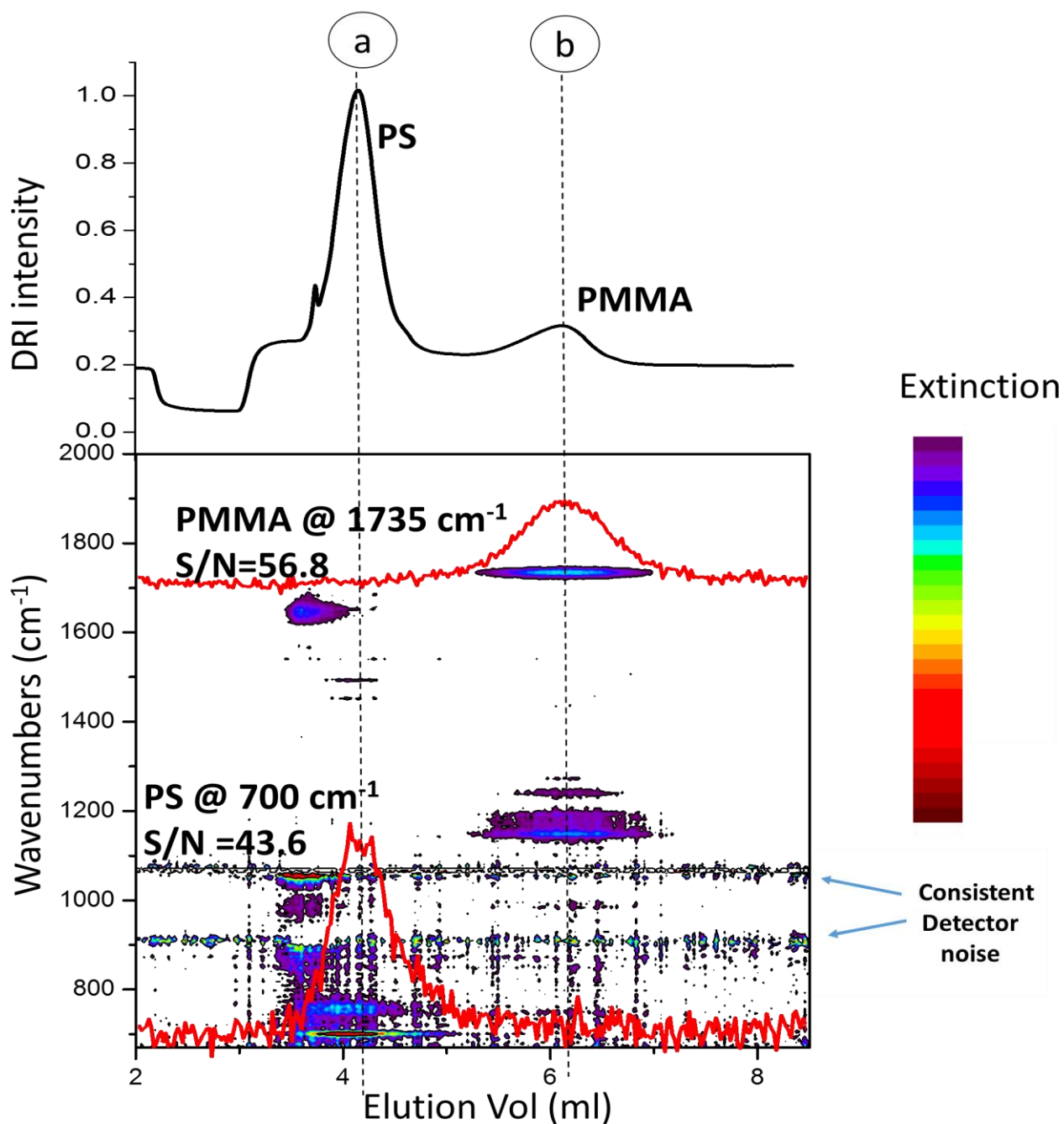
Figure 4.9: Contour plot of the 2D spectral elugram from the FTIR detection of the ThFFF separation of SM 1

The molecular heterogeneity of a particular complex polymer can be presented either in a three-dimensional diagram or a so-called "contour plot" (Figure 4.9). To obtain this, two analytical methods that are sensitive to one type of heterogeneity are used. In the present case ThFFF was used as being selective towards the molar mass, and FTIR was sensitive towards chemical

composition. For blends, discrete composition fractions are present, whereas in copolymers, a continuous drift in composition is expected[7].

The injected mass used to obtain Figure 4.9 was below the overload limit for the DRI detector and we were still able to obtain sufficient S/N values of 43.6 and 56.8 for PS and PMMA, respectively. For the two components in the blend, specific elugrams can be extracted from the data. Here we only show the elugrams at 700 and 1735 cm^{-1}, to which the peaks of the DRI detector (Figure 4.9 upper part) can be assigned to as they correlate with the FTIR elugram. Another elugram can be generated at 1150 cm^{-1} which can be used to identify the PMMA methoxy group.
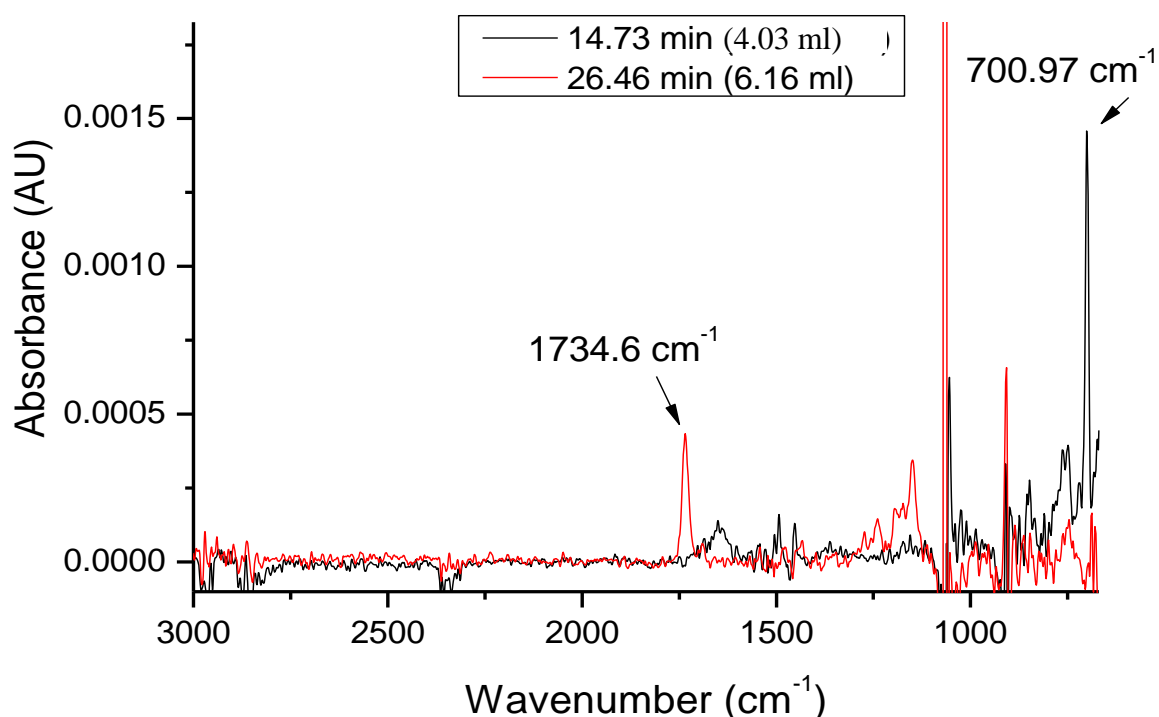
Figure 4.10: Spectra extracted at the peak maxima of the blend components, for PS at elution volume 6.16 mL and for PMMA at elution volume 4.03 mL from ThFFF-FTIR separation in Figure 4.8A

In addition, Figure 4.10 shows that it is possible to obtain full spectra from the various peak maxima in the ThFFF fractogram. The quality is sufficient to clearly identify the particular polymer by comparison to spectra available in standard spectral libraries.

Figures 4.11-4.13 show the chemical composition readings for the PS-PMMA blends SM3-5. Figure 4.11 shows that, even without baseline separation, the composition of a sample can still

be identified to be a blend because the PS and PMMA FTIR elugrams do not overlap[8,9]. This indicates the absence of covalent bonding between the two structural moities, confirming that the sample cannot be a copolymer[10]. A similar but not as obvious behaviour can be seen in Figure 4.13 for SM 5. The FTIR elution profile is the same as that observed in Figure 4.6B for the homopolymers.

The pronounced shoulder seen in Figure 4.5 for SM 5, is not seen in the FTIR elugram. This could be due to the increased noise and decreased sensitivity that comes from a coupled experiment.
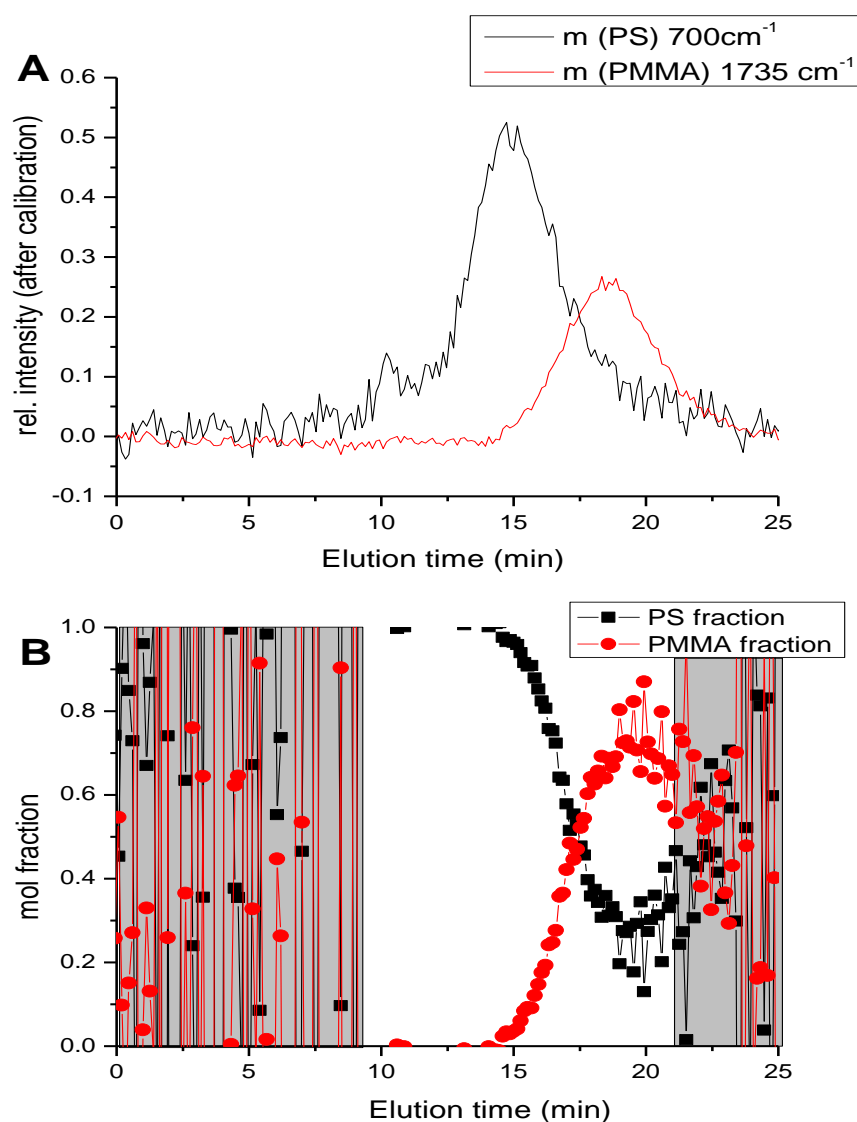
Figure 4.11: (A) FTIR elution profile, (B) chemical composition distribution for SM 3

Figure 4.12 shows that at any given elution time there is more PS than PMMA in SM4. This is because more PS was injected into the system than PMMA. Figure 4.12 is an example for the limitation of the ThFFF-IR system. Here a blend sample is seen that exhibits the same behaviour that is expected for a copolymer sample. The FTIR elugrams for the PS and PMMA blend fractions overlap similar to what they would in a covalently bonded copolymer sample. This means if a sample was completely unknown in terms of molar mass and chemical composition, it would be a challenge with this set-up, to say whether the sample is a copolymer or a blend.
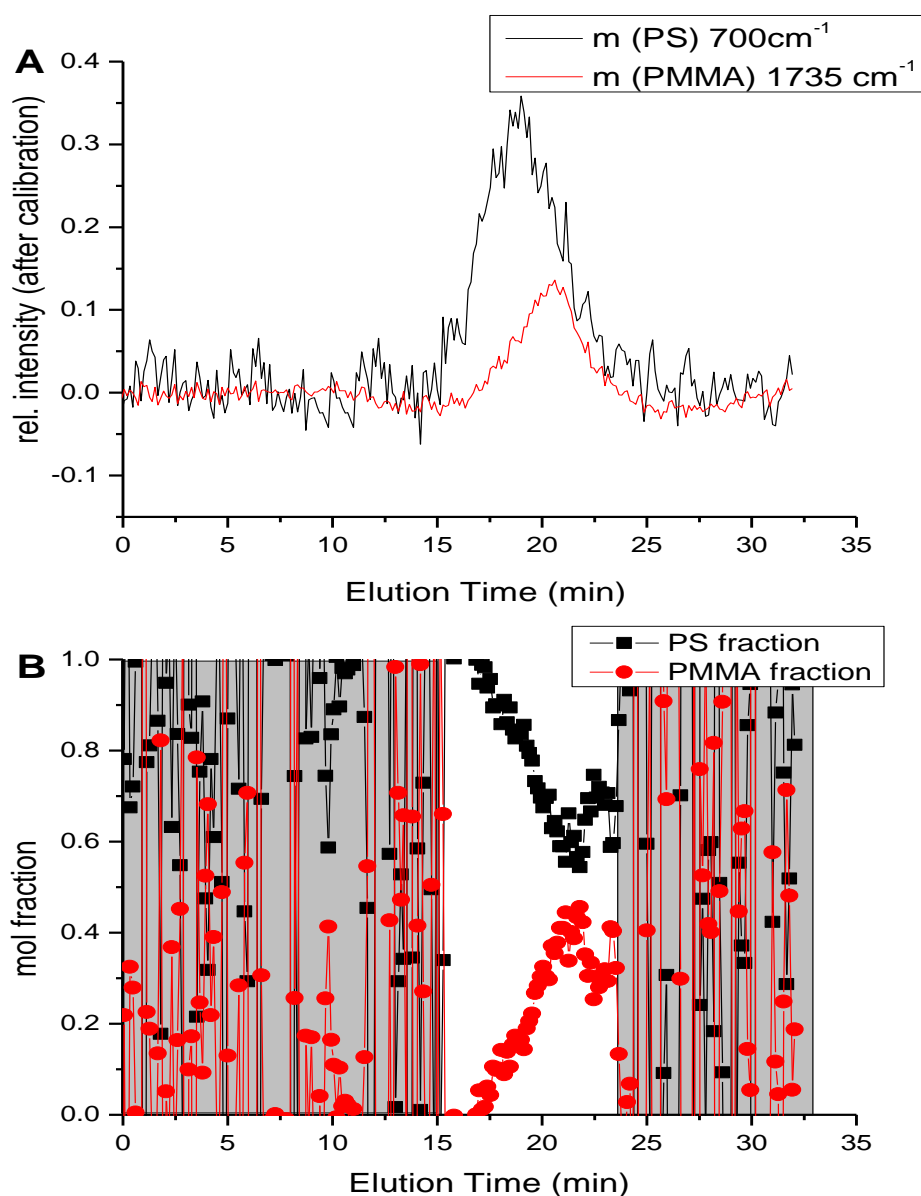
Figure 4.12: (A) FTIR elution profile, (B) chemical composition distribution for SM 4
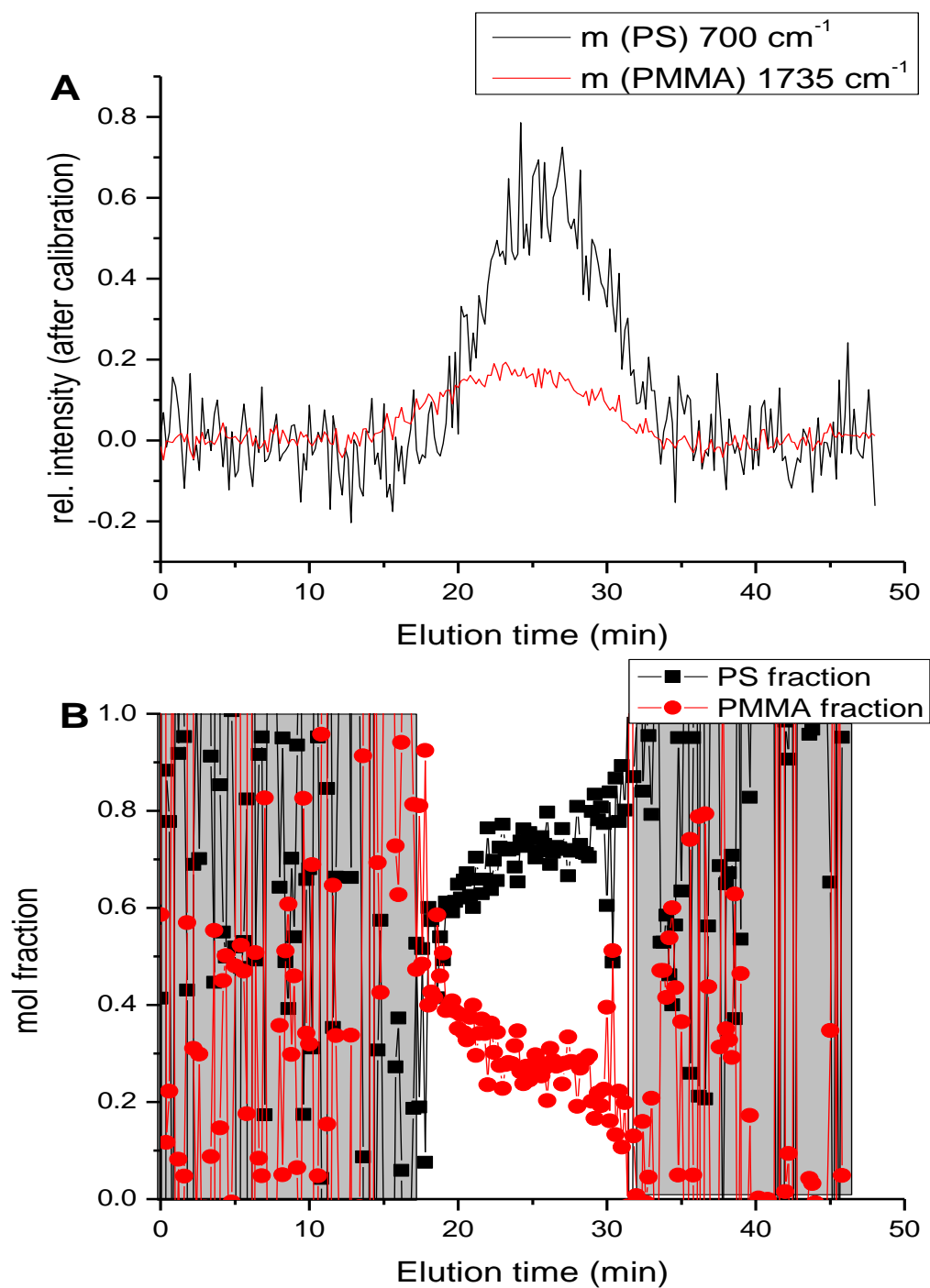
Figure 4.13: (A) FTIR elution profile, (B) chemical composition distribution for SM 5

4.2.3. Analysis of PS-PMMA blends regarding molar mass and size distributions by ThFFF-RI-MALLS and ThFFF-DLS

In addition to chemical composition information, with the present multidetector ThFFF system molar mass and hydrodynamic size information can be obtained. Similar to the typical multidetector SEC approach, molar mass information is based on MALLS detection while hydrodynamic size information is based on DLS detection. Before conducting these experiments, however, the specific refractive index increments (dn/dc) of the samples must be determined. The values for the homopolymers were determined using ThFFF-RI (method described in Chapter 3) and then the ThFFF-RI-MALLS detection set-up was used to determine peak-maximum molar masses (M_p). It is important to note that for copolymers dn/dc varies with composition of the two comonomers in the polymer. This means that the bulk dn/dc values cannot be used for copolymer samples with varying chemical composition contents. For copolymers the dn/dc at each elution volume must be calculated for the determination of accurate molar mass distributions. Furthermore, molar mass determination using MALLS is even more difficult when evaluating data for blends that are not baseline resolved into their homopolymer fractions. In this case, in the co-elution region dn/dc changes with the amounts of the blend components in each elution volume fraction. For this reason, information on molar masses is only presented for SM 1, SM 2 and SM 3. Even though SM 3 did not show baseline separation, the resolution was good enough to see a distinct peak for each homopolymer.

The dn/dc values of the homopolymers in THF at 25 °C were 0.171 ± 0.002 mL/g for PS, 0.079 ± 0.003 mL/g for PMMA. These values are comparable to those in literature[3]. The M_p values are approximations. For them to be absolute the change in dn/dc with elution time must be experimentally calculated for each point in the separation in cases where the blend components co-elute. For the blend samples that were relatively well resolved the molar mass distributions were determined by using the dn/dc values of the homopolymers.

Table 4.6: Peak molar masses (M_p) of the blend components in well separated SM blends.

Sample	Retention time (min)	M_p (kg/mol)
SM 1	10.9 (PS)	34.8
	22.5 (PMMA)	141.0
SM 2	14.4 (PS)	70.4
	21.1 (PMMA)	135.0
SM 3	14.2 (PS)	70.8
	18.8 (PMMA)	87.5

Below are the fractograms for SM 1, SM 2 and SM 3, superimposed with the molar mass readings from the MALLS detector. The molar mass distributions for SM 3 may contain some error because there is no baseline separation. However, the MALLS fractogram correlates well with the DRI from SM 3 in Figure 4.5 and the FTIR elugrams in Figure 4.11. The homopolymers in SM 4 and 5 co-eluted and, therefore, the molar masses could not be determined from the MALLS readings.
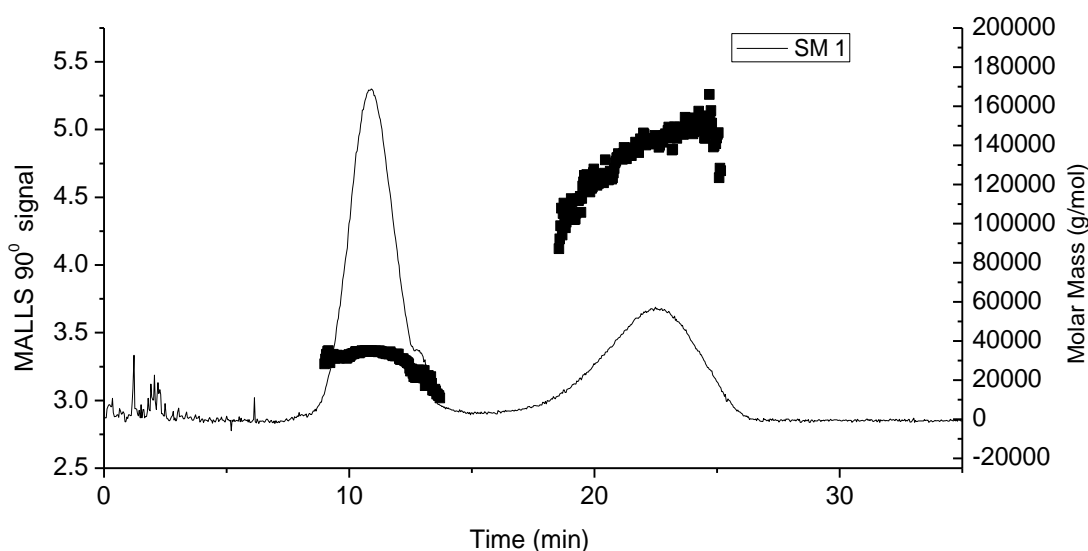
Figure 4.14: MALLS fractogram of SM1 overlaid with molar mass distributions

63
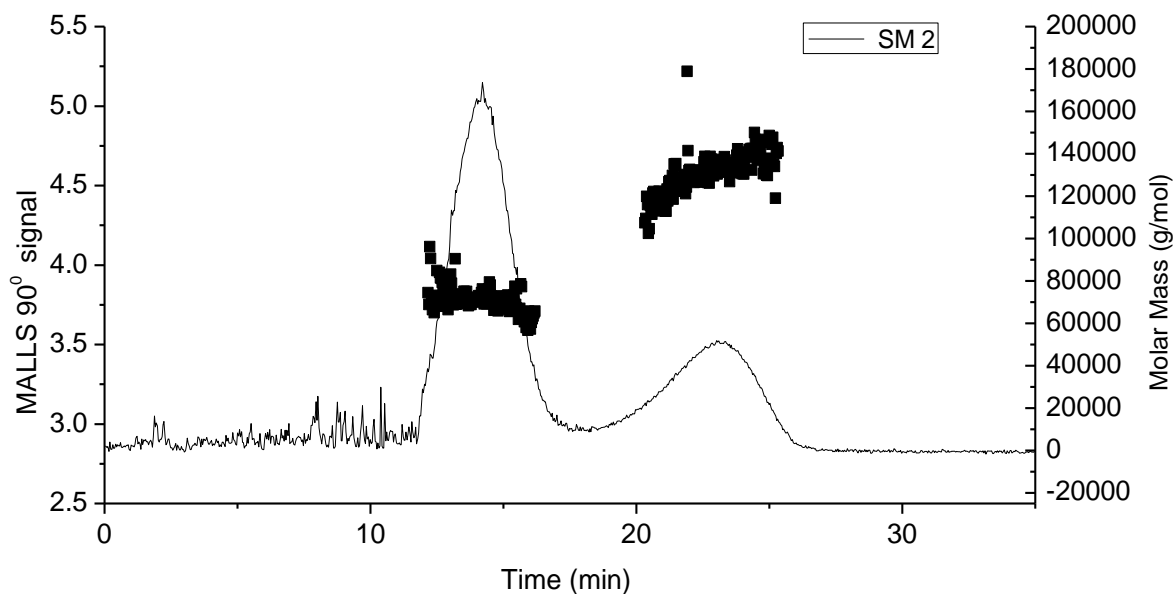
Figure 4.15: MALLS fractogram of SM2 overlaid with molar mass distributions
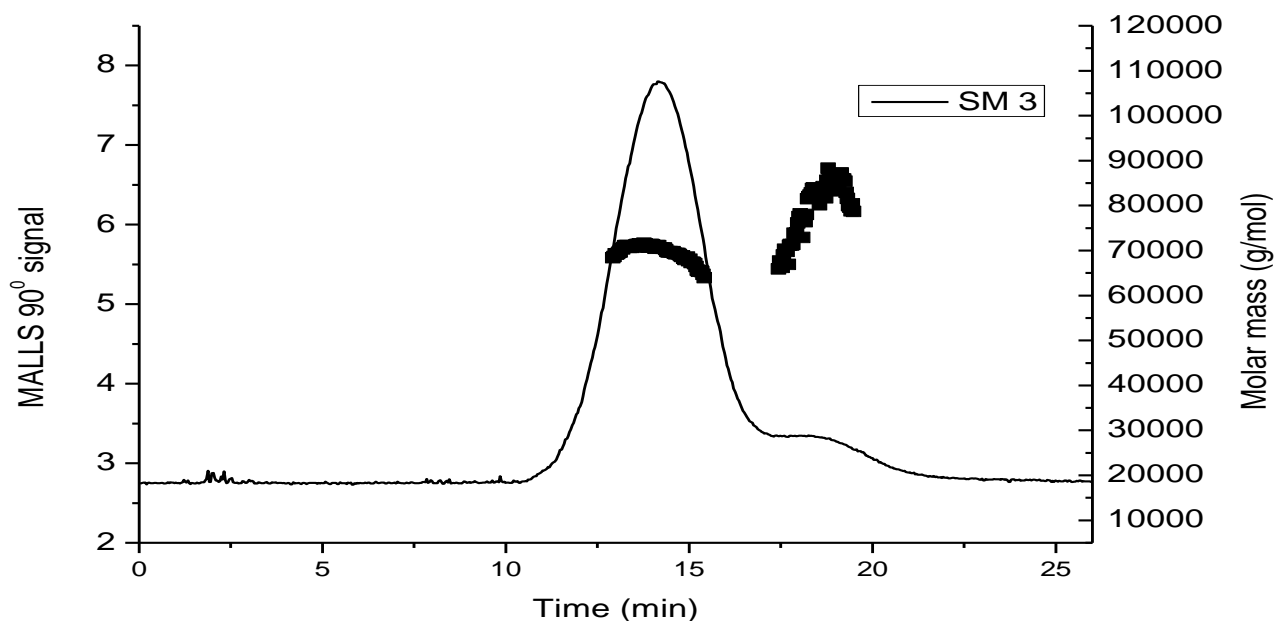
Figure 4.16: MALLS fractogram of SM 3 overlaid with molar mass distributions

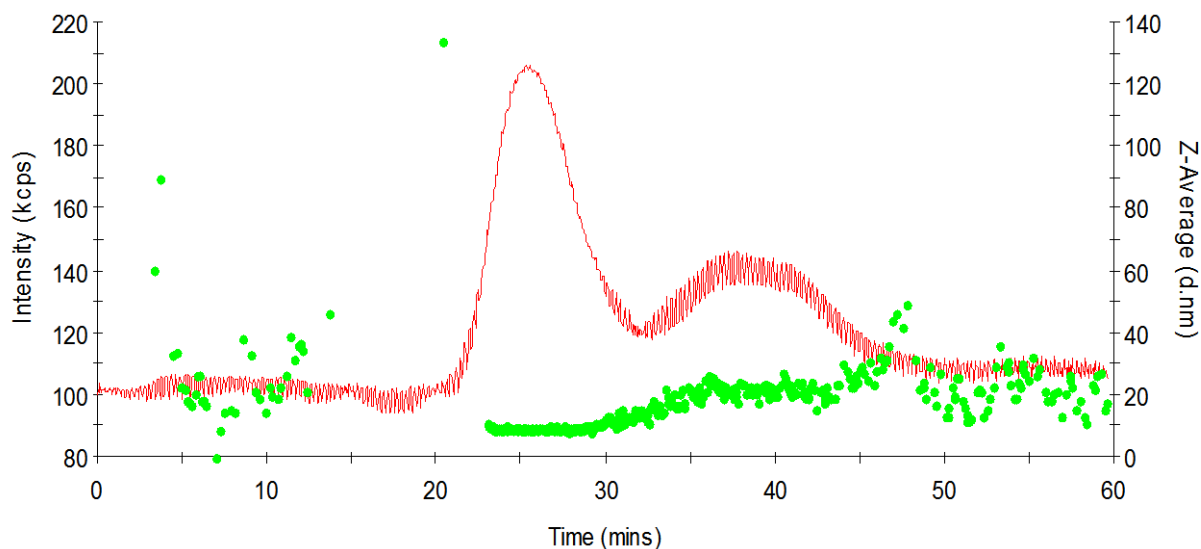Figures 4.17 and 4.18 represent the size distributions of the blends from the online DLS data. The green dots represent the Z-average hydrodynamic diameters (D_h) and the corresponding elution profiles are presented in red.

64

Figure 4.17: DLS fractogram for SM 1
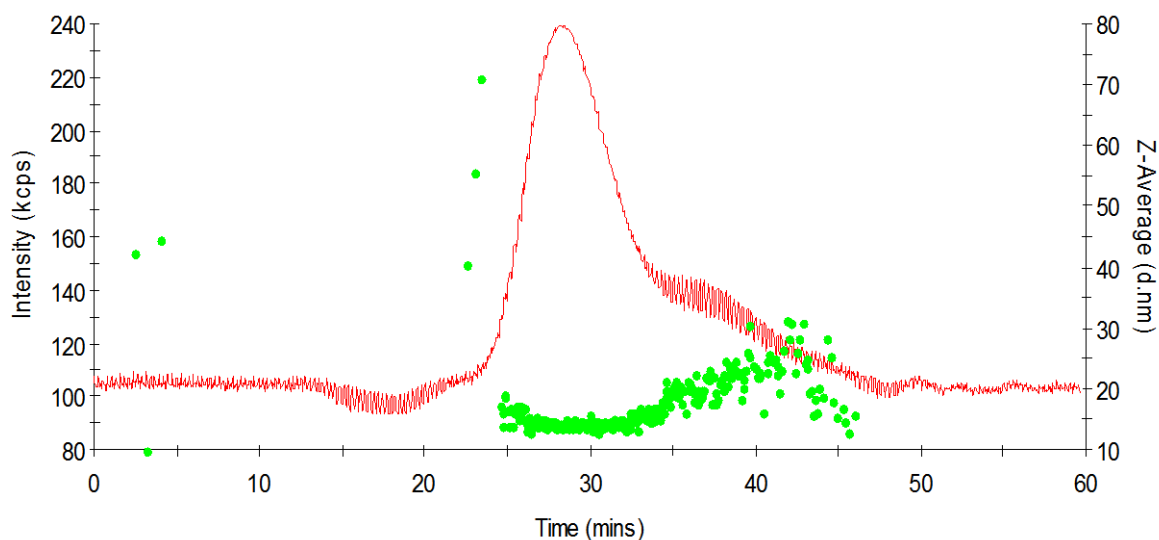
Figure 4.18: DLS fractogram for SM 2

In Figures 4.16-4.21 it is confirmed that separation is influenced by hydrodynamic size in addition to chemical composition since in each elution peak hydrodynamic size increases with increasing elution time. Furthermore, the influence of peak broadening is clearly demonstrated. Figure 4.14 and Figure 4.17 are representative of the same sample. The MALLS trace shows baseline separation whereas the DLS does not. This trend is similar for all samples and is indicative of peak broadening. In the instrumental set-up it is shown that the MALLS (cell volume = 63 µL) is the second detector and the DLS (cell volume = 500 µL) is the last detector

in series. Peaks elute later and become broader for detectors with a large cell volume. Between the MALLS and DLS detectors there is tubing as well as the DRI detector and the FTIR spectrometer. Therefore, mixing in the flow cells as well as the tubings is expected to lead to the band broadening observed. This can be countered by using shorter tubing between the detectors, however, the detector cell volumes cannot not be changed freely. The DLS fractograms for SM 3 and SM 4 show a very small variation in size for the two components. The difference between the FTIR and the DLS SM3 fractograms show the effects of band broadening between the detectors.
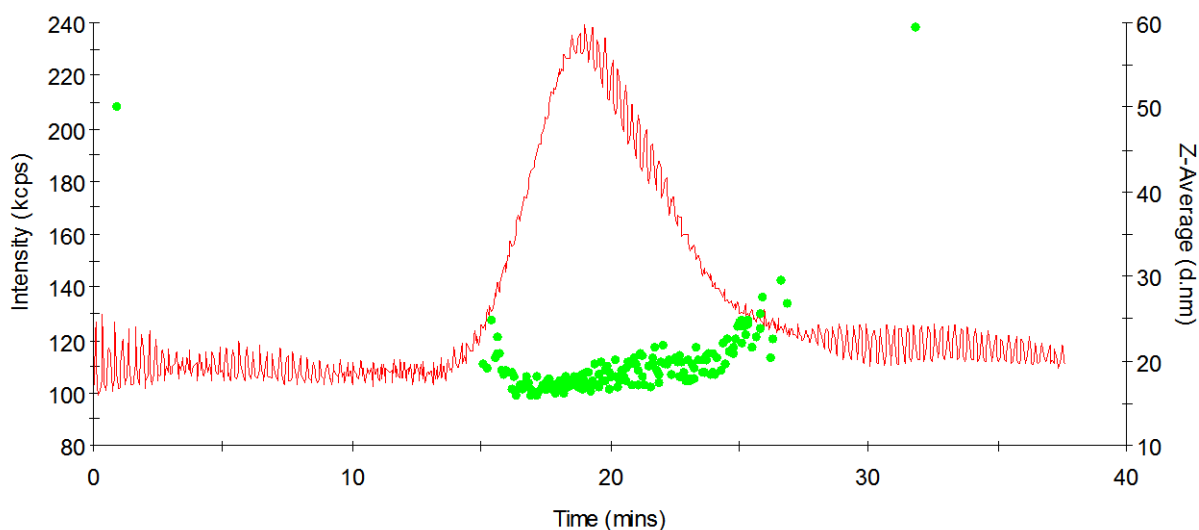
Figure 4.19: DLS fractogram for SM 3
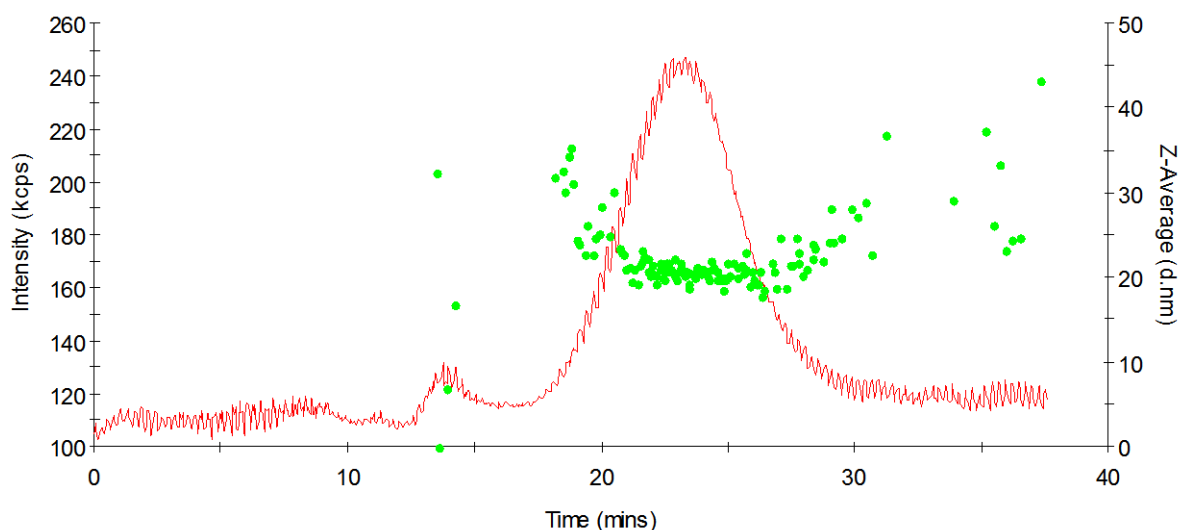
Figure 4.20: DLS fractogram for SM 4
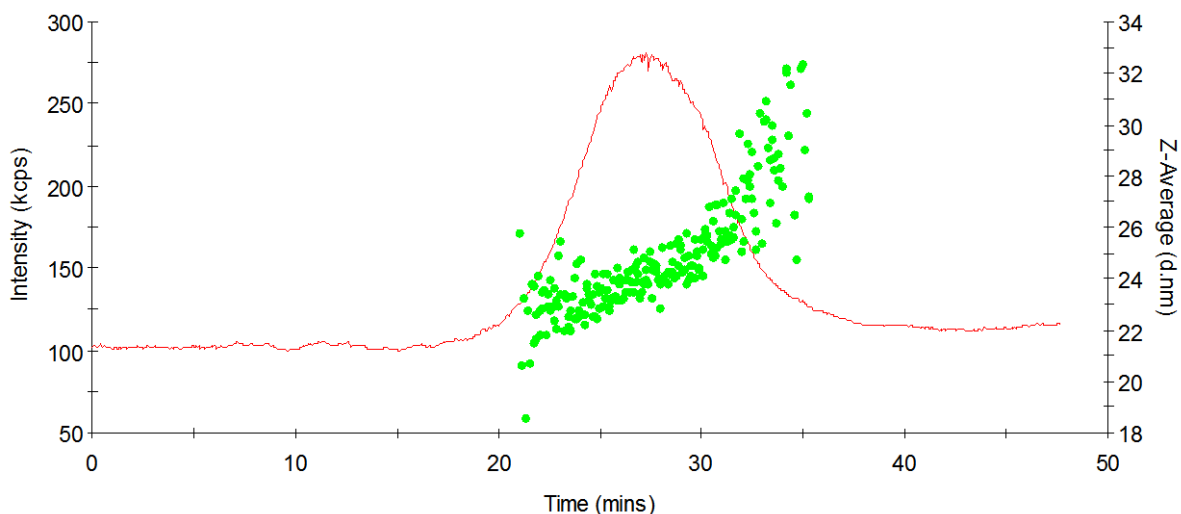
Figure 4.21: DLS fractogram for SM 5

The homopolymers that make up SM 5 have significantly different molar masses (PS 196 kg/mol and PMMA 88 kg/mol). It is, therefore, expected that they have a noticeable difference in size in solution. Figure 4.21 shows a gradual increase in size of the particles from ± 21 nm to ±33 nm and this correlates to the R_g values for the individual homopolymers shown in Table 4.4.

4.3   SMA Copolymers

In the previous sections, polymer blends were used to develop the experimental and data interpretation methods for ThFFF-FTIR, which are used as a basis for the analysis of copolymers. To prove the applicability of the ThFFF-FTIR coupling, four poly(styrene-co-methyl methacrylate) (SMA) samples were selected and analyzed. The compositions of the copolymers as provided by the manufacturer are summarized in Table 4.7.

4.3.1. Analysis of SMA copolymers regarding chemical composition by ThFFF-UV-RI

Table 4.7: Molar masses (M_w), chemical compositions and dispersity indexes (Đ) as provided by the manufacturer

Polymer	M_w (kg/mol)	Composition (wt. % styrene)	(Đ)
SMA 1	20	48	1.14
SMA 2	50	44	1.05
SMA 3	50	83	1.49
SMA 4	88	33	1.08

The copolymer samples in Table 4.7 were used as provided and were dissolved in THF at room temperature. Complete dissolution was confirmed using offline DLS.
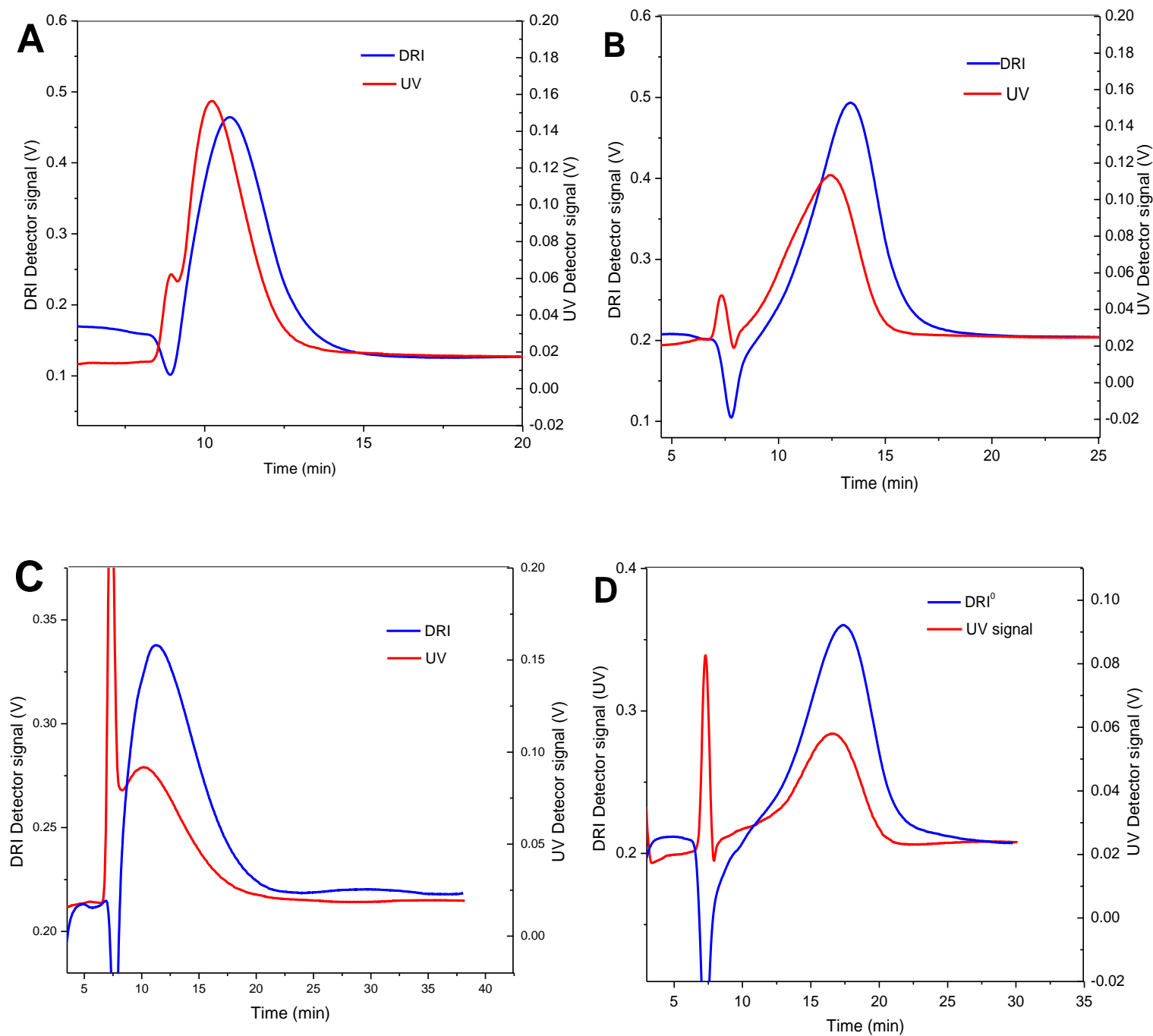
Figure 4.22: Superimposed fractograms for (A) SMA 1, (B) SMA 2, (C) SMA 3 and (D) SMA 4. Detectors: DRI (blue) and UV at 254 nm (red) fractograms

The superimposed DRI and UV fractograms of the copolymer samples show different elution profiles for the four copolymer samples. The relative intensities of the UV detector signals give an indication of the presence of UV absorbing components in each sample. All four copolymers

69

show UV activity indicating the presence of styrene units and through calibration of the two detectors, quantification was possible. In Table 4.8, the bulk compositions of the four copolymers are presented using the same method (UV/DRI) that was used for the blend samples that is based on the total peak areas of the eluting components.

Table 4.8: Bulk content (wt. %) of styrene in SMA copolymers and theoretical styrene content as stipulated by the manufacturer

Polymer	Styrene$_{Theo}$ (wt. %)	Styrene$_{Exp}$ (wt. %)
SMA 1	48	45.2 ($\pm$2.2)
SMA 2	44	40.0 ($\pm$3.2)
SMA 3	83	75.8 ($\pm$4.8)
SMA 4	33	36.2 ($\pm$3.3)

SMA 1, 2 and 4 show comparable results to those given by the manufacturer with a slight underestimation. This is because the three copolymers all start to elute with the void peak which could not be accounted for in the calculations. SMA 3 had a 7.2 % underestimation. This could be due to a portion of the copolymer eluting with the void peak. When calculating the area of the UV or DRI peaks, the void area is not accounted for.

4.3.2. Analysis of SMA copolymers regarding chemical composition distribution by ThFFF-FTIR

The chemical composition distribution of the four copolymers was measured by ThFFF-FTIR. For the calculation of the copolymer compositions, the absorption peaks at 700 cm^{-1} for PS and 1735 cm^{-1} for PMMA were used. The integrals of the elugrams were calibrated, and the chemical composition distributions as mass fractions were calculated therefrom.

Figure 4.23 depicts the elugrams of the block copolymers SMA 1 and SMA 2 after calibration correction. The elugrams correlate to the amounts of PS and PMMA that are present in the sample at each elution time. The calculation of the ratio for chemical composition distribution is relevant only where there is sufficient signal intensity. At intensities less than 5% of the

maximum intensity, noise dominates these regions. The areas that do not meet the requirements are clearly seen as grey areas.
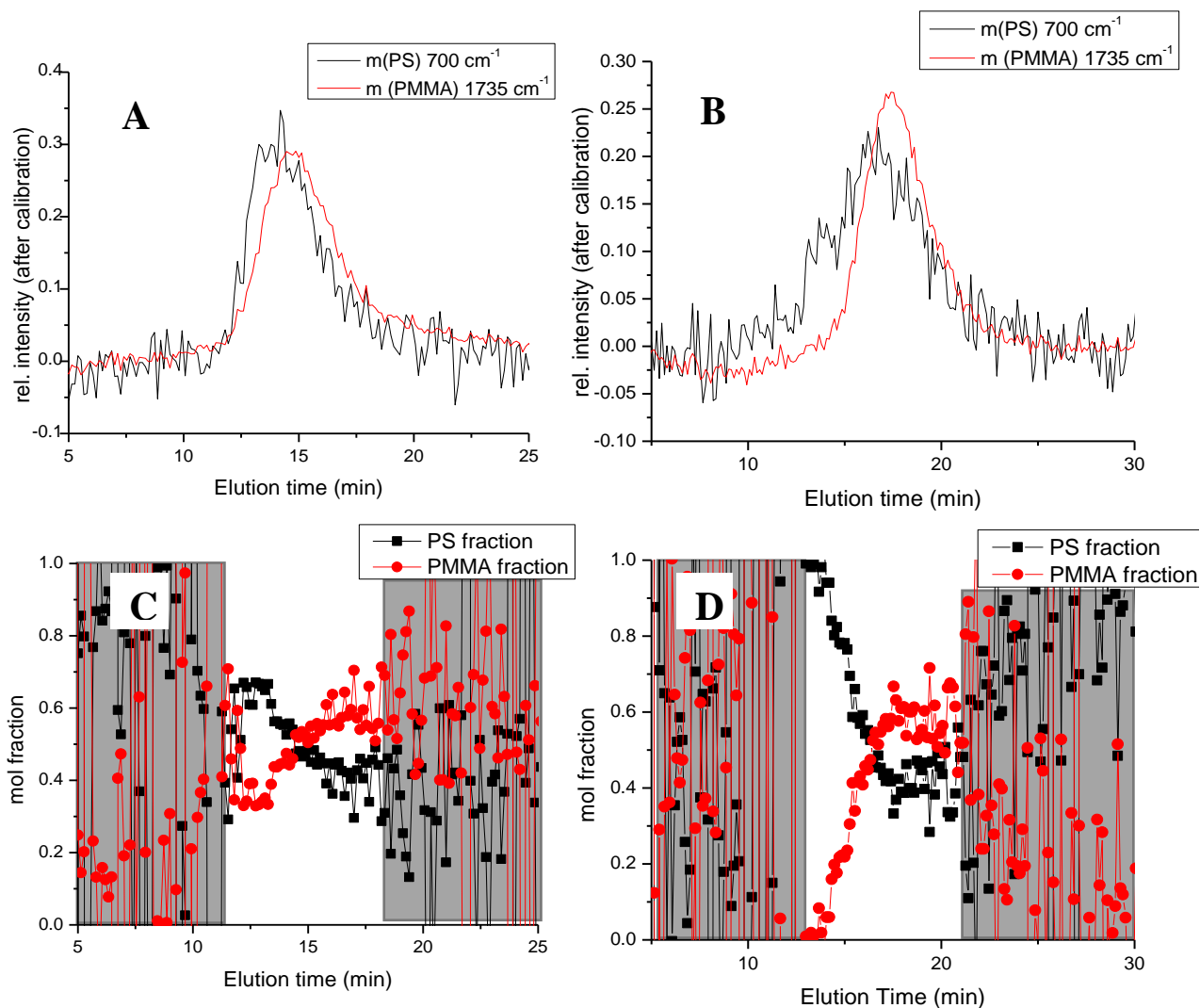
Figure 4.23: (A) and (B) ThFFF-IR elugrams of copolymer samples SMA 1 and SMA 2 after calibration. (C) and (D) show the weight fractions of styrene and MMA in the copolymer samples SMA 1 and SMA 2 as a function of elution time

71
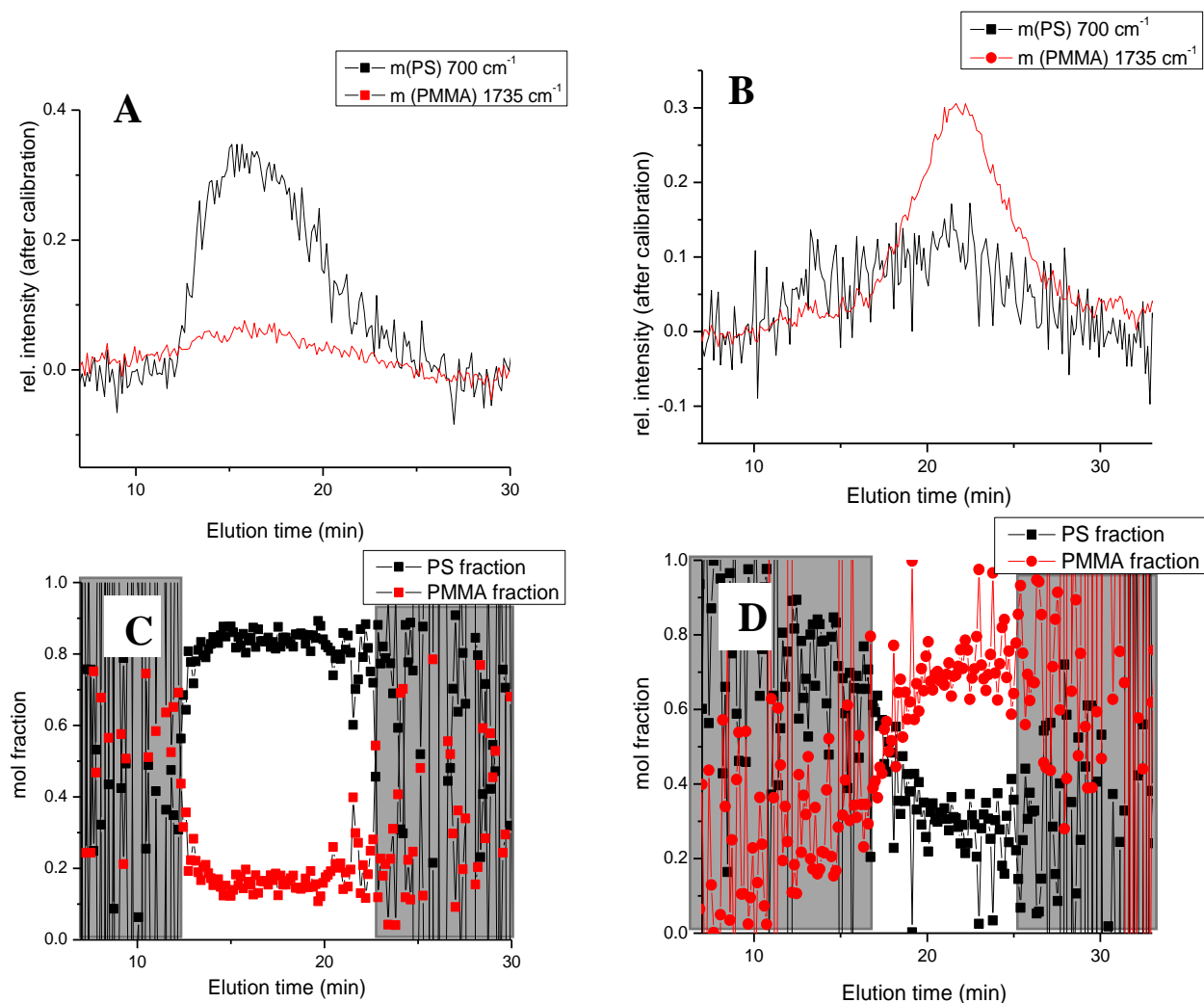
Figure 4.24: (A) and (B) ThFFF-IR elugrams of copolymer samples SMA 3 and SMA 4 after calibration. (C) and (D) show the mole fractions of PS and PMMA in the copolymer samples SMA 3 and SMA 4 as a function of elution time

If it assumed that ThFFF separation for homopolymers takes place according size in solution, with the smaller polymers in solution eluting first whilst the larger ones elute last, then size in solution can be related to molar mass. Copolymers elute according to size and chemical composition as has been shown for the blends of homopolymers. Only in the case that there is no molar mass dependence of chemical composition in the copolymers, which might be the case for random copolymers, elution time in ThFFF correlates with molar mass. In general, low molar mass polymers are small in solution compared to higher molar mass polymers that have a larger size in solution. Therefore, it can be said that the early elution times consist of low molar mass polymers and the polymers at the later elution times are high molar mass polymers.

This statement, however, must be confirmed by online MALLS detection as will be discussed later.

By recreating the calibrated mole fraction elugrams, from Figure 4.23 and 4.24 in Figure 4.25, it can be seen that all four copolymers have different chemical composition behaviours as a function of elution time. Figure 4.24A shows the relative FTIR peak intensity of sample SMA 3. This sample has the same molar mass as sample SMA 2 but a different chemical composition. Figure 4.24C illustrated that the PS mole fraction remains significantly higher with elution time than the PMMA content. SM3 shows a homogenous chemical composition throughout the separation. The PS fraction concentration is constantly between 80 to 90 % and the PMMA is between 10% and 20% throughout the elution profile. From here one of three conclusions can be made 1) this is a homogeneous copolymer or 2) a blend of two homopolymers or 3) a blend of homopolymer and a copolymer. But since a separation of homopolymer components is not seen, it is assumed that this is a chemically homogenous copolymer. Each molar mass fraction has the same chemical composition which is expected for random copolymers prepared by controlled polymerization techniques. This, however, is in contrast to the molar mass distribution which is relatively broad, defined by the polydispersity index of 1.49.

Figure 4.24B and D represent sample SMA 4. Although the PS elugram for the FTIR wavenumber 700 cm^{-1} is relatively noisy (S/N = 8.15), the mole fraction distribution correlates with the percentage composition given by the manufacturer. PS content starts at 60%, decreases to 20% and then increases to 40%. The PMMA content increases in a similar fashion from 40% to 80% and back to 60%. The PS absorbance at 760 cm^{-1} was not useful because it had a S/N ratio of 4.58. It is important to also note that any absorbance other than the one calibrated for would require a calibration that is specific to that signal.

At early elution times, SMA 4, exhibits a low concentration of MMA units and a high concentration of S units. Conversely, at higher elution times a high concentration of MMA is seen and a lower concentration of S. Again, if we assume that separation is according to total size which is related to molar mass, then the low molar mass components are rich in styrene and the high molar masses are rich in MMA. Therefore, it can be said that at higher molar masses longer MMA blocks are present and at lower molar masses longer styrene blocks are present. On average, the SM 4 copolymer has shorter styrene blocks and longer MMA blocks. According to both the bulk (33 wt. % styrene) and theoretical (36.2 ±3.3 wt. % styrene) compositions, this is true because the bulk reflects the molecules with the highest concentration.
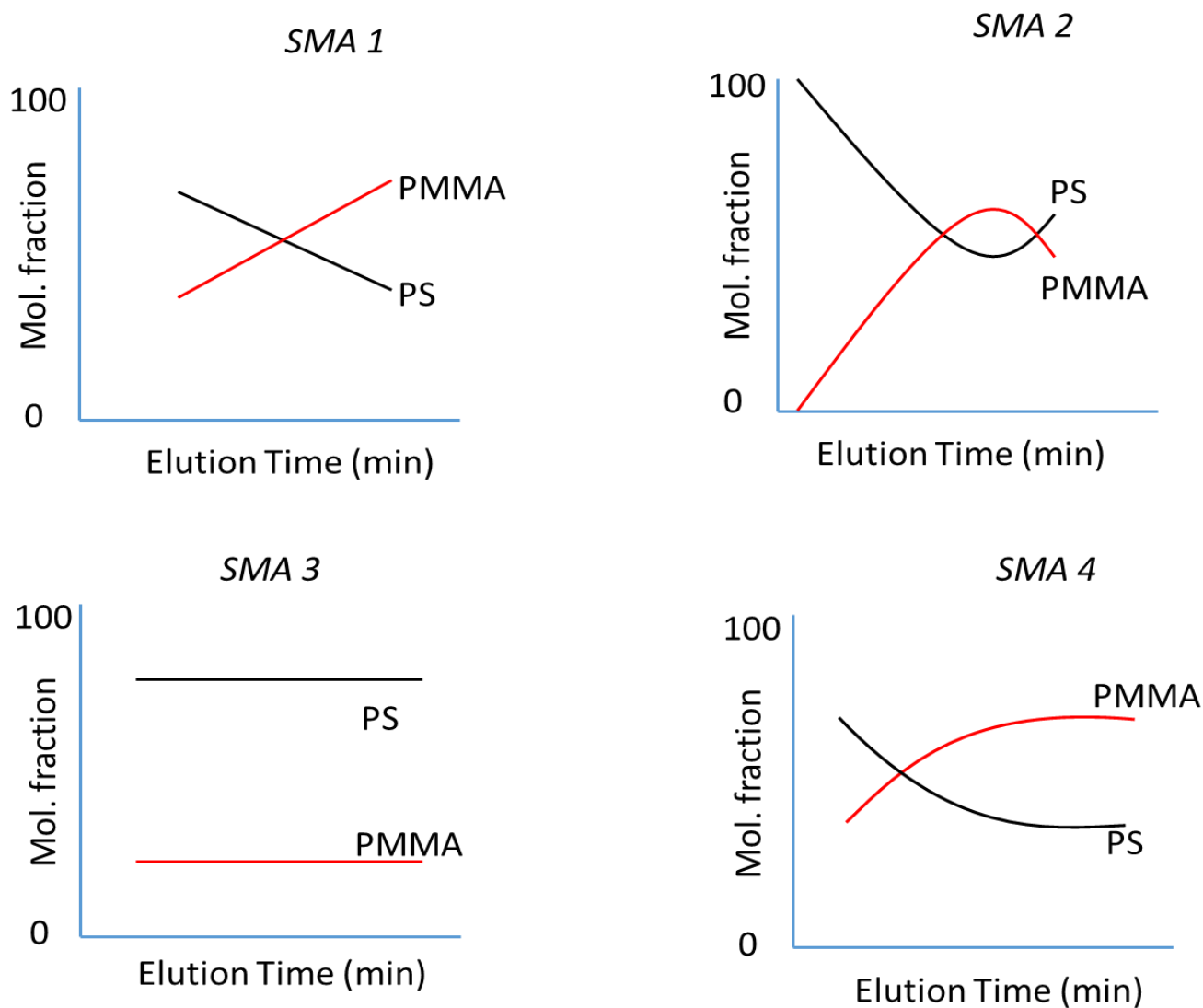
Figure 4.25: Schematic representation of chemical composition distribution as a function of elution time for the four copolymers

The mole fraction distributions of SMA 1, SMA 2 and SMA 4 show a drift in the chemical composition as a function of elution time. SMA 1 and SMA 2 display similarities in their copolymer structure. The PS content in the SMA 1 sample decreases from approximately 70 % to 10 % with increasing elution time. Similarly, the PS content of the SMA 2 sample decreases from 100 % to 30 %. At the early elution times of SMA 2, there are components that do not contain any MMA and only have S units. At later elution times we do not have any components with 100 % PMMA. Therefore, this could be a copolymer with a complex composition that contains PS as the homopolymer. The following conclusion can be made: in the first step, anionic synthesis was used to form a PS block, which had a fairly narrow molar mass

74

distribution. In the second synthesis step, the addition of MMA, chains were terminated continuously, resulting in fewer molecules with a high S content and more molecules with a high MMA content[11]. To prove this, two spectra were extracted at 13.96 min and at the peak maximum (17.42 min) seen in Figure 4.26. As expected, there is almost no detectable MMA (1736 cm^{-1}) at the early elution time. At the peak elution time, a significantly higher intensity of MMA is seen. Both spectra contain styrene units. Such detailed conclusions on the synthesis are difficult to access with other analytical methods.
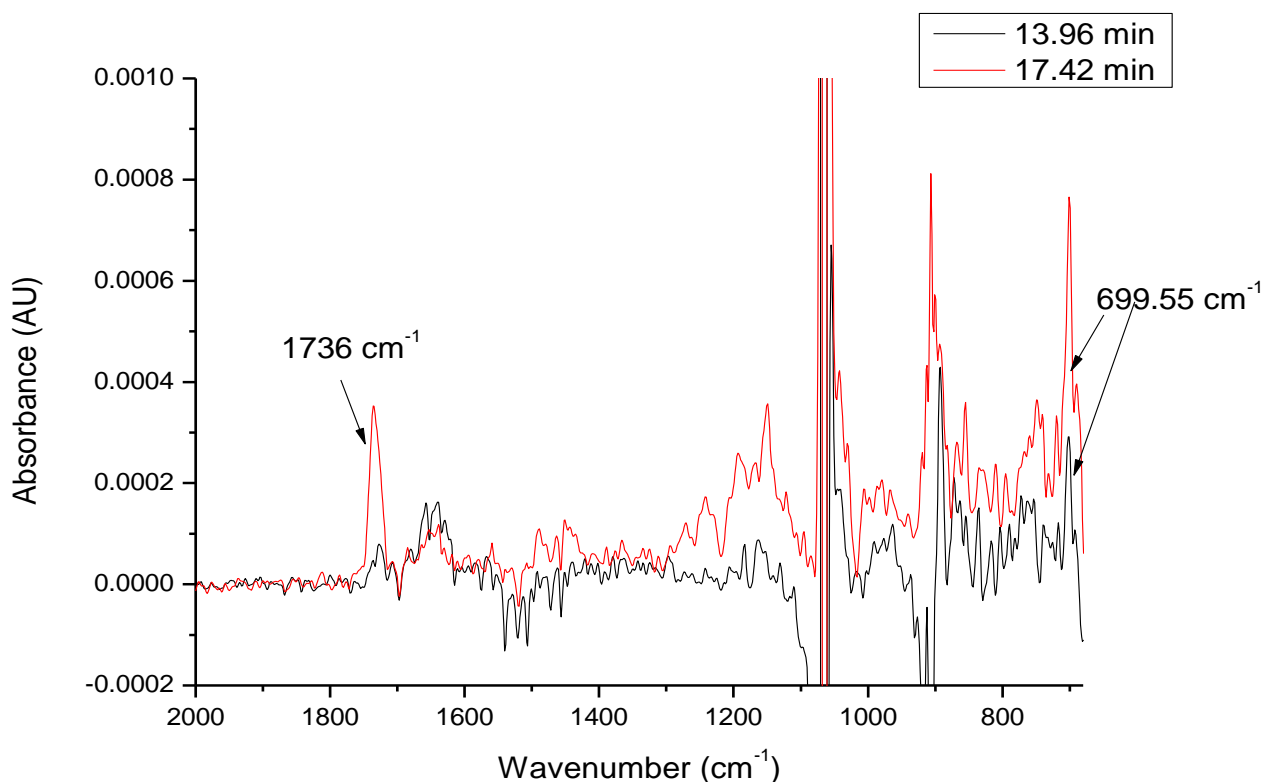
Figure 4.25: SMA 2 spectra extracted from elution times of 13.96 min and 17.42 min (peak max)

On average the results obtained by ThFFF-FTIR for the copolymer samples are comparable with those performed by ThFFF-UV/DRI.

It was, however noted that the S/N ratios from ThFFF-FTIR were significantly lower than those from the SEC-FTIR measurements that were done by the group of Wilhelm[8,9]. This was attributed to the fact that, fundamentally SEC shows better resolution than ThFFF and S/N is directly proportional to resolution. Therefore, SEC-FTIR will give FTIR peaks with better resolution and consequently a better S/N ratio[1,12].

75

4.3.3. Analysis of SMA copolymers regarding molar mass and size by ThFFF-MALLS-DLS

ThFFF-MALLS was used for the rapid detection of the molar mass heterogeneity of the copolymers. The retention times were based on the MALLS elugrams. The DLS detector provided the radius of gyration (R_g) from which the diffusion coefficient (D) could be calculated. Thereafter, the Soret coefficient (S_T) and the thermal diffusion coefficient (D_T) can be calculated.

The bulk dn/dc of the copolymers in THF at 25 °C for SMA 1, SMA 2, SMA 3 and SMA 4 were 0.122 ± 0.003 mL/g, 0.135 ±0.002 mL/g, 0.158 ± 0.002 mL/g and 0.112 ± 0.001 mL/g, respectively. These were used to determine the molar masses at the peak maximum. To determine the molar mass distribution, the dn/dc at each elution volume would have to be determined because it is not constant throughout the distribution as is indicated by the ThFFF-FTIR findings.

Table 4.9, shows that the Soret coefficient values for larger molecules correlates to longer retention times but for sample SMA 2 and SMA 3 having the same molar mass the Soret coefficient is the same. The thermal diffusion coefficients D_T for SMA 2 and SMA 3 have a difference of 0.77, which confirms that they have different chemical compositions. The styrene content of SMA 1 and SMA 2 differ by 4.0% and, therefore, they were expected to have similar D_T coefficients. The D_T coefficients are 3.86 ±0.22x10^{-7} cm^{2}s^{-1}K^{-1} and 3.40 ±0.55x10^{-7} cm^{2}s^{-1}K^{-1}, respectively.

Table 4.9: Peak molar mass (M_p), retention time (t_r), radius of gyration (R_g), diffusion coefficient (D), thermal diffusion coefficient (D_T) and Soret coefficient (S_T) of SMA determined by ThFFF at a temperature gradient (ΔT) of 60 K.

Sample name	M_p (kg/mol)	t_r (min)	R_g (nm)	D (10^{-10} cm^2 s^{-1})	D_T (10^{-7} cm^2 s^{-1} K^{-1})	S_T (K^{-1})
SMA 1	24.2	9.9	11.1	8.55 ±0.92	3.86 ±0.22	0.0022
SMA 2	53.7	12.5	15.9	5.97 ±0.81	3.40 ±0.55	0.0018
SMA 3	55.2	11.9	19.6	4.84 ±0.84	2.63 ±0.26	0.0018
SMA 4	80.3	22.6	22.5	4.22 ±0.57	4.34 ±0.68	0.0010

4.3.4. Analysis of a mixture of SMA copolymer and PMMA homopolymer

The properties of copolymers can be enhanced by the addition of a homopolymer. Therefore, it is important to have analytical techniques that are able to characterize a blend as a mixture of a homopolymer and copolymer. With this method, we are able to precisely do that.

Figure 4.26A shows a fractogram for a blend sample consisting of SMA 1 and PMMA with a molar mass of 138 kg/mol. The elution profile resembles the one of SM1 shown in Figure 4.4. From the concentration detector, it is not possible to confirm the exact chemical composition of the blend. The FTIR elugram is able to confirm that the first eluting component is the copolymer. The FTIR spectrum at 15.13 min consists of both MMA and styrene units of the copolymer whereas the spectrum at 27.0 min does not show a styrene moiety.
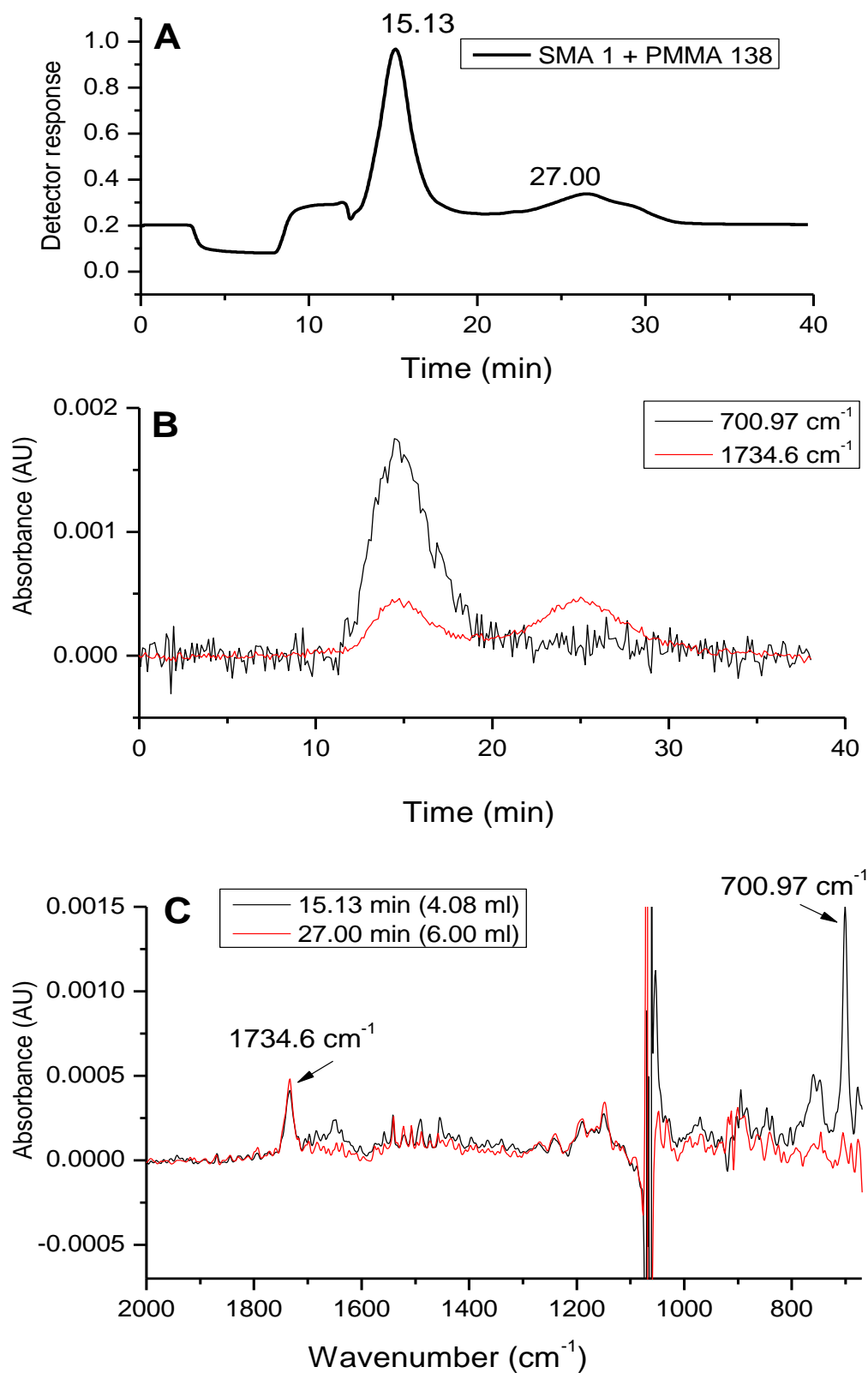
Figure 4.26: (A) DRI fractogram, (B) FTIR elugram, (C) spectra extracted from peak maxima for blend of SMA 1 and PMMA 138 g/mol

78

4.4   Poly (styrene-acrylonitrile) (SAN) copolymers

In this section, random copolymers of styrene and acrylonitrile (SAN) are investigated in DMF. SAN copolymers are prepared industrially by free radical polymerization. This method of polymerization has a major drawback due to its limited control over molecular parameters such as molar mass and chemical composition. SAN copolymers are interesting materials for typical FTIR spectroscopy analyses. They exhibit distinctive absorption peaks for the styrene and the acrylonitrile units that can be used to explore the molecular heterogeneity of the samples.

4.4.1.   Analysis of SAN copolymers by ThFFF-DRI-MALLS-DLS

The average comonomer compositions and molar masses of four SAN copolymers are presented in Table 4.10. The copolymers have rather similar chemical compositions but different molar masses.

Table 4.10: Molar masses (M_w), chemical compositions and dispersity indexes (Đ) as provided by the manufacturers.

Sample	Styrene (wt. %)	M_w (kg/mol)	Đ	Source
SAN 30	79	30	1.19	Polymer Source
SAN 50	70	50	1.35	Polymer Source
SAN 165	75	165	-	Sigma-Aldrich
SAN 185	70	185	-	Sigma-Aldrich

Figure 4.27 shows the superimposed DRI fractograms for all four SAN copolymers. The separation as monitored by the DRI detector is not desirable since some low molar mass material co-elutes with material/solvent in the the void peak. MALLS detection is not sensitive to low molar material that co-elutes in the void peak; traces in Figure 4.28 show well defined fractionation profiles. As can be seen, SAN 165 and SAN 185 exhibit similar elution profiles due to their similar molar mass and chemical compositions. In contrast, samples SAN 30 and SAN 50 with similar chemical compositions elute earlier due to their low molar masses.
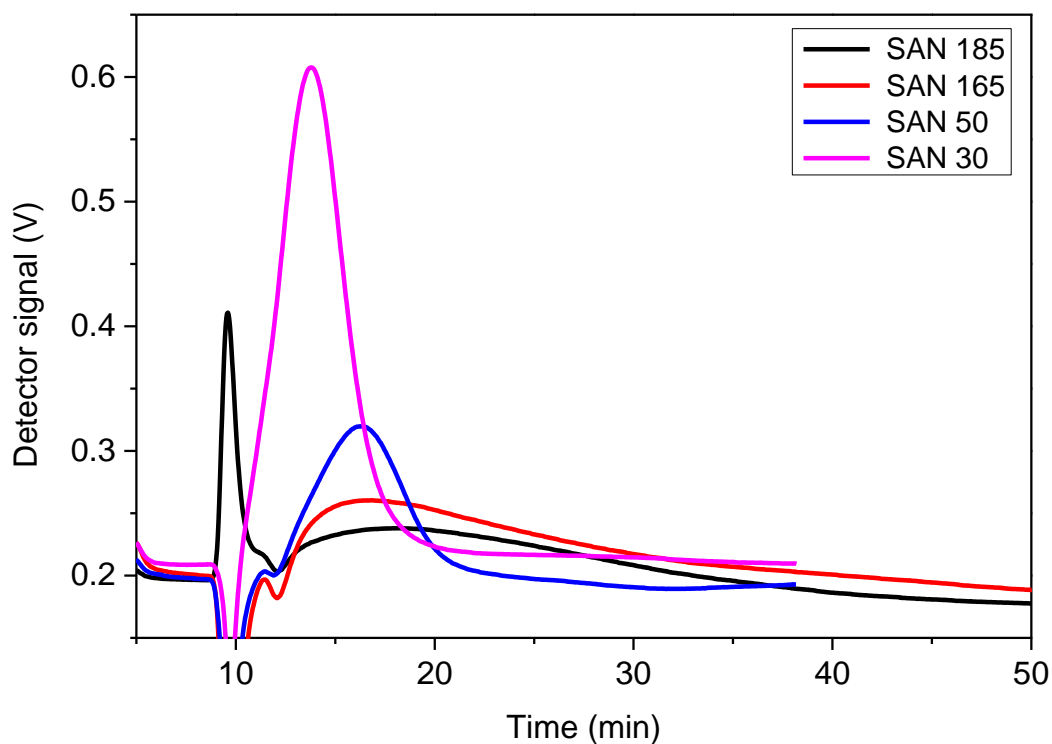
Figure 4.27: Superimposed fractograms of SAN 30, SAN 50, SAN 165 and SAN 185 as detected by DRI.
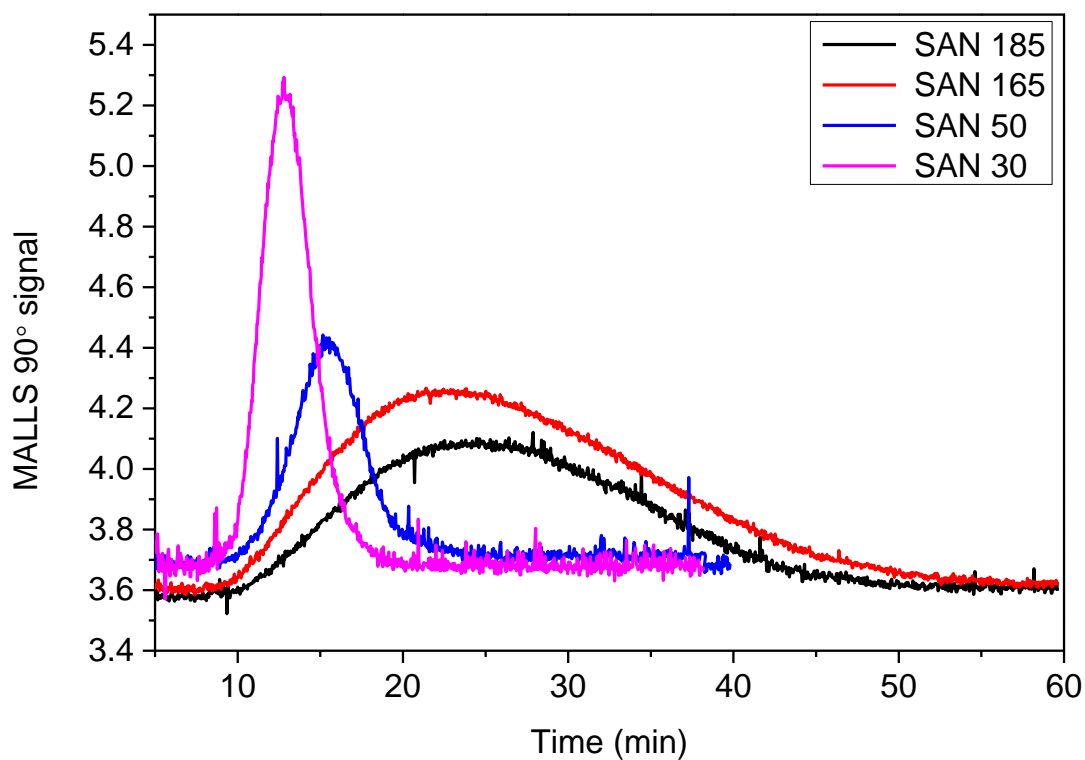
Figure 4.28: Superimposed fractograms of SAN 30, SAN 50, SAN 165 and SAN 185 as detected by MALLS at 90°.

80

Using the previously described multidetector ThFFF setup, different molecular parameters including the diffusion coefficients can be determined. In Table 4.11, the normal diffusion, thermal diffusion and the Soret coefficients are presented. As expected, the copolymers with the lowest molar masses have the highest normal diffusion coefficients. However, when samples SAN 165 and SAN 185 are compared, it is seen that the sample with the lower molar mass has the lower D. This is unexpected but, can be related to the different molecular microstructures of the samples and their interactions with the solvent.

Table 4.11: Retention time (t_r), radius of gyration (R_g), diffusion coefficient (D), thermal diffusion coefficient (D_T) and Soret coefficient (S_T) of SAN determined by ThFFF at a temperature gradient (ΔT) of 60 K.

Sample name	t_r (min)	R_g (nm)	D (10^{-8} cm^2 s^{-1})	D_T (10^{-5} cm^2 s^{-1} K^{-1})	S_T (K^{-1})
SAN 30	12.76	12.03	2.26	6.05	0.00037
SAN 50	15.67	21.85	1.25	4.09	0.00030
SAN 165	21.73	29.64	1.02	4.65	0.00022
SAN 185	24.23	24.17	1.13	5.72	0.00020

4.4.2.   Analysis of SAN copolymers regarding chemical composition distribution by ThFFF-FTIR

ThFFF-FTIR was used to determine the chemical composition distribution of the SAN copolymers. Different from the previous applications on styrene-MMA copolymers where both monomers exhibit strong adsorptions in the FTIR spectra, in the present case styrene is easily detectable while acrylonitrile exhibits only a weak absorption in the region of 2000 to 2250 cm^{-1} for the nitrile group[13]. Considering the fact that the present copolymers contain only 21 – 30 wt. % of acrylonitrile, it was a challenge to detect these units. Furthermore, the homopolymer poly(acrylonitrile) (PAN) is insoluble in DMF at the required concentration and, therefore, could not be investigated by ThFFF. Due to the fact that DMF is UV absorbing, the

UV data could not be used to determine the chemical composition via PS absorbance in the copolymer. Therefore, FTIR was used to confirm the presence of acrylonitrile (AN) and styrene (S) groups as well as the investigation of the chemical composition distribution of the copolymers.
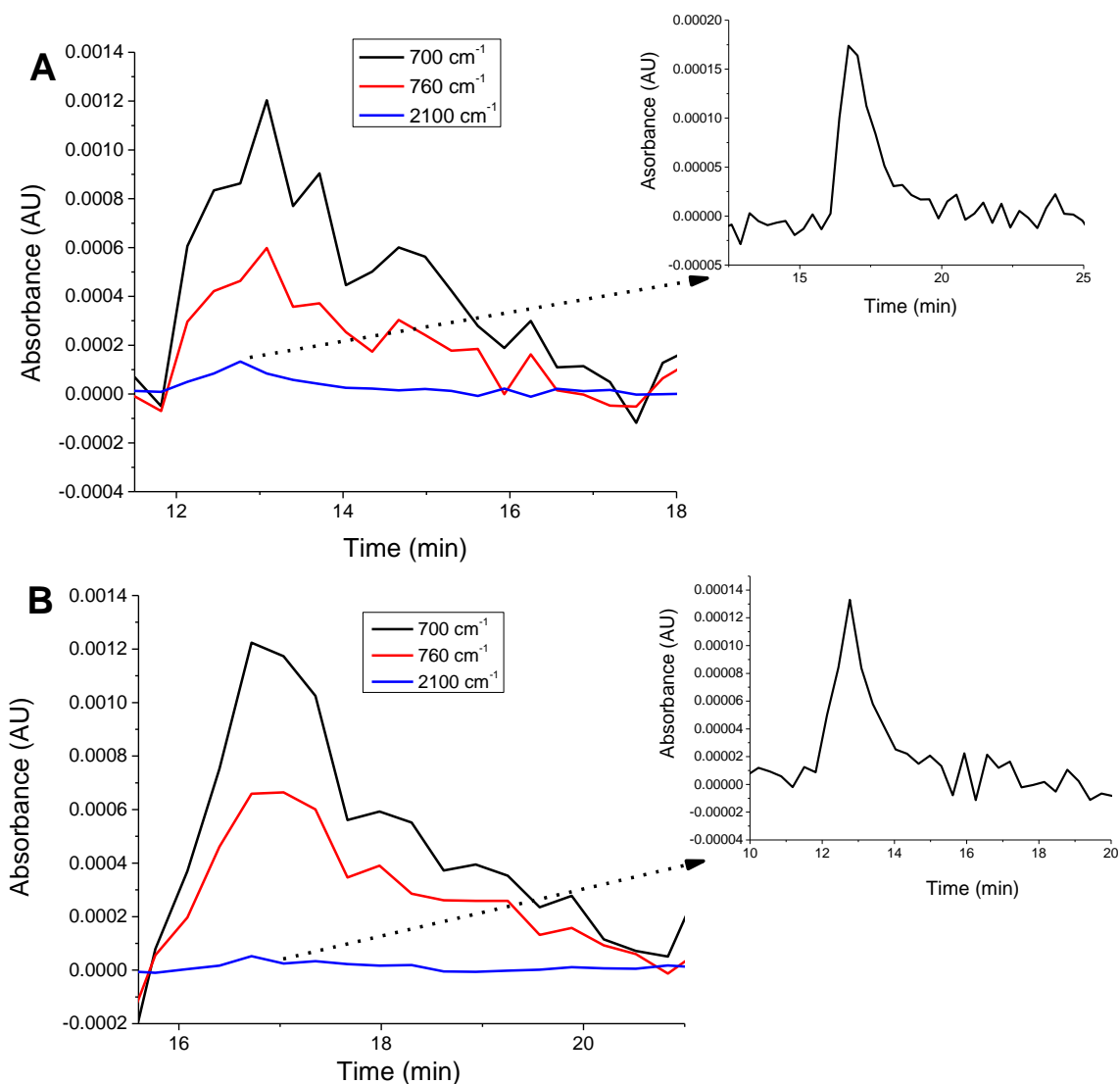
**Figure 4.29:** FTIR elugrams of (A) SAN 30 and (B) SAN 50. The inserts show enlarged elugrams for AN units at 2100 cm⁻¹.

The SAN copolymers under investigation had AN contents of 21 – 30 wt. %. Our aim was to explore the possibility of using the FTIR detector as a means to detail the chemical composition distribution. In order to investigate the chemical composition distribution, the characteristic

nitrile groups ($2000 - 2250$ cm^{-1}) and styrene units (760, 700 cm^{-1}) were explored. Figures 4.29 and 4.30 summarize the FTIR elugrams of the copolymers.
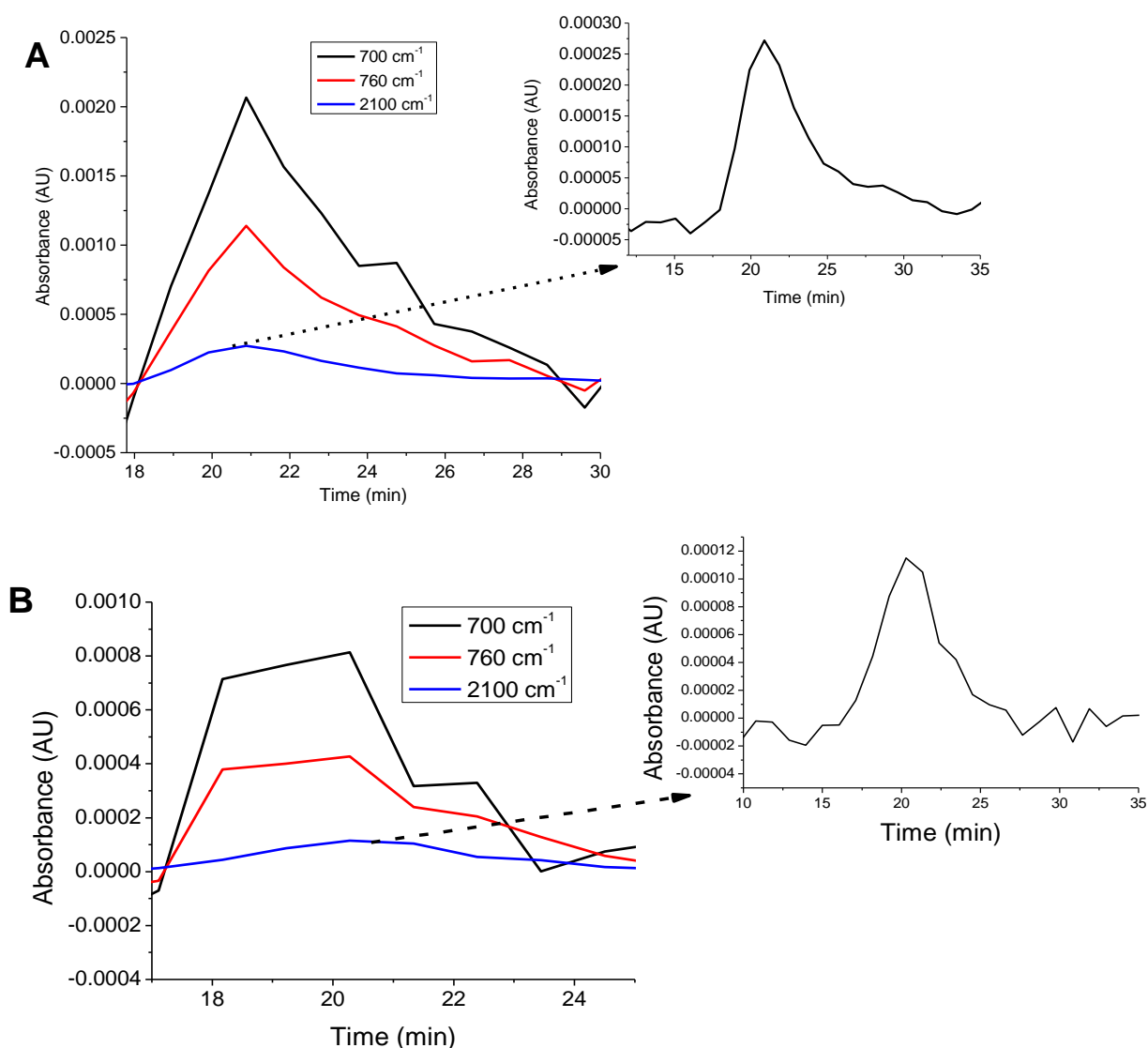
Figure 4.30: FTIR elugrams for (A) SAN 165 and (B) SAN 185. The inserts show enlarged elugrams while monitoring the AN unit at 2100 cm^{-1}.

As can be seen, the absorbances of the AN units in all cases are much lower than the absorbances of the S units. This makes it very challenging to obtain concentration profiles for the AN units as a function of elution time. Selected FTIR spectra show, however, that nitrile groups can be clearly seen. Although the intensity of the AN groups is quite low, an attempt to monitor the AN group concentration in the course of the ThFFF fractionation was made. As is

83

shown in the inserts in Figures 4.29 and 4.30, well defined elution profiles can be obtained by monitoring the AN groups.
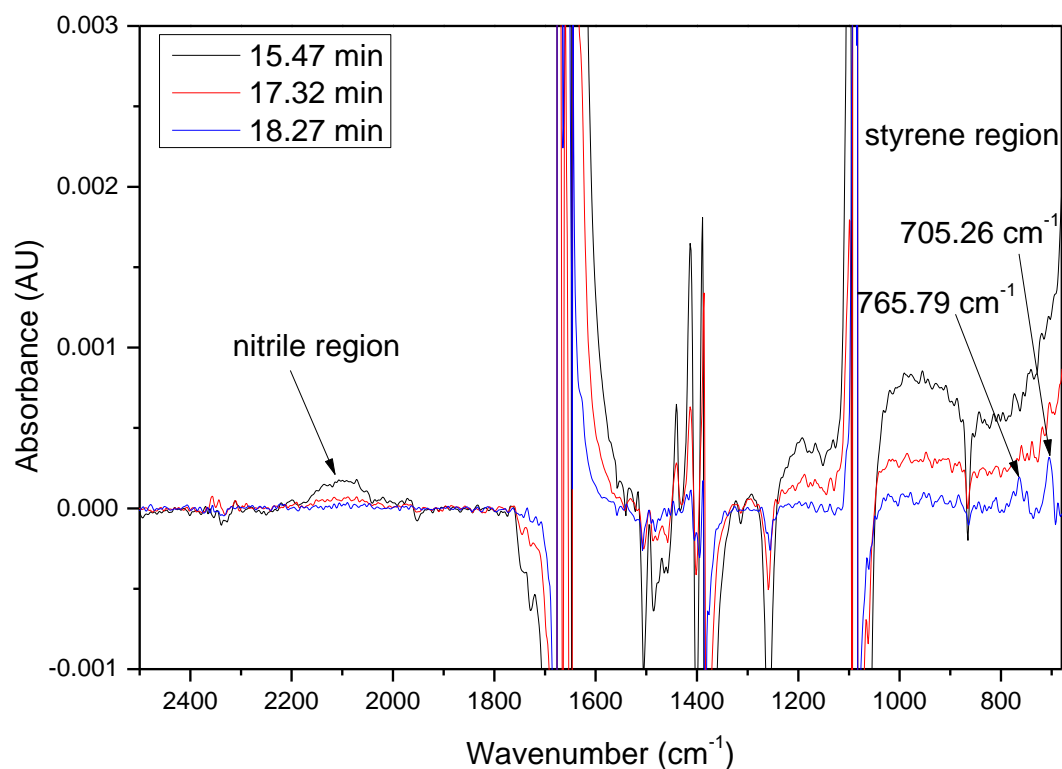

Figure 4.31: FTIR spectra of SAN 50 at 15.47, 17.32 and 18.27 min.

Figure 4.31 shows FTIR spectra of SAN 50 at three different elution times. The nitrile region is visible with a broad peak from 2100 to 2200 cm^{-1}. The group exhibits weak absorbances as compared to the styrene related peaks at 765.79 and 705.26 cm^{-1}. At 17.32 min, the nitrile band is even less intense as compared to the peak and at 18.27 min and, therefore, the nitrile absorbances cannot be distinguished from the signal noise. Styrene, however, shows intense absorbances. Figure 4.32 and 4.33 show an overlay of the MALLS and the FTIR elugrams. MALLS gives information on the molar mass distribution while the elugram obtained with FTIR detection of the AN component details the chemical composition distribution as a function of the molar mass. Both SAN 30 and SAN 50 have narrow molar mass distributions and the AN group shows high absorbances in the centre of the distribution. This was observed for both samples, see Figure. 4.32. However, AN is not distributed throughout the entire molar mass distribution.
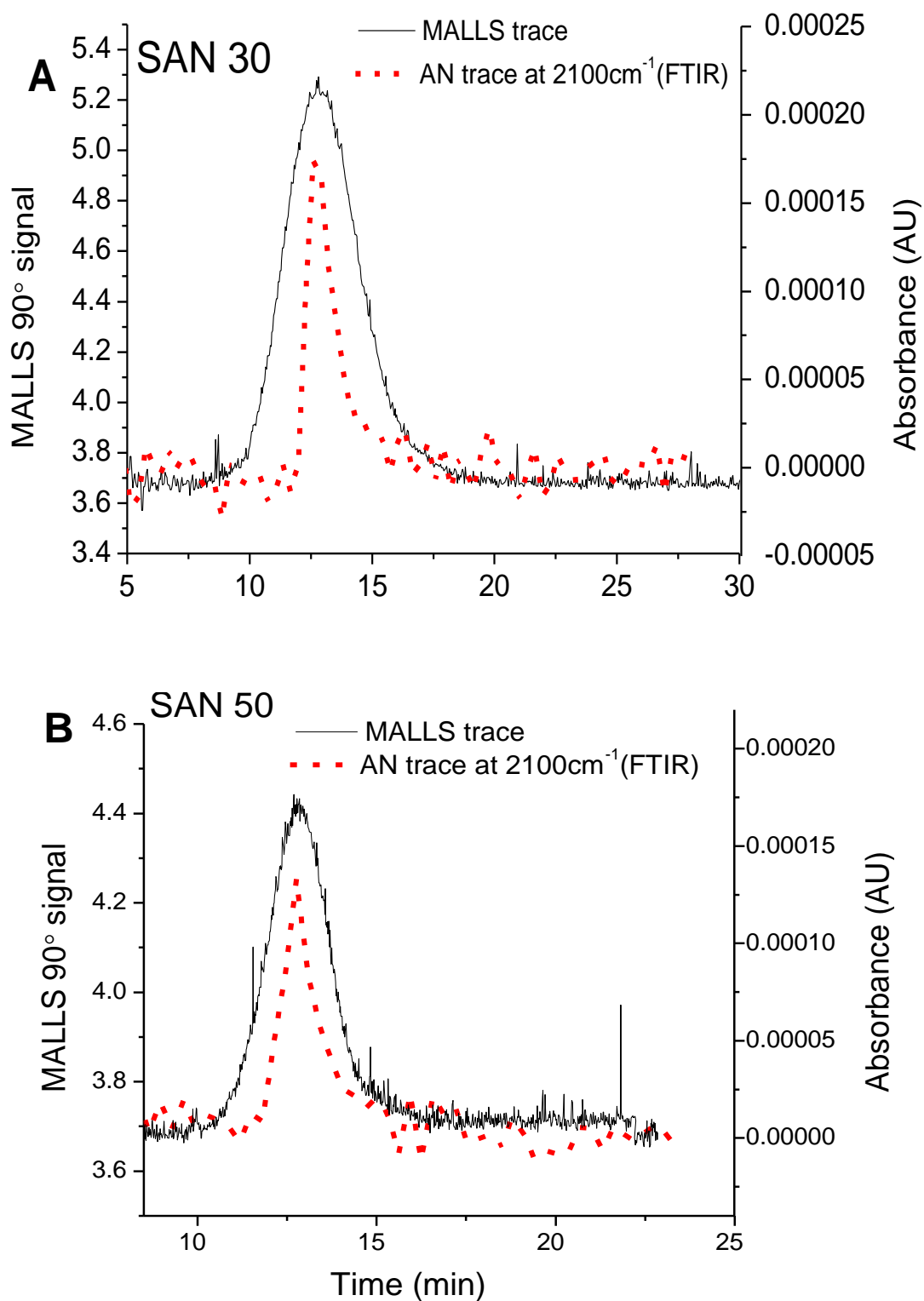
Figure 4.32: Superimposed MALLS and FTIR elugrams of (A) SAN 30 and (B) SAN 50.
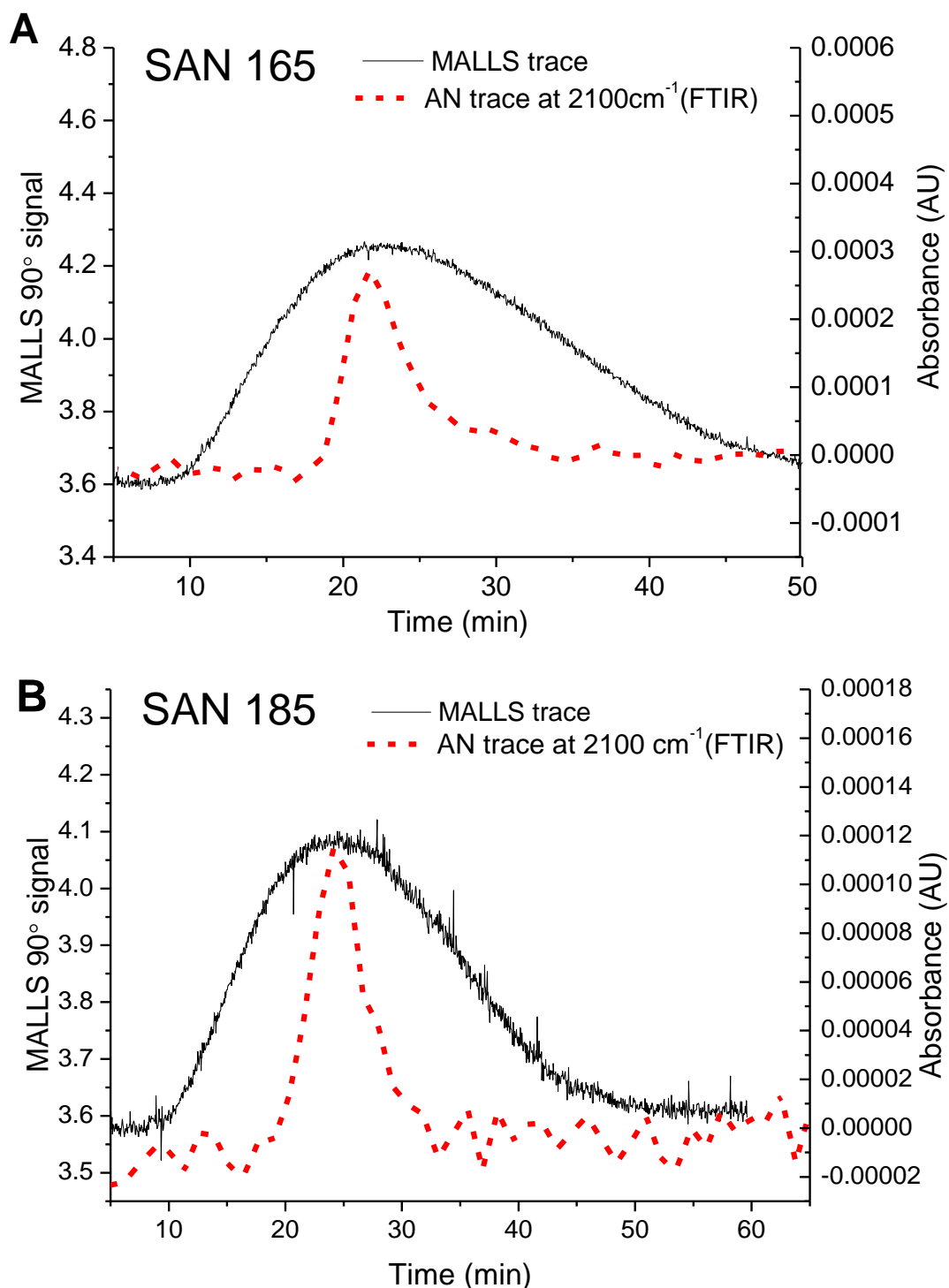
Figure 4.33: Superimposed MALLS and FTIR elugrams of (A) SAN 165 and (B) SAN 185.

For SAN 165 and SAN 185 copolymers, it is clear that the AN is not evenly distributed throughout the molar mass range. However, it is important to note that FTIR is not very sensitive towards the nitrile group of the AN functionality because of its low response factor and concentration within the copolymers. Furthermore, it was not possible to measure the absolute chemical composition of the copolymers due to the insolubility of PAN which

86

prevented a calibration with suitable homopolymers. Therefore, a calibration from PS-PAN blend samples could not be obtained. The poor solubility of PAN was confirmed using offline DLS. In cases where blends cannot be made using homopolymers, peak ratios at the peak maximum can be used to compare for the different samples or calculate the mean peak absorbance ratio over the elution range and use those values to compare them to the values given by the manufacturer.

Figure 4.34 shows the proposed molar mass distribution as a function of AN composition in the form of contour plots. The representation are based on ThFFF-MALLS-FTIR.
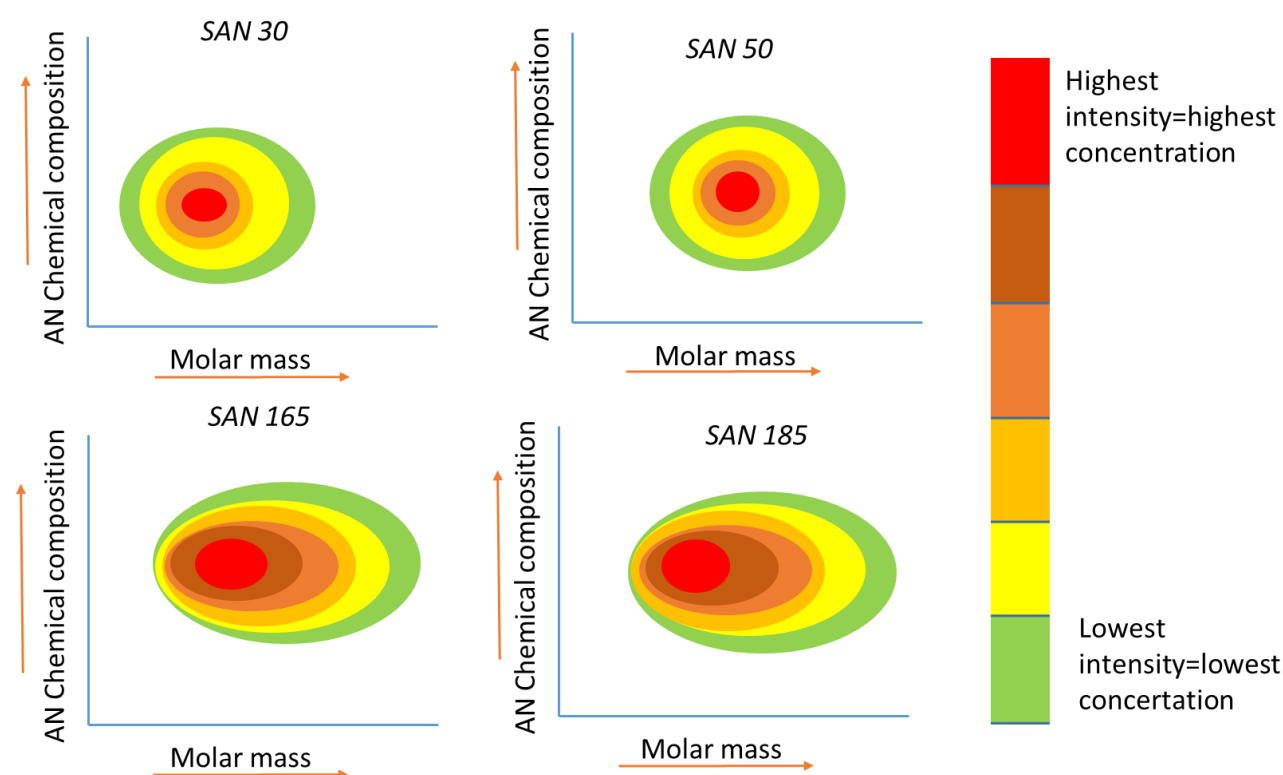
Figure 4.34: Schematic representation of contour plots detailing the distribution of AN functionalities in SAN 30, SAN 50, SAN 165 and SAN185.

As illustrated in Figure 4.34, it is proposed that SAN 30 and SAN 50 have similar molar mass distributions but at slightly different elution volumes (Figure 4.28 and 4.32). The highest concentration of the AN, is found at the highest point in the molar mass distribution plots of SAN 30 and SAN 50. SAN 165 and SAN 185 have broader molar mass distributions as detected by MALLS. (Figure 4.28 and 4.33). However, it is important to remember that these proposed plots do not consider the molar mass distribution and the chemical composition distribution in

each copolymer chain. This information can be attained through a more detailed study using ThFFF-NMR.

Table 4.12: AN wt. % and mean peak absorbance area ratios for SAN copolymers

Sample	AN content (wt. %)	Mean peak ratio ($\frac{2100\ cm^{-1}}{700\ cm^{-1}}$)	Mean peak ratio ($\frac{2100\ cm^{-1}}{760\ cm^{-1}}$)
SAN 30	21	0.0661	0.179
SAN 50	30	0.134	0.245
SAN 165	25	0.117	0.203
SAN 185	30	0.143	0.282

In Table 4.12 the mean peak absorbance ratios for the SAN copolymers were calculated using the absorbances at 700 and 760 cm^{-1} for styrene. In general, the peak at 700 cm^{-1} had more noise as compared to the one at 760 cm^{-1}, therefore, we found it valuable to present both sets of peak ratios in the same data set for comparative purposes. According to the manufacturer, SAN 50 and SAN 185 have the same AN content which is higher than that of SAN 30 and SAN 165. In Table 4.12, it is seen that SAN 50 and SAN 185 have higher mean peak ratios compared to SAN 30 and SAN 185. In addition, it is seen that SAN 30 has the lowest value, which corresponds well to it having the lowest AN content. These results indicate a qualitative agreement with the values from the manufacturers. It is important to note, however, that due to inherent noise from the ThFFF-FTIR, these results were determined with low accuracy.

4.5   References

1.   Smith, B. C. *Fundamentals of Fourier Transform Infrared Spectroscopy*. (CRC Press: Florida, U.S.A, 2011).

2.   Schimpf, M., Caldwell, K. & Giddings, J. C. *Field flow Fractionation Handbook*. (Wiley-Interscience: New York ,U.S.A, 2000).

3.   Podzimek, S. *Light Scattering, Size Exclusion Chromatography and Asymmetric Flow Field Fractionation*. (John Wiley & Sons: New Jersey, U.S.A 2011).

4.   Held, D. & Kilz, P. Characterization of Polymers by Liquid Chromatography. *Macromol.*

Symp. **231,** 145–165 (2006).

5. Mori, S. *Encyclopedia of Chromatography*. (Taylor & Francis Group: Florida, U.S.A, 2005).

6. Pasch, H. *Hyphenated Techniques in Liquid Chromatography of Polymers. Advances in Polymer Science* **150** (2000) 1-66

7. Pasch, H., Adler, M., Rittig, F. & Becker, S. New Developments in Multidimensional Chromatography of Complex Polymers. *Macromol. Rapid Commun.* **26**, 438–444 (2005).

8. Beskers, T. F., Hofe, T. & Wilhelm, M. Development of a chemically sensitive online SEC detector based on FTIR spectroscopy. *Polym. Chem.* **6,** 128–142 (2015).

9. Beskers, T. F., Hofe, T. & Wilhelm, M. Online Coupling of Size-Exclusion Chromatography and IR Spectroscopy to Correlate Molecular Weight with Chemical Composition. *Macromol. Rapid Commun.* **33,** 1747−1752 (2012).

10. Michler, G. H. & Verlag, C. H. *Atlas of Polymer Structures*. (Hanser Publishers: Munich, Germany, 2016).

11. Noshay, A. & McGrath, J. E. *Block Copolymers*. (Academic Press: New York, U.S.A, 1977).

12. Griffiths, P. R. & de Haseth, J. A. *Fourier Transform Infrared Spectroscopy*. (John Wiley & Sons: New Jersey, U.S.A, 2007).

13. Smith, B. *Infrared Spectral Interpretation.* (CRC Press: Florida, U.S.A, 1999)

Chapter 5 : Conclusions and future work

5.1   Summary

The main focus of this work was to set up and develop an online FTIR detection method for multidetector ThFFF. FTIR is one of the most selective detectors for chemical composition analysis of complex polymers. The FTIR detector adds in a powerful way to the existing multidetector ThFFF instrument comprising concentration (DRI and UV) as well as molar mass (MALLS) and size (DLS) sensitive detectors. The novel detector combination allows for the simultaneous analysis of chemical compositions, molar masses, molecular sizes and diffusion properties in one experiment. This is the first setup of its kind that allows for the comprehensive analysis of complex polymers, nanoparticles and large polymer assemblies regarding their molecular distributions.

Conclusions

The presented coupled method significantly enhances the capabilities of multidetector ThFFF. In addition to size analysis, the online coupling with FTIR spectroscopy allows for the detailed chemical composition analysis of complex polymers. With the present method, the time needed for FFF separation and subsequent analysis by FTIR is significantly decreased compared to the offline approach.

In one integrated procedure, THFFF-FTIR was able to provide molecular and structural characterization of complex multicomponent samples. By preparing blends and copolymer samples with distinct differences in chemical composition, FTIR was able to confirm chemical heterogeneity and subsequently quantify it. The multidetector setup (ThFFF-UV-MALLS-RI-FTIR-DLS) allowed for molar mass approximations, size distribution determination and thermal diffusion calculations. Furthermore, the ThFFF-FTIR results could also be compared to those calculated from ThFFF-UV-DRI.

Through a series of experiments, it was possible to determine the LOD and LOQ for two polymers, PS and PMMA. These limits were then correlated to the conditions of the ThFFF were overloading was not present. This ensured that the ThFFF separation quality remained intact without compromising on the spectral quality. The S/N ratio was, in general, well above the limit of quantification, which allowed for the calculation of the correlated weight fractions

at each elution time, after mathematical solvent suppression using the TIMO software. Furthermore, SAN copolymers, were qualitatively analysed using the abovementioned set-up. ThFFF-FTIR showed to be a useful technique in the analysis of copolymers with low concentrations of a specific monomer in a copolymer. A more comprehensive analysis of the SAN copolymers can be done using ThFFF-NMR.

In conclusion, for the first time, online coupling of ThFFF and FTIR for the determination of the chemical composition and the chemical composition distribution of blends and copolymers was developed.

5.2   Future work

Different complex polymers in different solvents should be analysed using this method. In future, it will be valuable to measure samples that cannot be measured using SEC (i.e. particles, micelles, proteins). Previous work using ThFFF has been presented on micelles and using ThFFF-FTIR will add a new dimension to these studies. Results can be compared to results obtained by the offline approach using the LC transform. This will help confirm the chemical composition distribution results from online ThFFF-FTIR. FTIR can also be coupled to AF_4, which unlike ThFFF separates only according to size. Combing FTIR with AF_4 will be useful for samples that are sensitive to heat and are likely to degrade if LC Transform is used on them. Particularly proteins that are only soluble in water and are heat sensitive could be analysed using the online FTIR coupling.